# ANALYTICAL AND NUMERICAL MODELING OF FOUNDATION HEAT EXCHANGERS

By

LU XING

Bachelor of Science in Mechanical Engineering

Huazhong University of Science & Technology

Wuhan, China

2008

Submitted to the Faculty of the
Graduate College of the
Oklahoma State University
in partial fulfillment of
the requirements for
the Degree of
MASTER OF SCIENCE
December, 2010

ANALYTICAL AND NUMERICAL MODELING OF

FOUNDATION HEAT EXCHANGERS

Thesis Approved:

J. D. Spitler

Thesis Adviser

D. E. Fisher

L. Cremaschi

Mark E. Payton

Dean of the Graduate College

# ACKNOWLEDGMENTS

I would like to thank my advisor, Dr. Spitler, for his useful guidance and his efforts in encouraging me to continue in every stage of this study. To my parents, who give me great support and endless love and patience; I owe them all of my education and success. To my fiancé, who always stays with me and supports me during the hard times of writing. I thank him for his great patience and love which supported me while finishing this thesis.

I would also like to acknowledge financial support for this project from the US Department of Energy and Oak Ridge National Laboratory. Our project monitors there, Piljae Im and John Shonder, have been particularly helpful. Also, I would like to thank the team of experimentalists, lead by Jeff Christian, that instrumented the house and monitor the data.

TABLE OF CONTENTS

Chapter Page

1. INTRODUCTION ..... 1

2. LITERATURE REVIEW ..... 6

2.1 Analytical HGHX Model ..... 7
2.2 Numerical HGHX Model ..... 14
2.3 Experimental Research on Horizontal Ground Heat Exchangers ..... 23
2.4 Foundation Heat Exchanger ..... 25
2.5 Models for Undisturbed Ground Temperature ..... 27
2.5.1 Analytical Model ..... 27
2.5.2 Numerical Model ..... 30

3. ONE-DIMENSIONAL GROUND HEAT TRANSFER MODEL ..... 33

3.1 1D Numerical Model ..... 34
3.1.1 Surface Heat Balance ..... 35
3.1.2 Heat Balance at the Bottom Boundary ..... 43
3.1.3 Soil Freezing/Melting ..... 44
3.2 Kusuda and Achenbach Model ..... 49
3.3 Experimental Validation ..... 50

4. FHX NUMERICAL MODEL ..... 62

4.1 Non-uniform Grid ..... 63
4.2 Finite Volume Equations ..... 67
4.3 Boundary Condition and Model Algorithm ..... 73
4.4 Short-Circuiting Heat Transfer ..... 75

5. FHX ANALYTICAL MODELS ..... 78

5.1 Single FHX Tube ..... 80
5.2 Sink/Source Method ..... 86

Chapter Page

5.3 Undisturbed Ground Temperature ..... 90
5.4 Load Devolution Superimposing Method ..... 92
5.5 Heat Pump Model ..... 97

6. VERIFICATION AND EXPERIMENTAL VALIDATION ..... 99

6.1 FHX Numerical Model Verification ..... 100
6.1.1 Time Step Independency Test ..... 100
6.1.2 Non-Uniform Grid Test ..... 102
6.2 Analytical Validation of Numerical Model ..... 103
6.3 Experimental Validation ..... 104
6.3.1 Validation of Undisturbed Ground Temperature Model ..... 111
6.1.2 Post-processing of Experimental Data ..... 115

7. INTERMODEL VALIDATION ..... 125

8. CONCLUSIONS AND RECOMMENDATION ..... 137

REFERENCES ..... 141

LIST OF TABLES

Table Page

3.1: Locations of SCAN sites and TMY3 weather data sites ..... 51
3.2: Annual maximum soil temperature at the depth of 50 cm (20") ..... 57
3.3: Annual maximum soil temperature at the depth of 100 cm (40") ..... 58
3.4: Annual minimum soil temperature at the depth of 50 cm (20") ..... 59
3.5: Annual minimum soil temperature at the depth of 100 cm (40") ..... 59

7.1: Climate zones ..... 125
7.2: Peak FHX ExFT error ..... 131
7.3: FHX sizing error ..... 131
7.4: Comparison of numerical and analytical model features ..... 132
7.5: Peak FHX ExFT error with adiabatic foundation ..... 133

LIST OF FIGURES

Figure Page

1.1: FHX. a) In basement excavation, b) extended into utility trench ..... 2
1.2: Cross-section of foundation heat exchanger ..... 3

2.1: Mirror-image method ..... 12
2.2: Floor heating system ..... 13
2.3: Schematic of ground coil ..... 15
2.4: Schematic of the frozen and non-frozen soil region ..... 17
2.5: Schematic of two-pipe arrangement ..... 18
2.6: Schematic of the grid ..... 20
2.7: Demir's model soil domain plot ..... 22
2.8: Schematic of different foundation heat exchangers ..... 24
2.9: (a) spiral pipe configuration (b) ring source approximation ..... 26

3.1: Soil temperature at 1 m (3.28 ft) deep, in Roger Farms, Nebraska ..... 42
3.2: Specific heat capacity of water in the soil ..... 45
3.3: Soil temperature at 0.5 m (1.64 ft) deep, in Mason, Illinois ..... 48
3.4: Soil temperature at 0.5 m (1.64 ft) depth in Nebraska ..... 52
3.5: Soil temperature at 1.0 m (3.28 ft) depth in Nebraska ..... 52
3.6: Soil temperature at 0.5 m (1.64 ft) depth in Pennsylvania ..... 53
3.7: Soil temperature at 1.0 m (3.28 ft) depth in Pennsylvania ..... 53
3.8: Soil temperature at 0.5 m (1.64 ft) depth in Minnesota ..... 55
3.9: Soil temperature at 1.0 m (3.28 ft) depth in Minnesota ..... 55
3.10: Snow cover sensitivity study at 50 cm (20") depth in South Dakota ..... 56

4.1: Cross-section of foundation heat exchanger ..... 63
4.2: Non-uniform grid ..... 64
4.3: Non-uniform grid detailed plot ..... 66
4.4 FHX tubes grid plot ..... 67
4.5: Earth surface cell ..... 70
4.6: Nodes around the FHX tube ..... 72

5.1: The schematic of a single FHX tube ..... 83
5.2: Application of mirror-image sources and sinks ..... 87
5.3: Thermal conductivity vs. water content in certain location in Oklahoma ..... 92
5.4: Thermal heat capacity vs. water content in certain location in Oklahoma ..... 92
5.5 Loads devolution method (hourly loads) ..... 94

Figure Page

5.6 Temperature response superimposition method (hourly loads) ..... 94
5.7 Loads devolution method (monthly loads)..... 97

6.1: HVACSIM+ time step independency study ..... 101
6.2: Inter numerical model time step independency study..... 101
6.3: Non-uniform grid test..... 103
6.4: FHX analytical model test against FHX numerical model ..... 104
6.5: Experimental house built in Oak Ridge, Tennessee ..... 105
6.6: SIP house and FHX pipes locations ..... 106
6.7: Cross-section of foundation heat exchanger..... 107
6.8: The geometry of FHX tubes: dimensions given in m ..... 110
6.9: The geometry of HGHX tubes ..... 110
6.10: Undisturbed ground temperature at 0.31m (1 ft) depth ..... 112
6.11: Undisturbed ground temperature at 0.61m (2 ft) depth ..... 113
6.12: Undisturbed ground temperature at 0.91m (3 ft) depth ..... 113
6.13: Undisturbed ground temperature at 1.52 m (5 ft) depth ..... 114
6.14: Undisturbed ground temperature at 1.83 m (6 ft) depth ..... 114
6.15: Heat pump flow rate and pressure drop correlation ..... 116
6.16: Correlation between flow rate and pressure drop ..... 117
6.17: Comparison of daily average simulated and measured FHX ExFT ..... 120
6.18: Comparison of FHX ExFTs with 1- and 15- minute data for 10 August..... 120
6.19: Daily average measured and modeled pipe wall temperature..... 121
6.20: Soil temperature at 0.38 m (15 ") depth, measured and modeled ..... 122
6.21: Soil temperature at 1.0 m (42 ") depth, measured and modeled ..... 123

7.1: FHX exiting fluid temperature predictions for Albuquerque, NM ..... 127
7.2: FHX exiting fluid temperature predictions for Knoxville, TN ..... 128
7.3: FHX exiting fluid temperature predictions for Phoenix, AZ ..... 128
7.4: FHX exiting fluid temperature predictions for SanFrancisco, CA ..... 129
7.5: FHX exiting fluid temperature predictions for Salem, OR ..... 129
7.6: FHX exiting fluid temperature predictions for Tulsa, OK ..... 130
7.7: Reasons for FHX ExFT difference between two model result in Salem,OR.. 134
7.8: Basement air temperature in Salem, OR ..... 135

# CHAPTER 1

## INTRODUCTION

Ground source heat pump (GSHP) systems are widely used in residential and commercial buildings due to their high energy efficiency. Horizontal and vertical ground heat exchangers are two types of heat exchanger usually used in ground source heat pump systems. However, the high costs of trench excavation required for horizontal heat exchanger installation and the high costs of drilling boreholes for vertical heat exchangers are often a barrier to implementation of the GSHP system. In the case of net zero energy homes or homes approaching net zero energy, the greatly reduced heating and cooling loads, compared to conventional construction, give the possibility of using a ground heat exchanger that is significantly reduced in size.

Recently, a new type of ground heat exchanger that utilizes the excavation often made for basements or foundations has been proposed as an alternative to conventional ground heat exchanger. By locating the pipes in the excavation made for the basement, "foundation heat exchangers" (FHX) can significantly reduce installation cost compared with the conventional ground heat exchangers. Although foundation heat exchangers have been installed in some homes and have worked successfully, no scientific design procedure has been developed in order to size the foundation heat exchangers for specific buildings. Therefore, both numerical FHX and analytical FHX models have been developed and are described in this thesis. These models can be used as design tools for sizing foundation heat exchangers, especially the analytical model, which

consumes much less computational time than the numerical model. The FHX models, especially the numerical model, can be used for analyzing the energy consumption of ground source heat pump systems with FHX. Both numerical and analytical FHX models consider several factors that effect the performance of the foundation heat exchangers; soil properties like soil thermal conductivity, soil density and soil heat capacity, pipe locations, pipe materials and pipe wall thickness, basement wall insulation R values, basement wall thickness, etc. Simplifying assumptions have been made in the two models; in both models the soil is assumed to be homogenous. The foundation heat exchangers investigated in this thesis are placed horizontally around the house basement, as shown in Figure 1.1.

a) b)

Figure 1.1: FHX. a) In basement excavation, b) extended into utility trench, (photo: Im 2009)

The numerical model is an explicit "two-dimensional" (2D) finite difference model coupled with a full energy balance on the earth's surface, including evapotranspiration, solar radiation, convection, thermal radiation and conduction. The two-dimensional simulation soil domain is as shown in Figure 1.2. The evapotranspiration sub-model (Walter, et al. 2000) is used with standard surface vegetation – grass of uniform 12 cm (4.7") height with a “moderately dry” soil surface. The freezing/melting of moisture in the soil is also considered in the model by using the effective heat capacity method (Lamberg, et al. 2004), which adjusts the specific heat capacity of water in the soil in such a way that, as it transitions from water in liquid form to water in solid form, the

total energy reduction is the same as in the actual freezing process. The inside basement wall and basement floor boundaries are convective, exchanging heat with the basement. Two approaches to setting the basement conditions have been investigated; the basement is held at a constant temperature and the basement unconditioned. Although evapotranspiration and freezing/melting of the soil are modeled, moisture transport and snow cover are not considered in this model. The numerical model was initially based on Liu's (2005) model, of pavement snow melting systems. However, the FHX numerical model utilizes different simulation domain, boundary conditions, and grid scheme from Liu's model; therefore, it is quite different from Liu's model. The numerical FHX model is covered in Chapter 4 of this thesis.

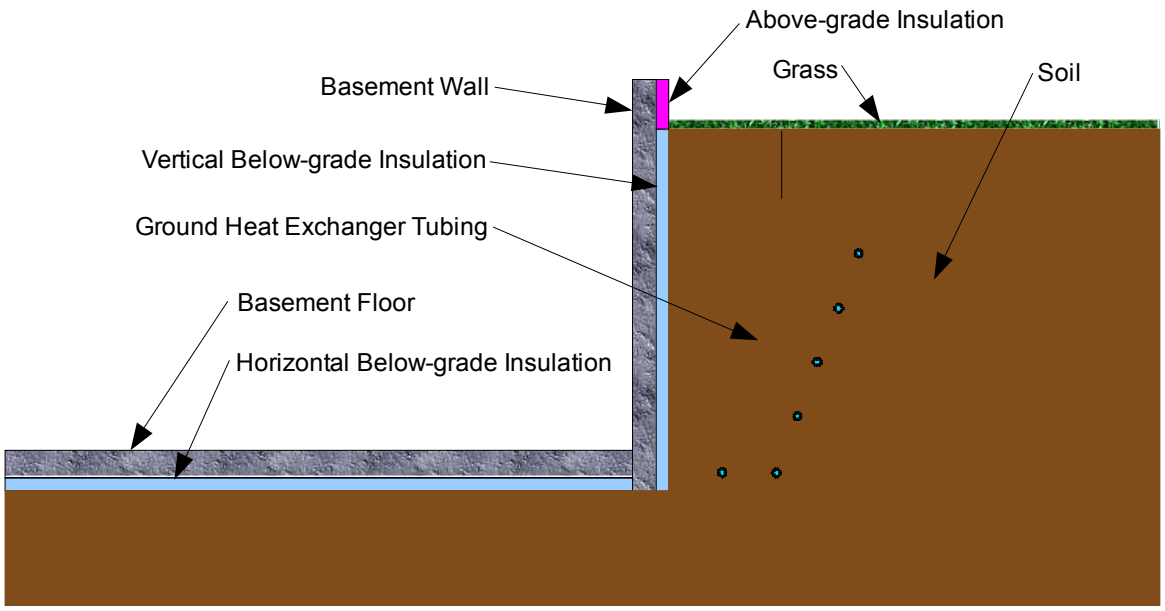


Figure 1.2: Cross-section of foundation heat exchanger (Spitler, et al. 2010)

Analytical models based on superposition of line sources, including mirror image sources, have been used to model horizontal ground heat exchangers for many years. Therefore, by simplifying the foundation geometry and eliminating the surface heat balance, two analytical models based on the line source solution have been developed in this thesis; an hourly time-step analytical model implemented in HVACSIM+ environment, and a monthly time-step analytical model

implemented in an interpreted language. Furthermore, the monthly time-step analytical model is very computationally efficient when a hybrid time step scheme (e.g. monthly time steps + monthly peak time steps) is used, thus used as a design tool. The design tool includes a user-friendly interface, which asks for building loads, soil properties, pipe locations, etc. It allows users to determine monthly peak or average fluid temperature entering or exiting heat pump in order to simulate the performance of GSHP systems with FHX. The analytical model is covered in Chapter 5 of the thesis.

Foundation heat exchangers have close contact with the soil, which means that for both numerical and analytical FHX models it is critical to determine the soil temperature at the site in order to evaluate the GSHP system performance. Ground temperatures for different soil depths over the year are also needed in fields like agriculture and biological sciences. However, there are few resources that provide soil temperature information. So a "one-dimensional" (1D) ground heat transfer model is developed; the goal is to predict soil temperatures bases on typical meteorological year data, then tune the analytical soil temperature model (Kusuda and Achenbach 1965) with the numerical model. The 1D ground heat transfer model will be validated with measured soil temperature at sites in the United State and will be covered in Chapter 3 of this thesis.

Various approaches have been investigated in order to verify the FHX numerical model before experimental validation, including a check on time step independency study, evaluation of the non-uniform grid and analytical validation of the numerical model. Then, the FHX numerical model is validated with experimental data collected from experiment operated in Knoxville, Tennessee, for a period of ten months. A 2D HGHX model is also used for the experimental validation; it is similar to the 2D numerical FHX model except for no foundation wall included. The FHX numerical model verification and validation is covered in Chapter 6 of this thesis.

The intermodel validation is covered in Chapter 7 of this thesis, which compares the simulation result of FHX numerical model and FHX analytical model. Six geographically-diverse locations are chosen for the parametric study; results of the two models are compared and differences between the results are investigated. Before proceeding to the material described above, Chapter 2 reviews the related literature. Conclusions and recommendations are presented in Chapter 8.

# CHAPTER 2

# LITERATURE REVIEW

This literature review describes previous work related to the modeling of foundation heat exchangers. The foundation heat exchanger, which is described in the thesis, is a new type of ground heat exchanger that utilizes the excavation often made for basements and foundation, in order to reduce the high cost of trench excavation. There are few models developed for the foundation heat exchangers. Braven and Nielson (1998) modeled a sub-slab heat exchanger that was placed besides the foundation footings using an analytical model of a ring source. Gao et al. (2008a) modeled ground heat exchangers embedded in foundation piles with a numerical solution. However, neither of the geometries is very close to the FHX proposed here. Horizontal ground heat exchangers (HGHX) are somewhat closer in geometry, but without the presence of a basement in close proximity to the heat exchanger tubing.

There are two types of approaches for solving the horizontal ground heat exchanger problem, including analytical solutions and numerical solutions. Analytical models based on superposition of line sources, including mirror image sources, have been used to model HGHX for many years. Likewise, numerical models based on finite volume or finite difference methods have also been developed. These models will be discussed in Sections 2.1 and 2.2. Experimental works for understanding the important factors which affect the system performance have been included in Section 2.3. Section 2.4 reviews foundation heat exchangers, though most of work that has been

done focuses heat exchangers integrated with piles; 2.5 reviews models for prediction of undisturbed ground temperature.

## 2.1 Analytical HGHX model

The analytical solution to horizontal ground heat exchangers is typically based on the line source solution or cylindrical source solution. The line source theory, which is first proposed by Kelvin(Philippe, et al. 2009), is most often applied. Ingersoll and Plass (1948) provides an elaboration of the Kelvin line source theory and treats the problem of obtaining the temperature field around a infinitely long line heat source or heat sink in an infinite soil domain(or other medium). The line source gives constant rate of emission $q$ to the soil. The soil is at an initial uniform temperature $T_0$ . When the line source is switched on at time $t = 0$ , the temperature at any point in the soil can be calculated by the equation:

$$T(r) - T_0 = \frac{q}{2\pi k_s} \int_x^\infty \frac{e^{-\beta^2}}{\beta} d\beta = \frac{q}{2\pi k_s} I(x) \tag{2-1}$$

$$x = \frac{r}{2\sqrt{\alpha_s t}} \tag{2-2}$$

Where:

$T(r)$ is the temperature in soil at any distance from the line source, in °C or °F;

$r$ is distance from the line source, in m or ft;

$T_0$ is the uniform initial soil temperature, in °C or °F;

$q$ is the heat transfer rate of the line source, in W/m or Btu/ft•hr;

$k_s$ is the soil thermal conductivity, in W/m•K or Btu/hr•ft•°F;

$\alpha_s$ is the soil thermal diffusivity, in $m^2/s$ or $ft^2/s$;

$t$ is the time since the start of operation, in seconds;

$\beta$ is the integration variable;

Equation 2-1 is exact only for a true line source, but it may be applied with negligible error, after a few hours of operation, to small (50 mm (2 inch) diameter or less) pipes. For larger pipes (100 - 200 mm (4 to 8 inch) diameter), and for periods less than few days, the solution has larger errors. However, the error can be calculated. The pipe has to be long enough so that the heat flow not perpendicular to the length of the pipe is negligible. In Equation 2-1, the integration of $\beta$ can be represented as a function of $x$. The values of $I(x)$ for various values of $x$ are provided by the Table 1 in the Ingersoll and Plass (1948) paper.

Ingersoll and Plass approach provides a simple treatment of the actual heat transfer process by solving a temperature field around a single pipe in infinite soil domain. It lays the ground work of more extensive system design methods that were developed later. However, it didn't consider some important real-life phenomenon such as multiple pipe configurations, semi-infinite medium, changing rate of heat transfer, and on-off cycling of the system.

Hart and Couvillion (1986) also evaluate Kelvin's line source theory and obtain a time-dependent temperature distribution around a line source of heat buried in homogeneous, infinite medium (*i.e.*, soil). The medium is at initial uniform temperature. The temperature distribution around a line source of heat is given by Equation 2-3, which is similar to the Ingersoll and Plass solution:

$$T(r) - T_0 = \frac{q}{4\pi k_s} \int_y^\infty \frac{e^{-s}}{s} ds \qquad (2\text{-}3)$$

$$y = \frac{r^2}{4\alpha_s t} \tag{2-4}$$

Where:

$T(r)$ is the soil temperature at any distance from the line source, in °C or °F;

$r$ is the radial distance from line source, in m or ft;

$T_0$ is the initial uniform soil temperature, in °C or °F;

$q$ is the heat transfer rate of the line source, in W/m or Btu/ft•hr;

$k_s$ is the soil thermal conductivity, in W/m•K or Btu/hr•ft•°F;

$\alpha_s$ is the soil thermal diffusivity, in $m^2/s$ or $ft^2/s$;

$t$ is the time since the line source is switched on, in seconds;

$\lambda$ is the integration variables;

From the integral table, the integral term in Equation 2-3 can be represented as a function of $y$, which is equal to $\left[ y - \ln y - \gamma - \frac{y^2}{2 \cdot 2!} + \frac{y^3}{3 \cdot 3!} + \cdots + \frac{(-1)^{N+1} y^N}{N \cdot N!} \right]$, where $\gamma$ is Euler's constant which is equals to 0.5772157. The value of $y$ can be calculated from Equation 2-4.

It is assumed that the heat rejected by the line source is absorbed by a cylinder around the line source with a radius of $r_\infty$. Theoretically, the correct value of the far field radius is $r_\infty = \infty$. For determining the temperature field around the line source, the far field radius is arbitrarily defined as:

$$r_\infty = 4\sqrt{\alpha_s t} \qquad (2\text{-}5)$$

Where:

$r_\infty$ is the far field radius, in m or ft;

$\alpha_s$ is the soil thermal diffusivity, in $m^2/s$ or $ft^2/s$;

$t$ is the time since the start of operation, in seconds;

Therefore, the value of $y$ can then be replaced with the value of $r_\infty$ and $r$, and the temperature distribution around the line source can be solved as:

$$T(r) - T_0 = \frac{q}{4\pi k_s}\left[\ln\frac{r_\infty}{r} - 0.9818 + \frac{4r^2}{2r_\infty^2} - \frac{1}{4\cdot 2!}\left(\frac{4r^2}{r_\infty^2}\right)^2 + \cdots + \frac{(-1)^{N+1}}{2N\cdot N!}\left(\frac{4r^2}{r_\infty^2}\right)^N\right] \qquad (2\text{-}6)$$

Where:

$T(r)$ is the soil temperature at any selected distance from the pipe centerline, in °C or °F;

$r$ is the radial distance from the pipe centerline, in m or ft;

$r_\infty$ is the far field radius, in m or ft;

$T_0$ is the initial uniform soil temperature, in °C or °F;

$q$ is the heat transfer rate imposed on the pipe centerline, in W/m or Btu/ft•hr;

$k_s$ is the soil thermal conductivity, in W/m•K or Btu/hr•ft•°F;

$t$ is the time since the start of operation, in seconds;

Equation 2-6 can calculate the temperature distribution around the line source at any distance, in conjunction with Equation 2-5. The soil temperature beyond the far field radius is assumed to be undisturbed and constant. According to Hart and Couvillion, Equation 2-6 is applicable for pipes when the value of $r_\infty$ obtained by Equation 2-5 is 15 times greater than $r_o$, the pipe outside radius. For case $r_\infty / r_o < 15$, the value of $r_\infty$ is calculated with another equation provided in the book. The multiple pipe configurations can be accounted for by superimposing the line source solutions (Hart and Couvillion 1986). In this situation, each pipe is represented as a line source, the temperature distribution around each pipe can be written as a line source solution (Equation 2-4). The resulting temperature distribution around a pipe is the summation of line source solutions.

For a vertical borehole, the ground in the radial distance may be considered infinite in extent. For the horizontal ground heat exchangers, though, the surface is relatively close and can not be treated as infinite. The temperature distributions around the pipes are affected by the earth surface as well. The heat transfer in a semi-infinite medium can be calculated by using the mirror-image method (or sink/source method) (Hart and Couvillion 1986). As shown in Figure 2.1, there is a HGHX tube at some depth *D* below the earth surface. There is a mirror heat sink lying on the same line drawn perpendicular to the earth's surface at a distance *D* above the earth surface. If the HGHX tube increases the earth temperature by adding a positive heat flow $q$, the heat sink decreases the earth temperature by imposing a negative heat flow of $q$ to the earth. Therefore, the earth temperature at the surface will stay constant at all the time. If the mirror heat sink is replaced with a mirror heat source, each time the HGHX tube is adding a positive heat flow to the earth, the heat source is adding a positive heat flow to the earth in the opposite direction, the earth surface will be adiabatic at all the time. In the FHX analytical model, the earth surface is treated as isothermal, but superimposed with the undisturbed earth temperature profile. The undisturbed earth temperature can be approximated as a function of depth and time of year (Hart

and Couvillion 1986). In the situation that the surface is insulated, the surface could be approximated as adiabatic surface.

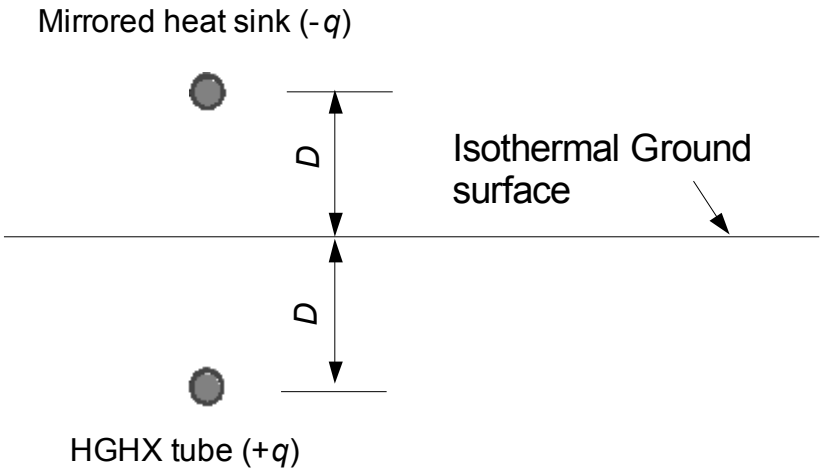


Figure 2.1: Mirror-image method

Hart and Couvillion (1986) provides comprehensive procedure for designing a more extensive ground heat exchanger. Based on the line source theory, it solves the heat transfer problem of multiple pipes buried in semi-infinite medium, and proves the possibility of applying the line source method to more complex modeling of heat exchangers.

Other than Kelvin's line source solution, some other analytical solutions have been derived to solve the temperature profile around a single or multiple line sources. Persson and Claesson (2005) calculate the temperature distribution of multiple pipes buried in a semi-infinite soil domain, by using the multipole method combined with the line source approach. Each pipe is treated as a line source, the center of the pipes are in Cartesian and complex coordinate. The analytical solution is expressed in a real part with an imaginary part; both of them satisfy the Laplace equation. The analytical solution becomes a line source plus the multipoles at the pipes. The line source represents the pipe's own influence on the surrounding temperature, while the

multipoles represent the other pipes' influence. The heat conduction problem is solved for steady state condition and for any arbitrary number of pipes.

Saastamoinen (2007)solves the unsteady and steady state temperature fields due to a single or several constant line sources in a slab or semi-infinite solid medium or ground, by using integral transform method. A floor heating system is simulated, as shown in Figure 2.2; multiple heating pipes are located in a conducting layer (slab), above the conducting layer there is a cover carpet, underneath the conducting layer is the insulation. A convective boundary at the cover carpet surface is applied, and a constant temperature condition is applied at the bottom of the insulation. The temperature distribution in the conducting layer after the pipe is switched on can be calculated. By eliminating the effect of bottom boundary and cover carpet, the heating floor system can be modified and turn into a heat conduction problem of multiple pipes buried in semi-infinite medium. The temperature field due to a single or several pipes in a semi-infinite solid medium or ground is solved.

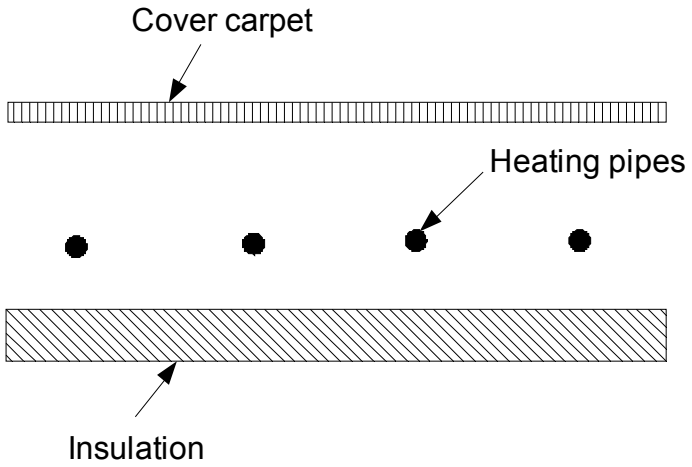


Figure 2.2: Floor heating system

## 2.2 Numerical HGHX model

Analytical solutions based on line source assumptions, are able to solve the heat conduction problem of multiple pipes buried in semi-infinite medium with constant heat extraction rate. And with superposition, they are able to solve problems with varying heat extraction rate. They are computationally efficient. However, they require approximations for non-infinite domains that may limit accuracy in practice. Compared with the analytical model, numerical models consume more computational time, but they are capable of calculating more realistically the performance of the system, by considering 1) soil freezing around the pipe in the winter operation, 2) soil dries out around the pipe in summer operation, 3) effect of moisture transportation, 4) snow cover and freezing on the earth surface. A number of horizontal ground heat exchanger models have been developed and are discussed below.

Metz (1983) developed a two-dimensional finite difference model to solve the underground heat flow of a buried tank. The soil domain is divided into up to 30 non-uniform rectangular cells. The tank is represented as a single cell, there are about 20 cells surround it. The temperatures of the 20 cells, once initialized, are solved at each time step by the finite difference heat conduction equations. Surrounding the 20 cells, there are about 10 cells which provide the far filed boundary conditions at all times. The far field soil temperature and initial soil temperature are estimated as a function of depth and time of year introduced in the paper. The size and shape of each cell is created based on the shape of the tank. The weekly average heat input into the tank is obtained from the experimental measurement and treated as an input for the model; the fluid temperature inside the tank is calculated and has been compared to the experimental data for four buried water tanks buried at depth range from 0.6-4 m (2-12 ft) and with an outer diameter range from 2.4-3.0 m (7.9-9.8 ft), in both winter and summer operation. Metz's model lays the ground of developing a numerical model for buried tanks or ground heat exchanger tubes; however, by representing the whole tank as one cell, the heat transfer between the tank and the soil is oversimplified.

Therefore, the comparison shows that the model, gives acceptable result when the heat input into the tank is small and with less satisfaction result when the heat is large. Furthermore, neither moisture transportation nor the freezing around the tank is considered in the model.

Mei (1985; 1986) developed a three dimensional explicit finite difference numerical model, for the case that a single pipe is buried under ground as shown in Figure 2.3. The soil is assumed to be homogeneous and the soil properties are constant. It is assumed that the earth surface is far enough from the center of the pipe; the distance between them is far field distance $r_{\infty}$ . The soil temperature beyond the far field boundary assumed undisturbed. The undisturbed soil temperature can be calculated from Kusuda and Achenbach (1965) model, which is a function of depth and time of the year.

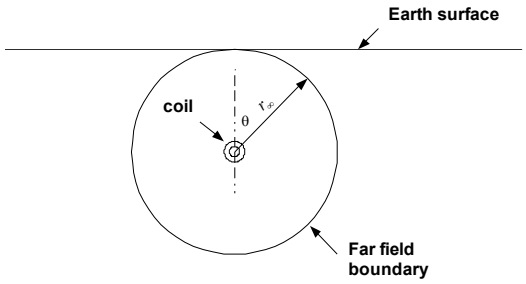


Figure 2.3: Schematic of ground coil

The temperature distribution within the far field boundary, can be solved with three heat conduction equations; the heat conduction equation in the soil, pipe wall and fluid. The unsteady state heat conduction equations are discretised in cylindrical coordinate, in $r$, $\theta$ and $z$. $z$ is the direction perpendicular to the intersection of the pipe. It is assumed that the soil and pipe wall temperature are constant along the length of the pipe, the fluid temperature changes along the length of the pipe. The fluid temperature is assumed to be uniform at any pipe cross-section. The initial temperature of soil, pipe wall and fluid are assumed to be known to the model, which either calculated from Kusuda and Achenbach model or obtained from experimental sites. The model

could also handle the off cycle period of the pipe, at when the fluid temperature is assumed to be equal to the pipe inner wall temperature. A follow up work is done (Mei 1986), and the effect of thermal backfilling material is included in the model. The single pipe model has been validated with measured data for a period of 44 days in winter operation, and for a period of 32 days in summer operation. The heat pump totally "on" time per day is provided by the experiment, the simulation was set up the run the same fraction of "on" time per hour. The simulated results of fluid outlet temperature and energy absorption from the ground have been compared to the experimental data. According to the validation result, the simulated daily average coil exiting fluid temperature (ExFT) is about 1°C (1.8 °F) higher than the experimental data, for most days in winter operation. For the summer operation, the simulation of coil ExFT matches quite well with the measured temperatures when the heat pump is on, but shows considerable derivations when heat pump is off. Mei found out that the during the heat pump is "off", the coil ExFT was measured inside the house and thus approach the room temperature, while the model is assuming the fluid temperature approaches the soil temperature. A parametric study is performed in the paper and found out the factors of soil thermal properties; pipe length and the pipe burial depth are important factors in determining the pipe performance.

A model (Mei and Emerson 1985; Mei 1986) for investigating the soil moisture freezing around a single pipe, during the winter operation, is developed. The soil domain around the single pipe is divided into two parts: frozen soil region non-frozen soil region. The schematic of frozen and non-frozen soil region is shown in Figure 2.4. The boundary temperature of the frozen and non-frozen soil region is defined as 0°C (32 °F). The latent heat change during the soil freezing is simulated in the frozen soil domain. Four heat conduction equations that describe the temperature distribution in the fluid, pipe, frozen soil region and unfrozen soil region are written. The model is validated with the experiment result for a period of 48 days in winter operation. The comparison of simulated and experimental results for exiting fluid temperature and total energy

absorbed from the ground is discussed. By investigating in the moisture freezing around the pipe in heating season, Mei and Emerson found out that unless the fluid inlet temperature is much lower than the soil freezing point, the effect soil freezing around the pipe is relatively minor.

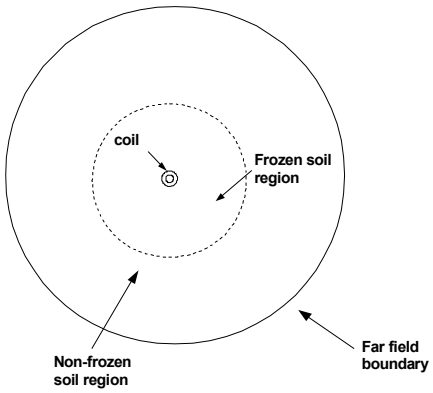


Figure 2.4: Schematic of the frozen and non-frozen soil region

Based on the single pipe model, a double pipe model has also been developed (Mei 1986; Mei 1988). The thermal interference between two pipes is investigated. The geometry of the double pipe is as shown in Figure 2.5; two horizontal ground pipes are buried in the same trench, one on top of the other. The same assumptions are made as in the single pipe model. The far field boundary is formed with the center located on lower pipe and the depth of the lower pipe as the radius. The heat conduction equation and boundary conditions of the each pipe is written exactly the same as in the single pipe model. The two pipe model is validated with the experimental results for a period of 28 days. Properties of pipe, soil and fluid are known as input for the model; the difference of measured and simulated daily energy absorbed from the ground indicated a maximum error of 27 percent, with the average error at less than 12 percent. Mei concludes from the two pipe model that there is a clear effect of thermal interference between two pipes that deteriorates each pipe's performance.

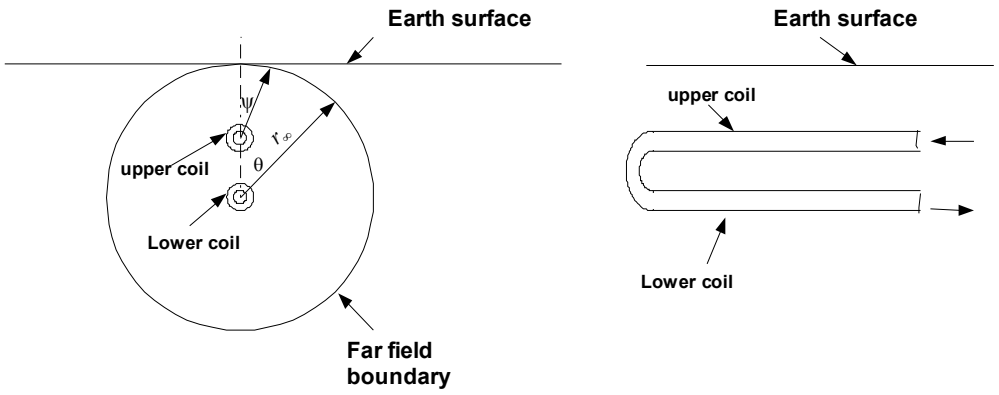


Figure 2.5: Schematic of two-pipe arrangement

Mei studies the freezing of moisture in the soil around a single pipe; however, when more than one pipe are buried under the ground, the frozen soil region around each pipe might sometimes merge into each other, thus, thus the method used for single pipe might be very complex or not computational efficient for solving the soil freezing around multiple pipes. Plus, the meshes derived in cylindrical coordinate are not very flexible to be applied to multiple pipes buried under the ground.

Piechowski (1996; 1999) developed a quasi-3D finite difference model for horizontal ground heat exchangers. The model can calculate the heat conduction problem of multiple pipes, but it is assumed that the distance between loops are big enough so that the thermal interference between pipes is not considered. It considers the moisture transport in the soil; soil freezing around the pipe is not included. There are some simplifying assumptions made in the model:

- The soil is homogeneous and soil properties are constant in all directions.
- The heat transfer in the soil is assumed to be axial-symmetric.
- The heat transfer in the soil is negligible in the direction along the length of the pipe.

- The fluid temperature and velocity at any cross section of the pipe are assumed to be uniform.

- For mass transfer equation in the soil, the influence of gravity on the soil moisture transfer in the unsaturated soil is assumed to be negligible.

The horizontal ground heat exchanger is sliced in the direction perpendicular to the pipe. For each slice, the circulating fluid temperature, and the corresponding soil temperature and moisture distribution can be calculated, by solving three equations; one is related to the energy balance of the circulating fluid, the two other equations describe transient, simultaneous heat and mass transfer in the soil region. For the equation calculating the circulating fluid temperature, it is assumed that the thermal capacity of the pipe material is sufficiently low compared with that of the circulating fluid and the soil, so that the heat diffusion equation for the pipe wall is neglected, and the pipe wall is represented by the overall heat transfer coefficient. A 2D grid is generated based on Cartesian coordinate, as shown in Figure 2.6; a secondary coordinate (cylindrical coordinate) is used surrounding the pipe, so that the soil temperature and moisture distribution in the vicinity of the pipe can be solved by heat and mass equations in cylindrical coordinates. The temperature at the outermost radius of the cylindrical around the pipe equals to the node temperature; in this way, it "stitches" the radial region together with the rectangular grid. The soil domain is bounded by a convective boundary on the top surface and three other far field boundaries on the two sides and the bottom. The typical mesh size used for the model is 0.3 m if a secondary coordinate around the pipe is used, instead, if only Cartesian coordinate is used in the model, the mesh size should be 0.05 m in order to assure the accuracy of the model. The concept of using a radial region around the pipe can achieve the same accuracy but with much coarser grid. The soil temperatures on the far field boundaries and initial soil temperature can be calculated with Kusuda and Achenbach correlation (1965). The initial fluid temperature is equal to the undisturbed soil temperature at the depth of the pipe. The cyclic operation of the system is

considered in the model, the initial fluid temperature and soil moisture content for the next ON cycle is assumed to be equal to the soil temperature on the pipe outside wall and soil moisture content after the previous OFF period of the system. The model is validated with experimental data collected from two horizontal ground heat exchangers installed at the University of Melbourne(Piechowski 1998). The case with the single pipes and two pipes with one on top of the other are both tested. Validation of the model was performed for the cooling mode operation of the system, but less than a 24 hour period.

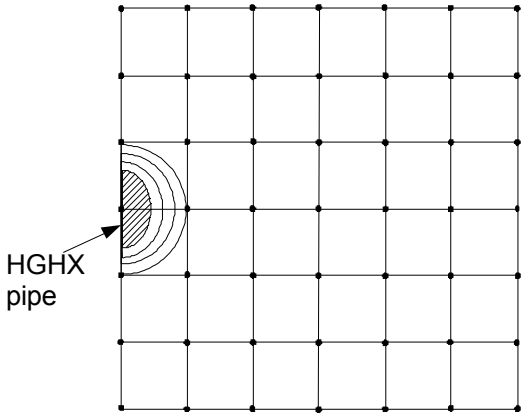


Figure 2.6: Schematic of the grid

Piechowski's model used a new approach which results in better accuracy and at the same time a reduced computational time, by concentrating the computational effort near the largest temperature and moisture gradients; for example, near the pipe-soil interface. Piechowski also found out for calculating the horizontal ground heat exchanger thermal performance, a proper estimation of the soil type and its initial moisture content is more important than the moisture transfer calculation capability of the model.

Esen et al. (2007a) developed a two dimensional finite difference model for horizontal ground heat exchangers. It is based on the same assumptions described above for Piechowski's model. Multiple pipes can be included in the model; however, it is assumed that the distance between

loops is big enough to avoid thermal interference between the pipes. The temperature of the soil and pipe wall does not change in the direction parallel to the pipe. The two-dimensional heat conduction equations in the soil and pipe-soil surface are written and discretised in Cartesian coordinate. The soil domain is bounded by a convective earth surface, a bottom boundary at deep depth and two adiabatic boundaries on the sides. The pipe is represented as a square pipe and located on the left boundary of the soil domain; eight cell centers are located on the pipe outside wall. 20 x 164 Uniform grids are used in the simulation and with a grid size of 0.008 x 0.008 m (0.31 x 0.31 inch). The initial soil temperature at all depth is assumed to the same and equals to the undisturbed soil temperature at a deep depth. The fluid temperature entering the ground heat exchanger is known as an input for the numerical model, the disturbed ground temperatures calculated from the model, at different fluid flow rates, are less than 1°C (1.8 °F) differences from the experimental results for a period of eight hours. The depth of the ground temperature used for the validation is not provided.

Demir et al. (2009) developed a two dimensional implicit finite difference model to solve the heat transfer problem of multiple HGHXs buried under ground. Neither of moisture transportation nor soil freezing is considered in the model. However, the effect of snow cover and precipitation are included in the model. The model assumes that for multiple pipes, all the pipes are at the same depth and the thermal interference between pipes are ignored, so that the soil domain becomes as shown in Figure 2.7. The left and right side boundary of the soil domain are assumed to be adiabatic. The model utilized a full heat balance on the top surface which includes the solar radiation, long wave radiation, convection heat transfer, conduction heat transfer through the earth surface (snow surface), heat transfer through evaporation on the soil surface (sublimation of snow), the heat transfer through the precipitation. The heat flux due to precipitation can be calculated by multiple the precipitation rates, the heat capacity of water and the difference of air and earth surface temperature. Uniform grid is used with a size of 0.1 x 0.1 m (3.9 x 3.9 inch). It

is assumed that the soil and pipe wall temperature does not change along the pipe axial. The temperature distribution of the fluid along the pipe can be calculated by applying conservation of energy in the fluid, the heat stored in the fluid equals to the heat conducted from the pipe wall. The calculated HGHX exiting fluid temperature (ExFT) and disturbed soil temperature near the ground heat exchanger are validated with experiment data for a period of 37 days in winter operation. The calculated HGHX ExFT from the model is less than 1.0 °C (1.8 °F) difference from the experimental result. Even though the snow cover and precipitation are included in the model, there is no clear evidence that the model is tested under the two surface conditions.

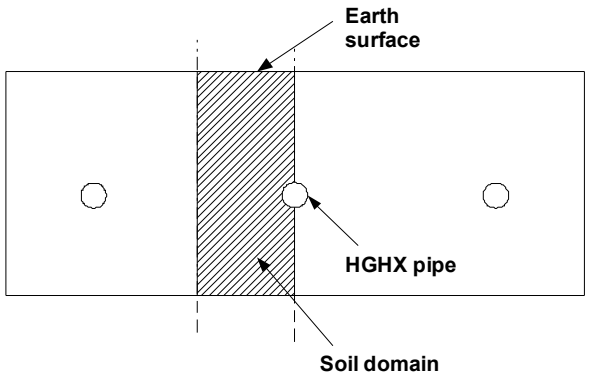


Figure 2.7: Demir's model soil domain plot

Tarnawski and Leong (1993)developed a two-dimensional finite element model for the horizontal ground heat exchangers. It considers the moisture transport in the soil and the freezing/thawing of the moisture in the soil. Complicated heat and mass transfer at the earth surface is considered, such as solar radiation, convection, evaporation, evapotranspiration, sublimation and condensation, the rainfall and snow cover. The longitude mean fluid temperature of the ground heat exchangers can be solved iteratively with simultaneous two-dimensional heat and moisture transfer in the ground discretised into triangular element, incorporated with a steady state heat pump model, once the heating and cooling loads of the house are known. The model results of HGHX ExFT and disturbed soil temperatures around the pipe are compared to the experimental

results for a time period of one year, starts on 1 September, 1988. However, there are few differences between the experiment and the conditions used in the model, for example, the experiment and model use weather data from different year, the experiment tested the spiral coil while straight pipe is simulated in the model, etc. Overall, the model is not well validated. Tarnawski and Leong model considers the water migration, snow cover on the surface, soil freezing, which will increase the accuracy of the model, but the complicated heat and mass transfer on the earth surface may also requires complex calculations, therefore, the model is not computational efficient.

From the previous studies on the HGHX numerical model, it can be concluded that soil properties, pipe depth and length are important factors that affect the performance of the pipes and need to be considered in the model. The detailed moisture movement calculation does not need to be included in the model, considering the computational time it takes and accuracy it gains. Instead, an initial guess of the soil type and its moisture content would be more beneficial in order to increase the accuracy of the model. Soil freezing and snow cover on the earth surface might be important factors which impact the performance of the heat exchangers, needs further investigation.

### 2.3 Experimental Research on Horizontal Ground Heat Exchangers

The experiment research on the HGHX pipes mostly evaluate the performance of the ground source heat pump(GSHP) systems with HGHX pipes and compare them with conventional heating and cooling systems. Some others investigated the effect of different factors on the performance of the HGHX pipes, such as the soil thermal properties, pipe burial depth.

A experiment work done in Turkey (Esen, et al. 2006), the GSHP system with HGHX pipes is compared to six conventional heating methods (electric resistance, fuel soil, liquid petrol gas, coal, and natural gas by using an economical analysis. The result shows that GSHP system with

HGHX pipes are more economical than first five conventional heating methods mentioned above, except for the natural gas. A techno-economic comparison between the GSHP system with HGHX pipes and an air-coupled heat pump (ACHP) system is presented(Esen, et al. 2007b), and the experimental result shows that GSHP systems are economically preferable to ACHP systems for the purpose of space cooling. The performance of horizontal ground heat exchangers used for the air preheating and cooling of the building in Germany is evaluated (Eicker and Vorschulze 2009), and it suggests a possibility for installing ground heat exchangers for office building cooling purpose. A GSHP system with HGHX pipes are installed in a secondary school in Canada (Minea 2006), it proves that GSHP systems are competitive to the conventional heating systems, in a cold climate, by improving the overall energy performance and lowering the initial capital cost. The GSHP system with HGHX pipes was operated and tested in the southern Marmara of Turkey (Pulat, et al. 2009)and it find out the GSHP systems are economic than the all other heating systems such as natural gas, coal, fuel oil, electric resistance, and liquid petrol gas by a economic comparison. It also concludes that the COP values may be improved by adjusting the distance between the pipes and the mass flow rate of the fluid.

Inalli and Esen (2004) tested the performance of HGHX pipes connected to a room with 16.24 $m^2$ (174.8 $ft^2$) floor area in Turkey. The experimental results were obtained from November to April in heating season. The effect of the pipe buried depth and fluid mass flow rate on the performance of the HGHX pipes are validated. The experimental result shows that the average performance coefficients of the system (COP) for HGHX pipes in different trenches, at 1 m (39.4") and 2 m (78.8 ") depth, were 2.66 and 2.81, respectively. It is also concluded from the experiment result that the increasing of the mass flow rate of fluid will lead to a decrease in the system COP. Bose and Smith (1992) studies the performance of a GSHP system with different pipe configurations; slinky coil, extended slinky coil, four pipe, horizontal U-bend pipe, the experiment is carried on

in Stillwater, US. It turns out that horizontal U-bend system has the highest performance rating value.

## 2.4 Foundation Heat Exchanger

The foundation heat exchangers are GHE pipes buried in the excavations made for the basement or footing of the building when the house is built, in order to reduce the initial boring cost or trenching fee. There are various types of foundation heat exchangers; sub-slab heat exchangers as shown in Figure 2.8 (a), vertical pile-foundation heat exchanger as shown in Figure 2.8 (b) and the FHX buried in the excavation made for the foundation wall as shown in Figures 1.1 and 1.2. The sub-slab heat exchangers are buried under the floor area when the house is first built. The vertical pile-foundation heat exchangers are GHE pipes put into the foundation piles of buildings. The foundation heat exchangers which are buried in the excavation made for the foundation wall is the topic of interest in the thesis. Most research works done in the field of foundation heat exchangers, including analytical/numerical models and experimental work, are about the sub-slab heat exchanger or vertical pile-foundation heat exchanger.

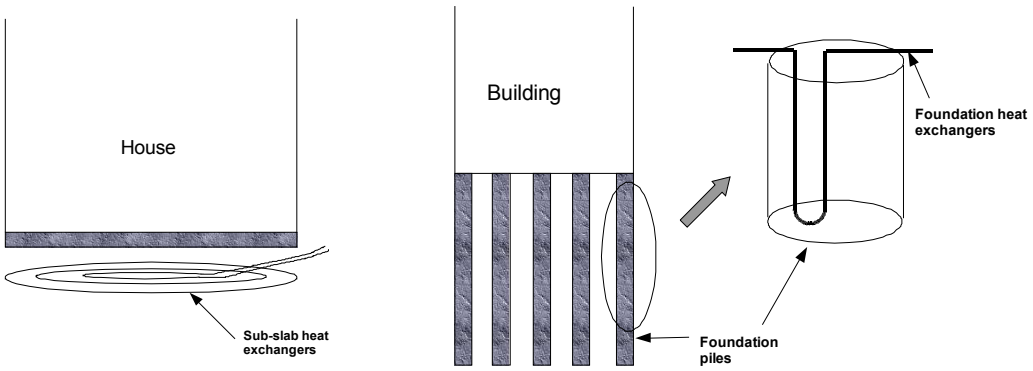


(a) sub-slab heat exchangers b) Vertical pipe-heat exchangers

Figure 2.8: Schematic of different foundation heat exchangers

Braven and Nielson (1998) developed an analytical model for sub-slab ground heat exchanger, based on the line source solution. The heat exchangers are buried under well insulated slab floor, which is close to the geometry of the foundation heat exchanger buried besides the foundation wall. The piping is laid out in a shape of spiral configuration and simplified as ring source in the model, as shown in Figure 2.9. The temperature change around a instantaneous ring source is solved by Carslaw and Jaeger (1959), based on the Kelvin's line source theory. The temperature change in the soil at a time due to heat extraction or rejection from a continuous ring source is the integration of instantaneous solution over time. The changing of heat transfer rate of the pipe can be accounted for by breaking the integral into time steps. The thermal interference between rings can be included by superposition. The adiabatic building floor and semi-infinite medium can be modeled by using the mirror image method. At any time, the temperature distribution around the ring source, buried under an insulated building floor, can then be calculated, by superimposing the temperature change at any distance to the undisturbed soil temperature file. The undisturbed soil temperature is estimated by a equation (Bose, et al. 1985), which is function of depth and time of year. The soil temperature at the wall of the ring source is calculated and assumed to be constant around the perimeter of each ring. For each ring, the outlet fluid temperature of the ring can be calculated with the NTU method, assuming the heat stored in the fluid equals to the heat transfer from the soil to the fluid.

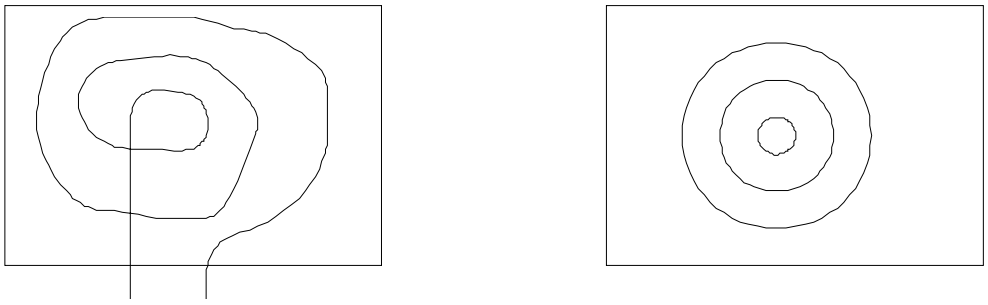

Figure 2.9: (a) spiral pipe configuration (b) ring source approximation

Few others work on the analytical solutions and experimental test for vertical pipe-foundation heat exchanger. In 1994, Morino and Oka (1994) carried out an experiment on heat exchanges in soil by circulating water in a single steel foundation pile. The quantity of heat transfer with the soil and variations of the water temperatures in the pile were investigated. A three-dimensional finite difference model was developed to compare with the experiment result. Laloui et al. (2006) studies the increased thermo-mechanical loads on the pile due to the thermal effects, based on experimental result and a finite element model developed. A ground-source heat pump system using the pile-foundation heat exchangers has been applied to a building in Shanghai (Gao, et al. 2008a; Gao, et al. 2008b). Four types of FHX pipes are investigated in the experiment; W-shape type, single U-shaped type, double U-shaped type and triple U-shaped type. The effect of pile type, fluid flow rate and inlet temperature on the system performance is evaluated and discussed. A three dimensional numerical model of a single foundation pile is developed to validate the experimental result. katsura et al.(2008; 2009) propose an analytical solutions for calculating the heat transfer of multiple energy piles in the soil by superimposing line source solutions. The result of the analytical solution is validated with experiment result.

## 2.5 Models for Undisturbed Ground Temperature

Earth temperature is one of the most important parameters affecting the heat transfer of the ground heat exchangers. The measurement of ground temperature profile is not easy and practical; therefore, modeling can be a useful tool for calculating diurnal and annual variations of the soil temperature at different depths. Modeling approach including: analytical model and numerical model.

### 2.5.1 Analytical Model

The analytical models developed mostly use a simple exponential-sinusoidal equation to predict the soil temperature at various depth and different time of the year. The equation is derived based

on a simple heat conduction theory, which assumes that earth is a homogeneous, heat conduction medium with constant soil thermal diffusivity in all directions, furthermore, the temperature of the surface exposed to the atmosphere varies periodically with time.

Using the heat conduction theory to solve the heat transfer in the soil has been discussed in various texts of heat transfer(Carslaw and Jaeger 1959; Eckert and Drake 1959; Van Wijk and de Vries 1966), since 1960s. Both the diurnal and annual soil temperature variations are accounted in the solutions.

Kusuda and Achenbach (1965) apply the equation, which was proposed by Carslaw and Jaeger(1959), Eckert and Drake(1959), to estimate the monthly average soil temperature at various depth $y$ and time $t$ of the year, with only the annual soil temperature variation accounted:

$$T(y,t) = T_{avg} - e^{-\sqrt{\frac{\pi}{\alpha_s t_p}}y} SA\cos\left(\frac{2\pi}{t_p}t - pl - \sqrt{\frac{\pi}{\alpha_s t_p}}y\right) \qquad (2\text{-}7)$$

Where:

$T(y,t)$ is the monthly average undisturbed soil temperature at the depth of $y$ and time $t$ of the year , in °C or °F;

$y$ is the soil depth, in m or ft;

$t$ the time of year, starting from January 1st, in hr;

$t_p$ is the period of soil temperature cycle (8766 hr), in hr;

$\alpha_s$ is the soil diffusivity, in $m^2/s$ or $ft^2/s$;

$T_{avg}$ is the annual average soil temperature of different depth and time, in °C or °F;

$SA$ is the surface amplitude, which can be assume to be half of the difference between the maximum and minimum monthly average temperatures in a year, in °C or °F;

$pl$ is the phase angle of the annual soil temperature cycle, in radians;

There are four parameter values that are needed to calculate the monthly average soil temperature from Equation 2-7; soil thermal diffusivity, surface amplitude, phase angle and annual soil temperature. The soil thermal diffusivity can be calculated from the observed data by using the amplitude and phase angle techniques introduced by the author. The other three parameters can be estimated by least-square fitting of measured soil temperature to Equation 2-7. There are measured soil temperature data for 63 stations located in 50 states in United States, compiled by Kusuda and Achenbach, based on some existing soil temperature data. Earlier research done by (Carslaw and Jaeger 1959; Eckert and Drake 1959; Van Wijk and de Vries 1966) provides equations to predict the soil temperature at different depths. Kusuda and Achenbach develops the procedure of applying the analytical model to predict the real site soil temperature, that is, estimating the four parameters needed in Equation 2-7 from experimental data, and then calculate the soil temperature with the four parameters and Equation 2-7. However, Kusuda and Achenbach's model does not consider the diurnal variation of soil temperature.

Moustafa et al. (1981)applied an analytical model similar to Equation 2-7, which only account for the annual soil temperature variation, to estimate the soil temperature in Kuwait. The annual soil temperature, surface amplitude and phase angle of the earth temperature cycle, which are parameters required as inputs for the analytical model, are estimated from experiment data collected from Kuwait Institute for Scientific Research Solar Energy site. The calculated soil temperatures at varies depths from the analytical model are then compared with the experimental data for an entire year in 1978.

Elias et al.(2004) gave a detailed description of Van Wijk and de Vries's (1966) model. Van Wijk and de Vries's model is also exponential-sinusoidal equation and but with extra term to account for diurnal soil temperature variations, compared with Equation 2-7. The daily surface amplitude in the equation is assumed to be constant. However, Elias et al. add more complexity to Van Wijk and de Vries's model by treating the daily amplitude as a sinusoidal function of time. The two models are compared and it is concluded that it is better to describe the daily amplitude by a sinusoidal function of time.

Droulia et al. (2009) develop an analytical model which implements the superposition of annual and daily sinusoidal fluctuations. The equation implemented in the model is similar to Equation 2-7 but with three more exponential-sinusoidal terms added, to accounts for the diurnal soil temperature variations. The calculated soil temperatures at the depth of 2 and 30 cm (0.8" and 11.8") are compared with experiment data for the period of one year.

### 2.5.2 Numerical Model

Analytical solutions, assuming a constant thermal diffusivity and a sinusoidal temperature fluctuation at the soil surface, are always applied to calculate soil temperature. However, those solutions lead to some inaccuracy in the simulation result because of non-uniform thermal diffusivity and non-sinusoidal soil surface temperature in realistic. Therefore, some numerical models are developed to study the sensitivity of soil temperature calculation to the assumption of constant thermal diffusivity. Some other models implement an energy balance in the earth surface, which includes the short wave solar radiation, long wave solar radiation, convection heat transfer or others, to calculate the surface temperature instead of representing the soil surface temperature as a sinusoidal function.

Hanks et al. (1971) developed a finite difference model based on the unsteady state, one dimensional heat conduction equation, in which the soil temperature is described as a function of

depth $y$ and time $t$. The finite difference approximation of the heat conduction equation allows for variation of soil thermal diffusivity over depth, at each depth the thermal diffusivity is assumed to be constant over time. The measured soil temperature at 1 cm (0.4") is used as the upper boundary conditions for the soil column, and is updated every time step. The bottom boundary condition is treated as adiabatic, at a depth which no heat flow occurred. The initial temperature was actual data measured as a function of depth. The computed and measured soil temperatures for a period of 24 hours at depth of 6 and 16 cm (2.4" and 6.3") agreed within 1.0 °C (1.8 °F) when actual soil thermal properties are used for the simulation. The differences between the simulated and measured data will increase to when assuming the soil thermal diffusivity is constant over depth and time. However, it is concluded in the paper that a reasonably accurate estimation of soil temperature can be made by assuming a reasonable value for the constant thermal diffusivity.

Sikora et al. (1990) developed a one-dimensional finite difference model to calculate the hourly soil temperature at various depth, based on Hanks et al.'s (1971) model. Measured soil temperatures at 1 and 30 cm (0.4" and 11.8") depths provide the upper and lower boundary conditions for the simulated soil domain. The soil thermal diffusivity varies at different depths. At each depth; the thermal diffusivity is constant over time. The predicted soil temperatures are validated against the experimental results at three depths and a period of 20 hours. A sensitivity study is performed by comparing the simulated soil temperature, with varying or constant thermal diffusivity, to the measured soil temperature. It is found out that the assumption of constant thermal diffusivity in all depth in the model is reasonable for hourly soil temperature predictions.

Herb et al. (2008) developed an implicit finite difference model based on 1-D unsteady state heat diffusion equation to calculate hourly soil temperature to a depth of 10 m (393.7 ft). The model includes two layers in the simulation soil domain, layer near surface with smaller cells and layer towards the lower boundary of the soil column with larger cells. The soil thermal properties vary

in different cells. The heat transfer due to moisture movement is not accounted in the model. A full energy balance is applied on the upper boundary of the soil column and an adiabatic condition is applied on the lower boundary. The vertical heat transfer at the soil surface includes long wave radiation, short wave radiation, evaporation and convection in dry weather. Under wet weather conditions, the heat fluxes due to precipitation and surface water runoff are added. The soil temperature at the earth surface is calculated by the heat balance equation on the surface, using recorded weather data as model input. The simulation of soil temperature has been made for eight different ground covers (asphalt, concrete, bare soil, lawn, tall grass prairie, corn and soy bean crops and forest). The different ground covers require changes in the soil thermal diffusivity, solar radiation absorptivity, and other parameter values. The parameter values for different ground cover are obtained by minimizing the root-mean-square-error (RMSE) of the simulated and measured soil temperature values. Herb et al.'s (2008) model implements a realistic energy balance at the ground surface to calculate the non- sinusoidal soil temperature at earth surface instead of using measured soil temperatures, as Hanks et al. (1971) and Sikora et al. (1990) did.

# CHAPTER 3

## ONE DIMENSIONAL GROUND HEAT TRANSFER MODEL

The interaction of buildings and ground source heat pump systems with the surrounding ground is quite important for design and energy calculation procedures. Analyses of building foundation heat transfer and ground heat exchangers often require as inputs the undisturbed ground temperature as a function of depth and time of year. There are at least three specific applications:

1. Foundation heat transfer – e.g. heat loss from basements, crawlspaces, and slabs-on-grade.
2. Horizontal ground heat exchangers and foundation heat exchangers – here the surface effects are very important.
3. Vertical ground heat exchangers.

Kusuda and Achenbach (1965) provides a simple analytical model for calculating the undisturbed soil temperature. The analytical model uses an exponential- sinusoidal equation to predict the undisturbed soil temperature at various depth and time of year. The foundation heat exchanger analytical model discussed in Chapter 5 of the thesis calculates the undisturbed soil temperature with the Kusuda and Achenbach model. The FHX numerical model generally depends on the Kusuda and Achenbach to set the initial temperature profile in the ground and, in some cases, to set the lower boundary conditions. However, the result of the equation depends on having the Kusuda and Achenbach parameters: annual average soil temperature, surface temperature.

amplitude and phase delay. Yet, the value of the three parameters are, at best, sketchily available from a couple figures in the ASHRAE Handbook series, and the phase delay parameter is not available

In order that the design and simulation tools be maximally usable and for estimating the undisturbed ground temperature with Kusuda and Achenbach model, a simple one-dimensional ground heat transfer model has been developed for estimating the three parameters. The One-dimensional numerical model utilizes a full surface heat balance coupled with TMY3 (Typical Meteorological Year 3) weather files (or other equivalent weather files) to calculate the undisturbed ground temperature; the simulation result will be tuned with the Kusuda and Achenbach model for calculating the parameters. For testing purposes, simulation is run for 20 years until well beyond when it reaches a steady periodic response, and then output a soil profile which is independent of initialization. Initial testing for independency shows that 6 years may be sufficient, even with a relatively poor guess of the parameters.

The TMY3 weather data files used are provided by National Solar Radiation Data Base; there are now files for over 1000 locations within the United State. For international locations, 227 IWEC (International Weather for Energy Calculations) files for locations outside the U.S. and Canada have been release by ASHRAE. ASHRAE will soon release IWEC2 files for over 2500 locations worldwide. The availability of the weather data files provides a possibility of estimating undisturbed ground temperatures based on the 1D model.

## 3.1 1D Numerical Model

The one-dimensional numerical model is explicit finite volume model, using non-uniform grid. The way of generating the non-uniform grid and deriving the finite volume equation for the 1D numerical model, is identical to what has been used in the two-dimensional foundation heat exchanger numerical model, which will be introduced in Section 4.1 and 4.2.

The simulation of 1D numerical model utilizes a full surface heat balance and a typical value of the geothermal gradient is used as the lower boundary condition. The geothermal gradient is the rate that ground temperature increases with depth; it indicates the heat flux from the earth hot interior to its outside surface. The freezing/melting of moisture in the soil is also considered.

### 3.1.1 Surface Heat Balance

The simulation implements a full heat balance at the earth surface, which includes long wave radiation, short wave radiation, heat conduction, convective heat transfer, and the effect of evapotranspiration. The final form of the heat balance equation for the upper surface boundary becomes:

$$R_{ns} - R_{nl} + k_s \frac{\partial T_s}{\partial y} + h_c\left(T_a - T_s\right) + \rho_w L_w ET = 0 \qquad (3\text{-}1)$$

Where:

$R_{ns}$ is the solar radiation absorbed by the surface, in W/m$^2$ or Btu/ ft$^2$•hr;

$R_{nl}$ is the net long wave radiation leaving the earth surface, in W/m$^2$ or Btu/ ft$^2$•hr;

$k_s$ is the soil thermal conductivity, in W/m•K or Btu/ft•°F•hr;

$T_s$ is the soil temperature at the earth surface, in °C or °F;

$h_c$ is the convection coeficient, in W/m$^2$•K or Btu/ft$^2$•°F•hr;

$T_a$ is the air temperature, in °C or °F;

$\rho_w$ is the density of the water, in kg/m$^3$ or lb/ft$^3$;

$L_w$ is the heat released when water vaporizes, in J/kg or Btu/lb;

$ET$ is the loss of water through evapotranspiration, in m/s or ft/s;

The short wave radiation absorbed by the earth surface $R_{ns}$ is determined by multiplying the incident short wave radiation on a horizontal surface and the absorptivity of the surface. The incident short wave radiation can be read from the TMY3 weather file. An absorptivity of 0.77 is chosen for grass cover, based on the recommendation of Walter et al. (2005). The net long wave radiation $R_{nl}$ is calculated based on the procedure recommended by Walter et al. (2005), which utilizes an effective sky emissivity, based on humidity and cloudiness. The convection heat transfer term $h_c(T_a - T_s)$ is estimated with the approach described by Antonopoulos (2006). This approach gives the convection coefficient as linearly proportional to the wind speed, as shown in Equation 3-2. The term $\rho_w L_w ET$ represents the heat loss through "evapotranspiration" at the earth's surface. Evapotranspiration (*ET*) is a term which describes the loss of water from the earth's surface through evaporation and plant transpiration. The transpiration represents the movement of water within a plant and subsequent loss of water from the plant surface through evaporation. Overall, the evapotranspiration is the loss of water through the evaporation of soil and plant surfaces. When water evaporates at the soil and plant surfaces, the earth's surface temperature will decrease as there is a large amount of latent heat absorbed by the water through the phase change process. Therefore, the heat loss through the evapotranspiration can be calculated by multiplying the *ET* rate (loss of water) by density of water $\rho_w$ and the latent heat of evaporation $L_w$; the latent heat of evaporation is calculated from (Allen, et al. 1998), as a function of air temperature. The evapotranspiration model (Walter, et al. 2005) gives the evapotranspiration rate in mm/hr as a function of the type of vegetation. For results presented here, a 12 cm (4.7 inch) clipped or cool-season grass surface has been used. Inclusion of

evapotranspiration has a significant impact in the prediction of the ground temperature. The term $k_s \frac{\partial T_s}{\partial y}$ is the conduction heat transfer from the surrounding cells. The convection coefficient $h_c$ used in Equation 3-1 can be calculated as (Antonopoulos 2006);

$$h_c = \frac{\rho_a c_{pa}}{208} u_{wind} \tag{3-2}$$

Where:

$h_c$ is the convection coefficient, in W/m$^2$•K or Btu/ft$^2$•°F•hr;

$\rho_a$ is the density of the air, in kg/m$^3$ or lb/ft$^3$;

$c_{pa}$ is the specific heat of the air, in J/kg-K or Btu/lb•°F;

$u_{wind}$ is the wind velocity, in m/s or ft/s;

The density and specific heat of the air in Equation 3-2 are both functions of air temperature; however, the changes have small effect on the value of $h_c$. Therefore, constant values of 1.205 kg/m$^3$ (0.08 lb/ft$^3$) and 1005 J/kg•K (0.24 Btu/lb•°F) are chosen. Equation 3-2 is only valid for grass reference surface, the value of 208, which is related to aerodynamic resistance of air, can be recalculated for different surface covers(Allen, et al. 1998).

The net long wave radiation, $R_{nl}$, is the difference between the long wave radiation emitted from the earth's surface to the sky and the long wave radiation from the sky absorbed by the surface. Usually, the long wave radiation from the earth's surface and the sky can be calculated based on Stefan-Boltzmann law, which calculates the radiation from an object (sky or earth) by multiplying $\sigma$ the Stefan-Boltzmann constant, to the effective emissivity $\varepsilon$ of the object and to the

temperature of the object to the power of four $T^4$, which becomes $\sigma\varepsilon T^4$. However, this method requires the sky temperature and the earth's surface temperature, the emissivity which are hardly known and need to be calculated or estimated. Walter et al. (2005) recommended the following equation for calculating hourly $R_{nl}$, which uses the cloudiness and air humidity to calculate the effective emissivity, only measured air temperature is needed for the calculation. The equation is valid only for SI units:

$$R_{nl} = \sigma T_a^{\,4}(0.34 - 0.14\sqrt{e_a})(1.35\frac{R_s}{R_{scs}} - 0.35) \qquad (3\text{-}3)$$

Where:

$R_{nl}$ is net long wave radiation, in MJ/m$^2$•hr;

$\sigma$ is Stefan-Boltzmann constant, $2.042 \times 10^{-10}$ MJ/ K$^4$•m$^2$•hr;

$T_a$ is mean hourly air temperature, in K;

$e_a$ is actual air vapor pressure, in KPa;

$R_s$ is measured incident short wave radiation on a horizontal surface, in MJ/hr;

$R_{scs}$ is the calculated clear sky short wave solar radiation, in MJ/m$^2$•hr;

Equation 3-3 is similar to $\sigma\varepsilon T^4$ which is used according to Stefan-Boltzmann law. However, the term $\sigma T_a^{\,4}$ is used in Equation 3-3 which assumes no sky temperature and earth's surface temperature is known for the calculation. The air humidity and cloudiness is used for calculating the effective emissivity $\varepsilon$. The term $(0.34 - 0.14\sqrt{e_a})$ represents the effect of air humidity, it

decreases when the air humidity increases. The term $(1.35\frac{R_s}{R_{scs}} - 0.35)$ expresses the effect of the cloudiness. When the cloudiness increases, there are more clouds in the sky, therefore, $R_s$ decreases, and the value of the term decreases. The term is always in the range $0.05 \le 1.35\frac{R_s}{R_{scs}} - 0.35 \le 1.0$. During the period of sunset and night time, the $R_s$ goes to 0, the value of $(1.35\frac{R_s}{R_{scs}} - 0.35)$ equals to the last hour before sunset and is kept the same until sun rises the next day. The value of $R_{scs}$ is the amount of solar radiation that would be received at the earth's surface under conditions of clear sky (no cloud), it can be calculated based on the solar radiation emitted at the sun surface, the distance between the earth and the sun, and the longitude, latitude, attitude of the earth, and the solar angle at different time of the year (Walter, et al. 2005).

The water loss from the earth surface through the evapotranspiration $ET$, is calculated by a model (Walter, et al. 2005) developed based on Penman-Monteith method. The Penman-Monteith method provides the way of calculating water evaporation from vegetated surfaces. In 1948, Penman (1948) combined the energy balance with the mass transfer equation at the earth surface and derived an equation which calculates the evaporation on an open water surface with recorded climate data, including the air temperature, humidity, wind speed, incident short wave radiation on a horizontal surface. Various derivations of the Penman-Monteith equation have been made during the past 60 years, Howell and Evett(2004) reviews the history of the development of the Penman-Monteith method. In 1999, the Task Committee on Standardization of Reference Evapotranspiration of the Environmental and Water Resources Institute of the American Society of Civil Engineers recommended a standardized form of the evapotranspiration calculation for a reference earth surface, which becomes:

$$ET = \frac{0.408\Delta(R_{ns} - R_{nl} - G) + \frac{C_n}{T + 273} u\gamma(e_s - e_a)}{\Delta + \gamma(1 + C_d u)} \quad (3\text{-}4)$$

Where:

$ET$ is the loss of water on the reference surface through the evapotranspiration, the reference surface can be a short grass (12 cm (4.7 inch) height) surface or a tall grass (50 cm (19.7 inch) height) surface, in mm/hr;

$R_{ns}$ is the solar radiation absorbed by the surface, in W/m$^2$;

$R_{nl}$ is the net long wave radiation leaving the earth surface, in W/m$^2$;

$G$ is the heat stored in the soil, in MJ/m$^2$•hr;

$\Delta$ is slope of the saturation vapor pressure-temperature curve, which is $(e_s - e_a)/(T_s - T_a)$ (where $e$ is the saturated vapor pressure, $T$ is temperature, the subscript "s" represent the soil surface, and "a" represent the air), in kPa /°C;

$\gamma$ is psychrometric constant, it relates the partial pressure of water in the air to the air temperature, in kPa;

$u$ is measured hourly wind speed at 2 m height, in m/s;

$e_s$ is saturated air vapor pressure, in kPa;

$e_a$ is actual air vapor pressure, in kPa;

$C_n$ is a non-dimensional constant which indicates the reference surface type, for short grass surface simulation it is 37 and it is 66 for tall grass surface;

$C_d$ is a non-dimensional constant which indicates the reference surface type, for day time, it is 0.24 (short grass) and 0.25 (tall grass at surface), for night time, it is 0.96 (short grass) and 1.7 (tall grass at surface);

Equation 3-4 calculates the evapotranspiration based on the energy balance on the earth surface. The net short wave radiation $R_{ns}$ entering the earth surface equals to the summation of net long wave radiation leaving the earth surface $R_{nl}$, the heat stored in the soil $G$, the heat loss through evapotranspiration, which is proportional to $ET$, and the convection heat transfer which is expressed by the term $\frac{C_n}{T+273}u\gamma(e_s-e_a)$. The term $\frac{C_n}{T+273}u$ represents the convection coefficient, which is linearly proportional to the wind speed $u$, the term $\gamma(e_s-e_a)$ indicates the difference between the air and soil temperature.

The value of $R_{ns}$, the net short wave radiation, is calculated based on the measured incident short wave radiation and the absorptivity of the grass surface. The net outgoing long wave radiation $R_{nl}$ is calculated by Equation 3-3. The hourly $G$ used in Equation 3-4 correlates well with net radiation and the type of vegetative cover; therefore, it can be calculated as a fraction of $R_{ns}-R_{nl}$. The value of saturated air vapor pressure, $e_s$, is calculated based on the measured air temperature; actual air vapor pressure $e_a$ is related to the value of $e_s$ and relative humidity in the air. The psychrometric constant $\gamma$ is linearly proportional to the atmospheric pressure, the atmospheric pressure equal to standard atmospheric pressure (101.3 kPa (14.7 Psi)) multiplied by a function of attitude of the simulation site. The slope of the saturation vapor pressure-temperature curve $\Delta$ is a function of measure hourly air temperature. Therefore, according to Walter et al.'s model (2005), the value of $ET$ can be calculated, if air temperature, air humidity, incident solar radiation on a horizontal surface and wind speed are known.

Considering the heat loss through evapotranspiration in the earth surface heat balance equation makes a significant improvement in the simulation results. As explained before, the evapotranspiration discussed in this thesis represents the loss of water through the evaporation of soil and plant's surfaces. The heat loss of evapotranspiration is calculated by multiplying the water loss through the evapotranspiration by the density of water and the latent heat of evaporation. The water loss through evapotranspiration is calculated by Equation 3-4, based on Walter, et al. model(2005). As can be seen in Figure 3.1, it shows the comparison of simulated soil temperature (with/without evapotranspiration accounted) and measured soil temperature at the depth of 0.5 m (1.64 ft) in Nebraska. The curve marked" experimental measurement" is five years measured data at a site (Roger Farms) in Nebraska, collected by the USDA Soil Climate Analysis Network, (See http://www.wcc.nrcs.usda.gov/scan/index.html). The curve marked "numerical model_ with evapotranspiration" is the simulation result, which includes the evapotranspiration. The curve marked "numerical model_ w/o evapotranspiration" is the simulation result when no evapotranspiration is considered on the earth surface, by assuming there is no water loss at the earth's surface.

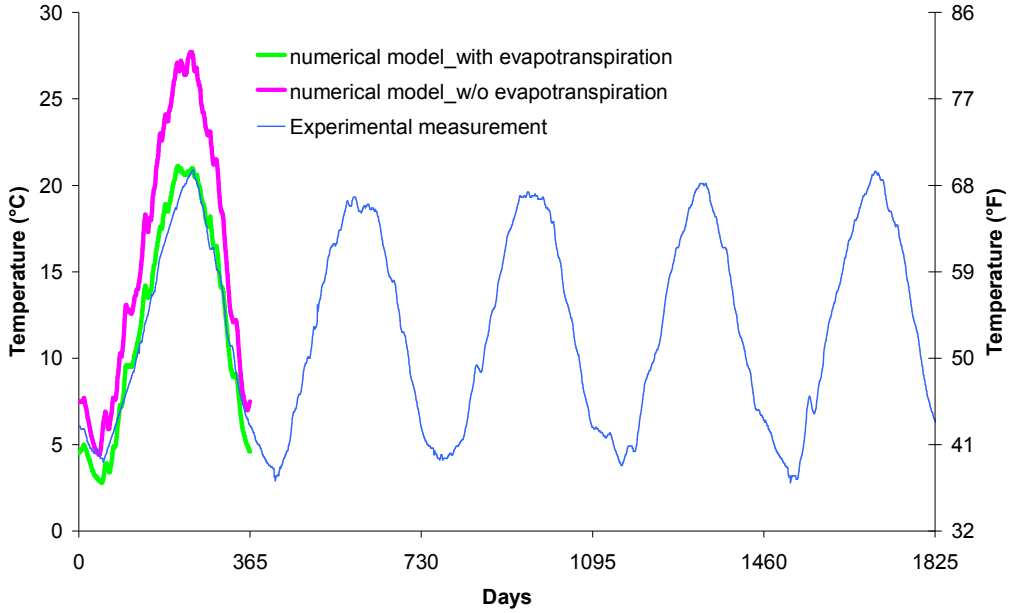


Figure 3.1: Soil temperature at 1 m (3.28 ft) deep, in Roger Farms, Nebraska

As can be seen, the simulation result, with evapotranspiration considered, is less than 2°C (4 °F) difference from the measured data. However, the simulation result without evapotranspiration included in the model is about 7°C (12 °F) difference from the measured data. Without accounting the evapotranspiration heat transfer at the earth surface, the model can only predict poorly result compared with the measured data. The same test has been done in few other locations. The results of the case study show that, the evapotranspiration is not negligible in the calculation of the surface heat balance, when the earth surface is covered by grass or other plants. For the calculation of the evapotranspiration, the numerical model now calculates the evapotranspiration at the earth's surface assuming it is covered by a grass with 12 cm (4.7") height all the year. In practice, the grass height varies at different time of year. Therefore, this method can be further improved by multiplying a seasonal factor to the evapotranspiration calculated based on a constant height grass surface. For example, in winter, when the grass goes dormant, the seasonal factor can be set to near 0, which represents there are almost no evapotranspiration on the earth's surface.

### 3.1.2 Heat Balance at the Bottom Boundary

The bottom boundary is set to be a depth of 10 m (32.4 ft) which is far from the earth surface; the boundary temperature will not be disturbed by the surface heat transfer. A typical value for the geothermal gradient of 25 °C/Km (0.0137 °F/ft) is imposed on the bottom boundary, which represents the flux conducted from the Earth's warm interior towards the earth surface. Therefore, the heat balance equation at the bottom boundary becomes:

$$K_s \frac{\partial T}{\partial y} + Q = 0 \qquad (3\text{-}5)$$

Where:

$K_s$ is the soil thermal conductivity, in W/m•K or Btu/hr•ft•°F;

$T$ is the soil temperature, in °C or °F;

$Q$ is the heat flux coming from the earth's warm interior, in W/m$^2$ or Btu/hr•ft$^2$;

Equation 3-5 calculates the soil temperature at the bottom boundary. The term $K_s \frac{\partial T}{\partial y}$ is the conducted heat from the cell above the bottom boundary cell. The heat flux from the earth's interior $Q$ can be calculated by multiplying the soil thermal diffusivity $K_s$ to the geothermal gradient.

### 3.1.3 Soil Freezing/Melting

When validating the simulation result of undisturbed ground temperature, against SCAN experimental measurements, it became apparent that freezing and melting of moisture in the soil can be important for colder climates. Therefore, freezing and melting of water in the soil is also considered. The effective heat capacity method (Lamberg et al., 2004) is utilized to minimize computation time while maintaining accuracy.

In the actual freezing process, there is great amount of latent heat released to the soil when the water in the soil freeze into ice, usually, the latent heat $L$ is added into the heat balance equation of each cell in the soil domain in order to account for the soil freezing. However, the effective heat capacity method accounts for the latent heat released during the phase change by artificially adjusting the specific heat capacity of the water in the soil as it transitions from water in liquid form to water in solid form. As Figure 3.2a shows, under normal conditions, the specific heat capacity of water in liquid form with constant value $C_{pw}$ and the specific heat capacity of water in solid form (ice) is with the value of $C_{pi}$. Figure 3.2b shows the water specific heat calculated after

utilizing the effective heat capacity. As seen in Figure 3.2b, the specific heat of water, during the temperature range $T_1$ (0°C (32°F)) and $T_2$ (-0.5°C (31°F)) when the soil freezing/melting, increases to the value of $C_{pwf}$. The value of $C_{pwf}$ is adjusted so that the cross-hatched area (▨) shown in Figure 3.2 equals to the latent heat released during the phase change $L$. The temperature range between $T_1$ and $T_3$ (0.05°C (31.9°F)), $T_4$ (-0.45°C (31.2°F)) and $T_2$, are transition areas.

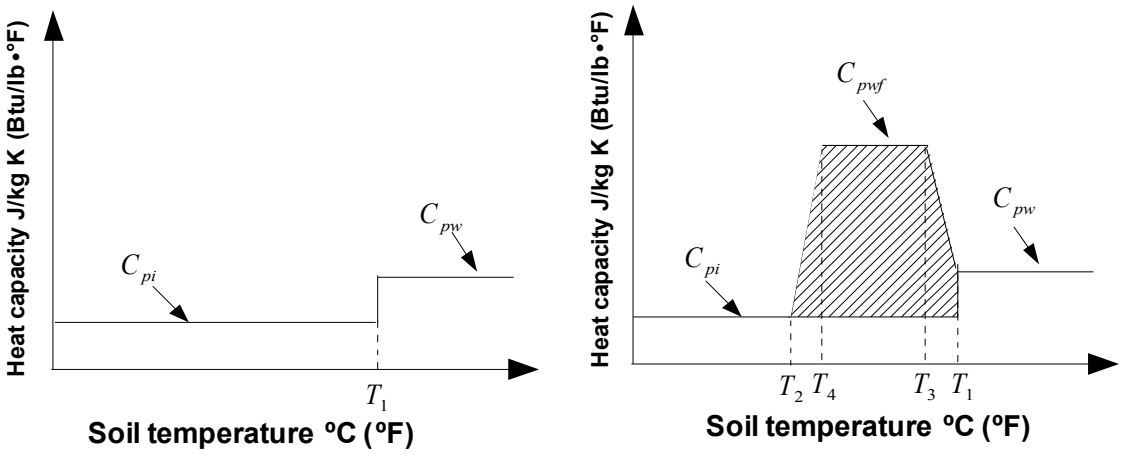


a) b)

Figure 3.2: Specific heat capacity of water in the soil

The value of $C_{pwf}$ during the freezing/melting process can be calculated as:

$$L + C_{pi}(T_2 - T_1) = C_{pwf}(T_4 - T_3) + \frac{C_{pi} + C_{pwf}}{2}(T_4 - T_2) + \frac{C_{pw} + C_{pwf}}{2}(T_1 - T_3) \quad (3\text{-}6)$$

Where:

$L$ is the latent heat released during the soil freezing or melting, in J/kg or Btu/lb;

$C_{pi}$ is the specific heat capacity of ice, in J/kg•K or Btu/lb•°F;

$C_{pw}$ is the specific heat capacity of water in liquid form, in J/m$^3$•K or Btu/ft$^3$•°F;

$C_{pwf}$ is the specific heat of water in the soil during freezing and melting process, in J/kg•K or Btu/lb•°F;

$T_1$ is the temperature at which soil starts freezing, in °C or °F;

$T_2$ is the temperature at which soil stops freezing, in °C or °F;

$T_3$ is the temperature, in °C or °F;

$T_4$ is the temperature, in °C or °F;

Equation 3-6 calculates the specific heat capacity of water in the soil $C_{pwf}$ during the freezing and melting process. The values of $T_1$ and $T_2$ depend on the type of soil, the value used in the 1D model is estimated from the soil freezing curve for clay loam. The values of $T_3$ and $T_4$ should be chosen so that they are close to $T_1$ and $T_2$, respectively. The volumetric heat of the soil is calculated (Niu and Yang 2006)based on the volumetric heat of dry soil, volumetric water fraction in the soil and volumetric heat of water for both liquid and ice conditions:

$$C_{pvs} = C_{pvsd} + C_{pw}\rho_w\theta_w \qquad 0°C\ (32°F) < T_s \qquad (3\text{-}7)$$

$$C_{pvs} = C_{pvsd} + C_{pwf}\rho_w\theta_w \qquad -0.45°C\ (31°F) \le T_s \le -0.05°C\ (32°F) \qquad (3\text{-}8)$$

$$C_{pvs} = C_{pvsd} + C_{pi}\rho_i\theta_i \qquad T_s < -0.5°C\ (32°F) \qquad (3\text{-}9)$$

Where:

$C_{pvs}$ is the volumetric heat capacity of soil, in J/m$^3$•K or Btu/ft$^3$•°F;

$C_{pvsd}$ is the volumetric heat capacity of dry soil, in J/m$^3$•K or Btu/ft$^3$•°F;

$C_{pw}$ is the specific heat capacity of water in liquid form, assumed to be 4180 J/kg•K (1.00 Btu/lb•°F), in J/kg•K or Btu/lb•°F;

$\rho_{pw}$ is the density of water in liquid form, assumed to be 1000 kg/m$^3$ (62.4 lb/ft$^3$), in kg/m$^3$ or lb/ft$^3$;

$C_{pwf}$ is the specific heat of water in the soil during freezing and melting process, in J/kg•K or Btu/lb•°F;

$C_{pi}$ is the specific heat capacity of ice, assumed to be 2066 J/kg•K (0.49 Btu/lb•°F), in J/kg•K or Btu/lb•°F;

$\rho_i$ is the density of ice, assumed to be 917 kg/m$^3$ (57.2 lb/ft$^3$), in kg/m$^3$ or lb/ft$^3$;

$\theta_w$ is the water content of the soil, in m$^3$/m$^3$ or ft$^3$/ft$^3$;

$\theta_i$ is the ice content of the soil, in m$^3$/m$^3$ or ft$^3$/ft$^3$;

$T_s$ is the soil temperature, in °C or °F;

Equations 3-7, 3-8 and 3-9 calculate the volumetric heat capacity of the soil. The value of $C_{pwf}$ is calculated from Equation 3-6. The values of volumetric heat of dry soil $C_{pvsd}$ , water content $\theta_w$ and ice content $\theta_i$ depend on the soil type simulated. Including the freezing and melting of water in the soil is important for colder climate. Figure 3.3 shows a comparison of experimental measurement of undisturbed soil temperature with the simulation result (with or without freezing

considered). The line marked "experimental measurement" is the five year experimental measurements of undisturbed soil temperature, at 0.5 m (1.64 ft) depth, at the measurement sites Mason, IL, provided by the USDA Soil Climate Analysis Network. The line marked "numerical model_ with freezing" is the computed soil temperature which considers the freezing of the soil. The simulation result is computed for clay loam soil containing 30% water by volume. The line marked "numerical model_ w/o freezing" is the simulated soil temperature without freezing of soil taken care of. Both the numerical results with or without freezing of soil considered include the effect of evapotranspiration on the earth's surface. As seen in the figure, the measured annual minimum soil temperature for each of the five years, at the depth of 0.5 m (1.64 ft), is about 3°C (37°F). The computed annual minimum soil temperature, with freezing of soil considered, is about 3°C (5°F) difference from the experimental results. If the soil freezing is not considered, the calculated annual minimum soil temperature will be about 11°C (20 °F) different from the measured results.

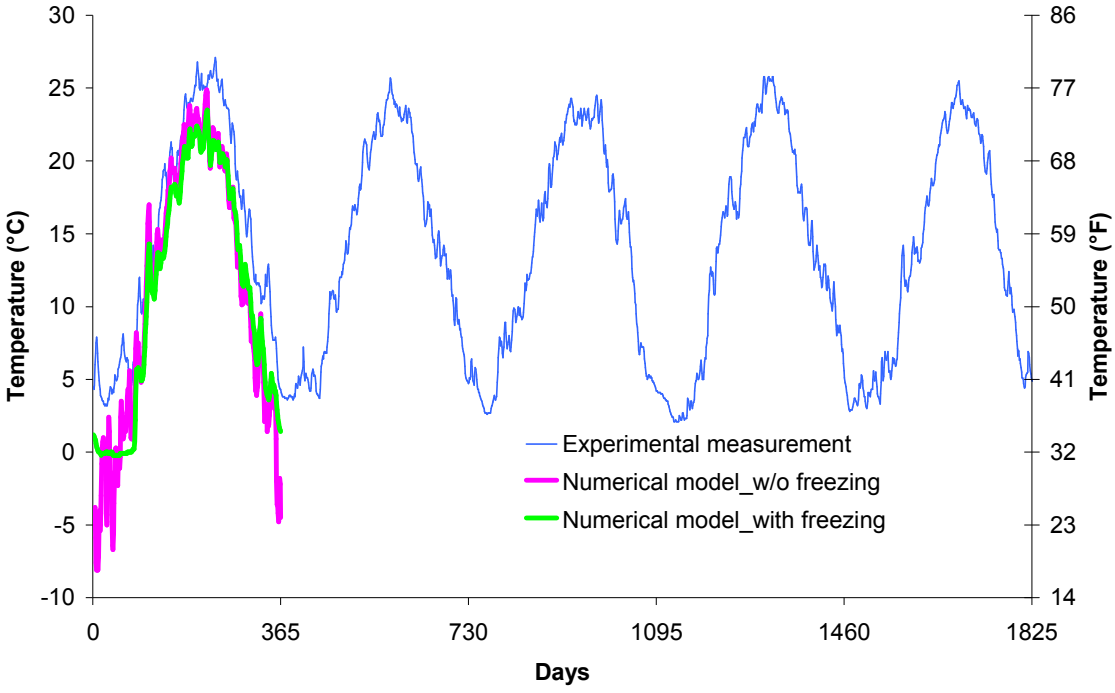


Figure 3.3: Soil temperature at 0.5 m (1.64 ft) deep, in Mason, Illinois

## 3.2 Kusuda and Achenbach Model

Kusuda and Achenbach model (1965) proposed a simple form of equation for computing the undisturbed ground temperature. The form of equation has been introduced in Section 2.5.1, in which temperature is expressed as a function of depth and time of year. As discussed before, there are three parameter values unknown; annual average soil temperatures, surface amplitude, phase delay. The computed results from the one-dimensional numerical model, by implementing a full heat balance at the earth surface and impose a geothermal gradient on the bottom boundary, are utilized to estimate the Kusuda and Achenbach parameters. Mathematically, this is done by minimizing the sum of the squares of the errors:

$$SSQE = \sum_{i=1}^{4} \sum_{j=1}^{365} \left( T_{soil\_1D} - T_{K\&A} \right)^2 \qquad (3\text{-}10)$$

Where:

$SSQE$ is the sum of square of the error;

$T_{soil\_1D}$ is the computed undisturbed ground temperature from the 1D model, in °C or °F;

$T_{K\&A}$ is the computed undisturbed ground from the Kusuda and Achenbach model, in °C or °F;

This is done at four depths and for a period of an entire year treating the annual average soil temperature, annual surface temperature amplitude and phase delay as the independent parameters that are adjusted to minimize the $SSQE$. The minimization is done with the Nelder-Mead Simplex method. The undisturbed soil temperature can then calculated from the Kusuda and Achenbach model with the three estimated parameters. This parameter estimation procedure

seems to work reasonably well, but it is limited by the accuracy of the 1-D numerical model used with TMY3 weather data.

### 3.3 Experimental Validation

The undisturbed soil temperature computed from 1D numerical model and Kusuda and Achenbach model with parameters fitted by the 1D model result are validated with the experimental data provided by Soil Climate Analysis Network (SCAN) of the USDA NRCS. The provided experimentally measured soil temperature data includes soil temperature files for an entire year, at the depths of 0.5, 1.0 and (for some locations) 2.0 m depth at a range of US locations. (See http://www.wcc.nrcs.usda.gov/scan/) Temperature measurements are available in some cases for a number of years.

Eleven geographically diverse SCAN measurement sites are chosen for the validating the simulation results over a range of weather conditions. The 1D model was run coupled with a typical meteorological year (TMY3) weather data, the locations at which the weather data are measured are selected so that they are close to the SCAN measurement site. The TMY3 data sets are derived from the 1961-1990 and 1991-2005 National Solar Radiation Data Base (NSRDB) archives. They are data files of hourly values of solar radiations, air temperatures, humidity, and other weather data for a one-year period. There are over 1000 locations within the U.S. (See http://rredc.nrel.gov/solar/old_data/nsrdb/1991-2005/tmy3/). The Kusuda and Achenbach model result is tuned from the 1D model result. The name, longitude, latitude and attitude of the eleven SCAN measurement sites and TMY3 data sites, in different states of the U.S., are listed in Table 3.1. The unit of the latitude and longitude in Table 3.1 is °.

Figures 3.4-3.9 shows a comparison of experimental measurements made at depths of 50 cm (20 inch) and 100 cm (40 inch) at three SCAN sites, Nebraska, Pennsylvania and Minnesota, to predictions made with the 1D numerical model and Kusuda and Achenbach model. The Kusuda

and Achenbach model result is calculated from the model parameters, which have been fit to the 1D numerical model. Figures 3.4 and 3.5 show the comparison of the simulation result from both models to the measured result collected, in Nebraska, at two depths for an entire year. As can be seen, the 1D numerical model result is quite close to the measured result with a difference no more than 2°C (4°F) at the maximum. Therefore, the Kusuda and Achenbach model which is tuned from the 1D model result matches the experimental result very well. Figures 3.6 and 3.7 also show that both the 1D model and Kusuda and Achenbach model give a good prediction of the undisturbed soil temperature compared with the measured data in SCAN sites, Pennsylvania.

Table 3.1: Locations of SCAN sites and TMY3 weather data sites

| States in the U.S. | Measurement sites | Name of Measurement Site | Latitude (°North) | Longitude (°West) | Attitude, m(ft) |
|---|---|---|---|---|---|
| Nebraska | TMY3 | Lincoln Muni. AP. | 40.83 | 96.77 | 357.0 (1171.0) |
| | SCAN | Roger Farm | 40.85 | 96.47 | 370.3 (1214.7) |
| Alabama | TMY3 | Huntsville Intl. AP | 34.65 | 86.78 | 190.0 (623.0 ) |
| | SCAN | WTARS | 34.90 | 86.53 | 190.5 (624.8) |
| North Dakota | TMY3 | Bismarck Muni. AP. | 46.77 | 100.77 | 502.0 (1646.6) |
| | SCAN | mandan | 46.77 | 100.92 | 588.3 (1929.5) |
| Minnesota | TMY3 | St.Cloud Muni. AP. | 45.55 | 94.05 | 311.0 (1020.0) |
| | SCAN | Cresent Lake | 45.40 | 93.95 | 298.7 (979.7) |
| South Dakota | TMY3 | Sioux Falls-Foss Field | 43.58 | 96.75 | 433.0 (1420.2) |
| | SCAN | Eros Data Center | 43.73 | 96.60 | 488.3 (1601.6) |
| Illinois | TMY3 | Peoria-Greater Peoria AP. | 40.67 | 89.68 | 199.0 (652.7) |
| | SCAN | Mason | 40.30 | 89.90 | 173.7 (569.9) |
| Pennsylvania | TMY3 | State College-Penn.State Univ. | 40.72 | 77.93 | 376.0 (1233.3) |
| | SCAN | Rock Spring | 40.70 | 77.93 | 371.9 (1219.7) |
| Ohio | TMY3 | Ohio State Univ. AP. | 40.07 | 83.07 | 283.0 (928.2) |
| | SCAN | Molly Caren | 39.95 | 83.45 | 323.1 (1059.7) |
| South Carolina | TMY3 | Florence Rgnl. AP. | 34.18 | 79.73 | 44.0 (144.3) |
| | SCAN | Pee Dee | 34.30 | 79.73 | 36.6 (120.0) |
| Georgia | TMY3 | Athens-Ben Epps.AP. | 33.95 | 83.33 | 244.0 (800.3) |
| | SCAN | Watkinsville | 33.88 | 83.43 | 234.7 (769.8) |
| Virginia | TMY3 | Frankin Muni. AP. | 36.70 | 76.90 | 12.0 (39.4) |
| | SCAN | Tidewater AREC | 36.68 | 76.77 | 24.3 (79.7) |

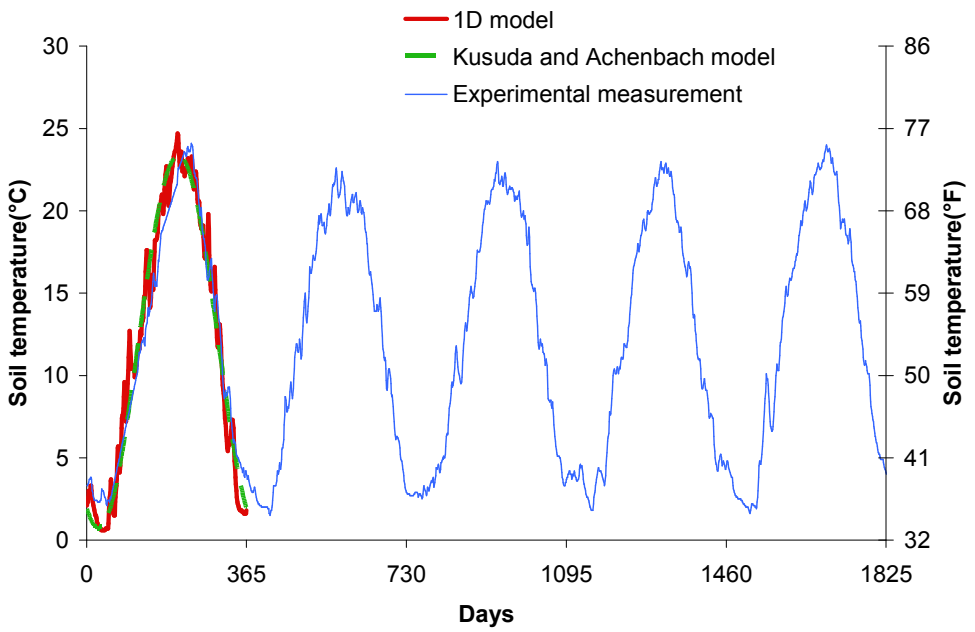


Figure 3.4: Soil temperature at 0.5 m (1.64 ft) depth in Nebraska

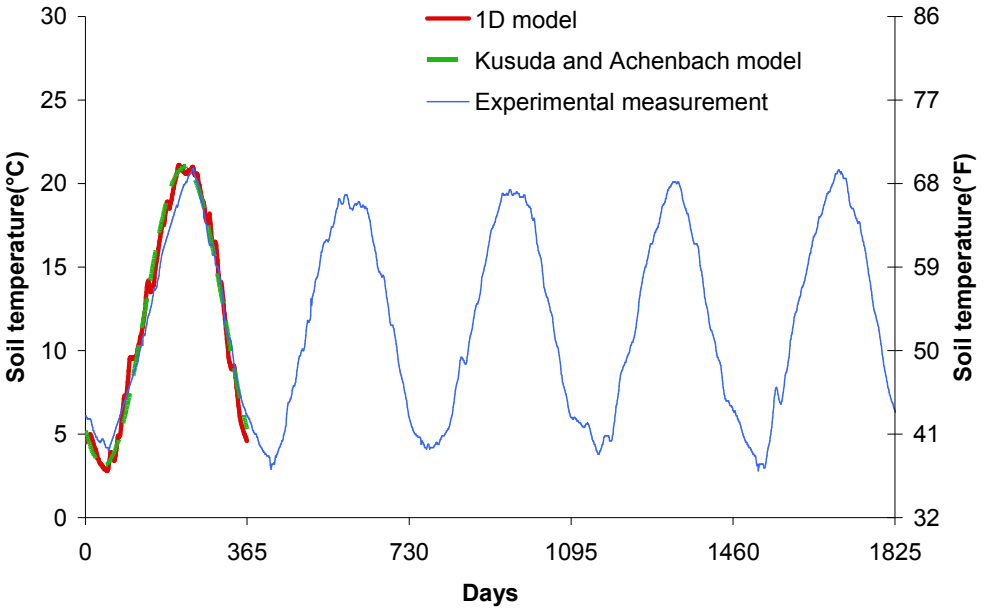


Figure 3.5: Soil temperature at 1.0 m (3.28 ft) depth in Nebraska

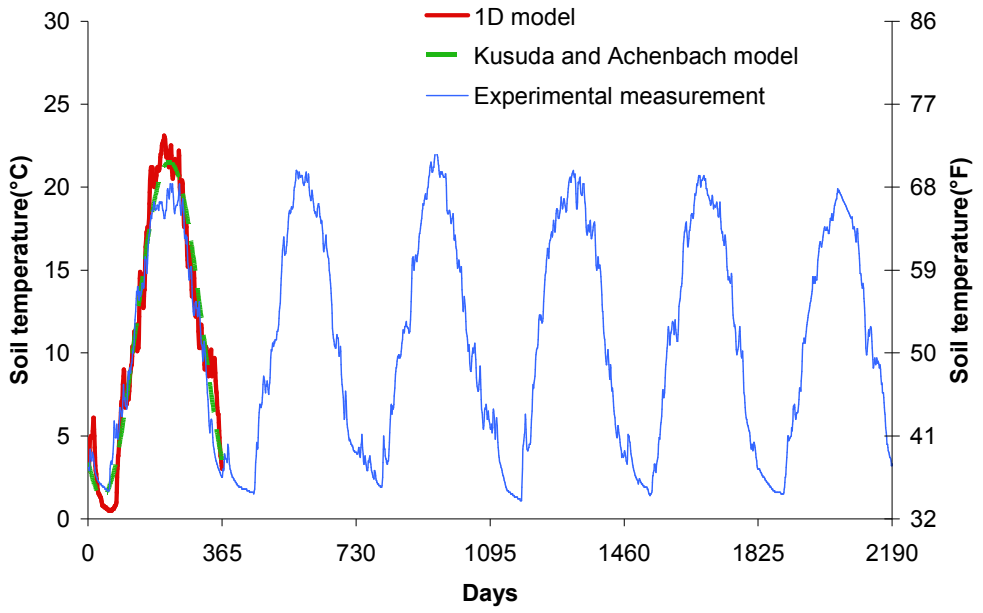


Figure 3.6: Soil temperature at 0.5 m (1.64 ft) depth in Pennsylvania

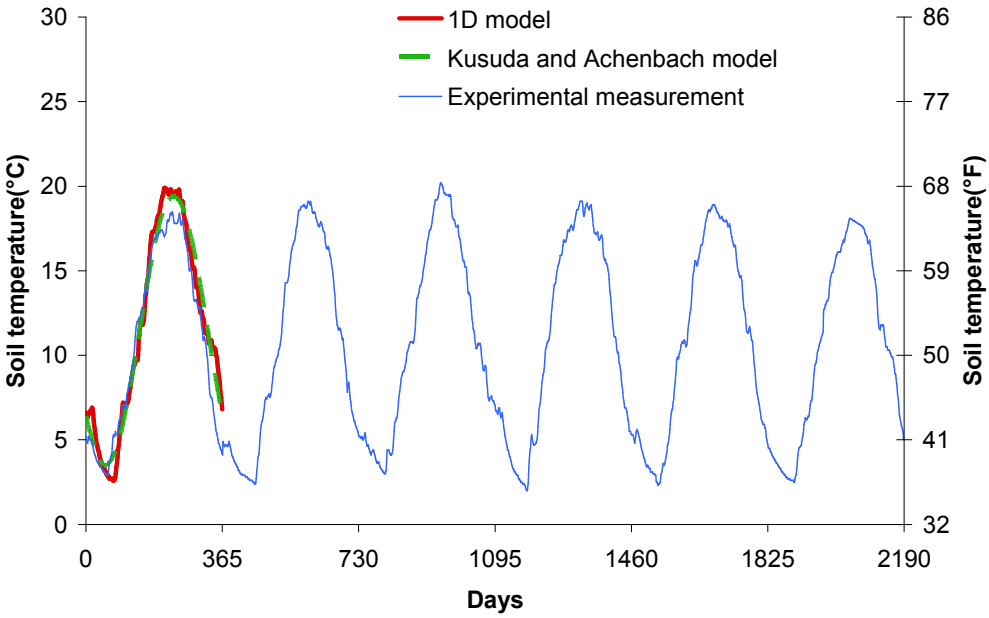


Figure 3.7: Soil temperature at 1.0 m (3.28 ft) depth in Pennsylvania

Figures 3.8 and 3.9 show less satisfactory results for Minnesota. Both the 1D model and the Kusuda and Achenbach model results fall significantly below the actual recorded minimum. One hypothesis is that snow cover significantly affects the downward migration of the cold front. Figure 3.10 shows results from a sensitivity analysis for a location in South Dakota. In this case, snow cover has been added for an 88 day period shown in the graph. (This work is accomplished with the cooperation of Xu, H. N., a visiting student from Harbin Institute of Technology University.) The line marked "1D model_without snow effect" is the simulation result of 1D model which does not account for the snow cover on the earth's surface. The line marked "1D model_10 cm (4") snow layer" and "1D model_50 cm (20") snow layer" represent the simulation results of 1D model which assumes a constant layer of snow cover on the earth's surface with a thickness of 10 cm and 50 cm (4" and 20") respectively. When there is a constant layer of snow cover with low thermal conductivity compared with the soil on the earth's surface, the snow cover serves as insulation with a high thermal resistance. In winter, the soil loses heat to the surrounding air; the insulation (snow cover) in the earth's surface decreases the heat loss of the soil and thus increases the soil temperature. Therefore, as can be seen in Figure 3.10, the simulation result with snow cover considered in the 1D model is much higher than the simulation result without snow cover included in winter, as expected. Furthermore, the simulation result with snow cover considered in the 1D model matches the experimental results much better. The preliminary conclusion of the snow cover sensitivity test is that it is probably important to include the snow cover effect in colder climate. From the measurement validation of 1D numerical model and Kusuda and Achenbach model in the site Minnesota, it can be concluded that the accuracy of 1D numerical model has a great effect on the validity of the analytical model. In order to improve the analytical model result, the accuracy of 1D numerical model should be greatly considered. Further more, comparing the simulation results from 1D model and Kusuda and Achenbach model in Figure 3.9, it shows that the simplified three-parameter Kusuda and Achenbach model gives a poor representation of the 1D model results when the soil of freezing/melting occurs. The

Kusuda and Achenbach model assumes soil is homogenous, thermal properties of soil are constant in all directions, which limit the application of the model when soil freezing/melting occurs.

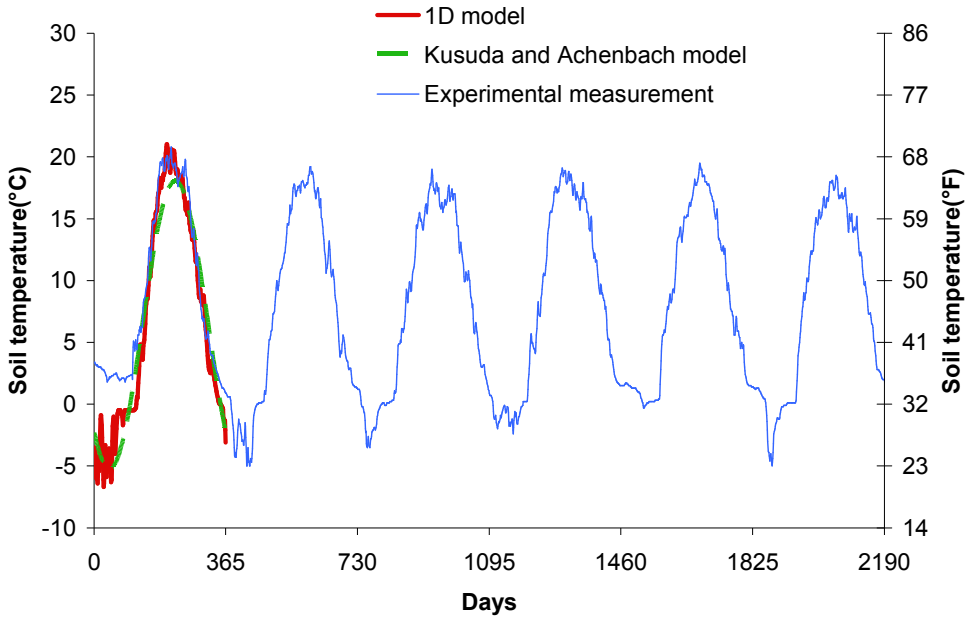


Figure 3.8: Soil temperature at 0.5 m (1.64 ft) depth in Minnesota

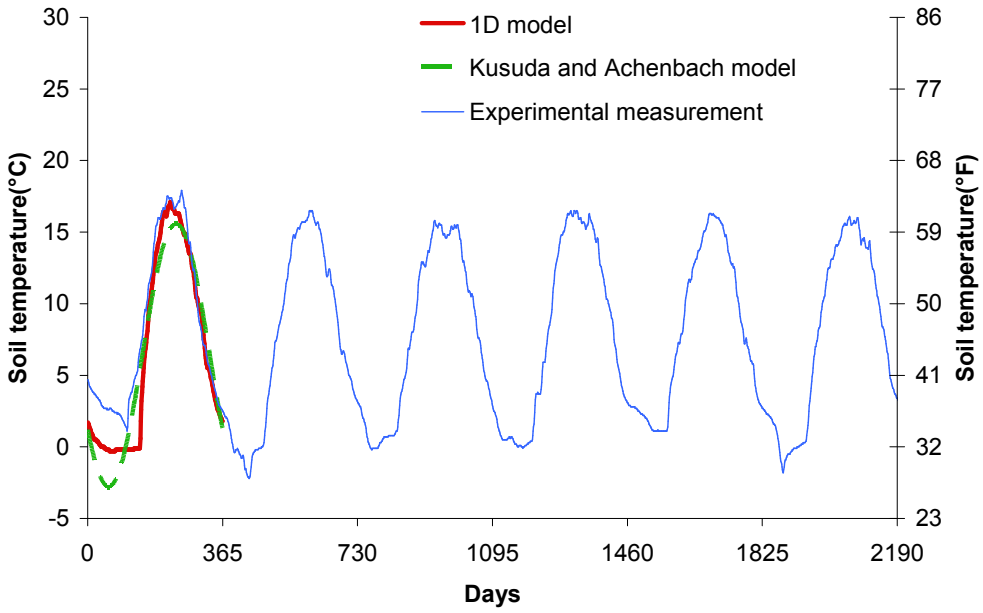


Figure 3.9: Soil temperature at 1.0 m (3.28 ft) depth in Minnesota

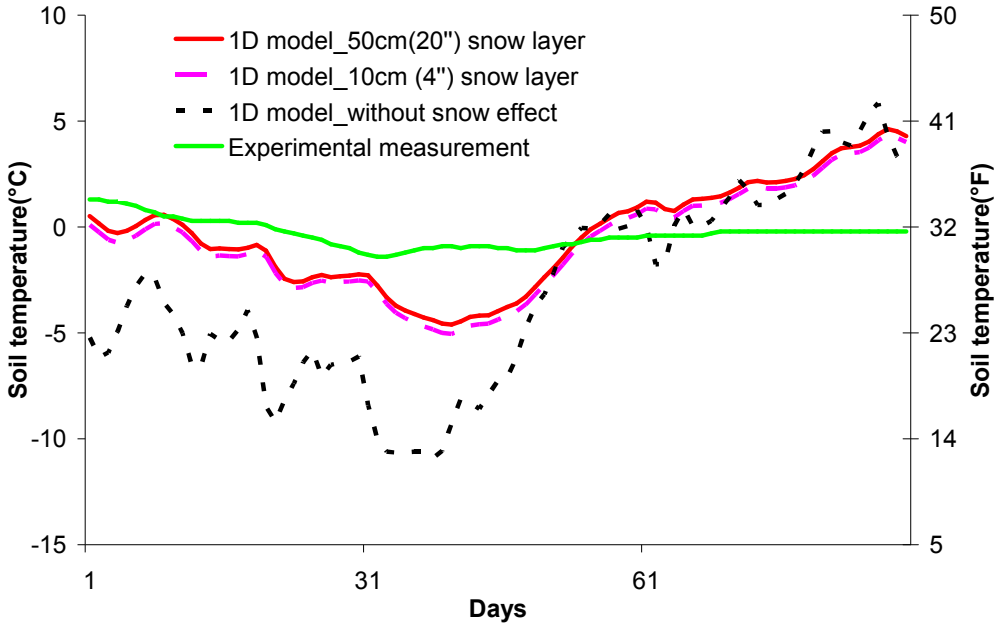


Figure 3.10: Snow cover sensitivity study at 50 cm (20") depth in South Dakota

The validation results of eleven measurement sites are tabulated in Tables 3.2, 3.3, 3.4 and 3.5. For validation of each measurement site, the differences between the Kusuda and Achenbach model results, 1D numerical model results and experimental results, vary at different depths and for different times of the year, thus hard to be categorized. Therefore, the annual maximum and minimum soil temperatures at different depths, which are the important factors that control the size and performance of the foundation heat exchangers, are used for the comparison of simulation results and measured results.

Tables 3.2 and 3.3 shows the comparison of annual maximum soil temperature calculated, with the 1D numerical model and K&A (Kusuda and Achenbach) model, to the SCAN measurement data, at the depth of 50 cm (20") and 100 cm (40"). The annual maximum soil temperature is marked as "$T_{\max}$". The SCAN measurement data for several years is used for the validation, for example, in Figure 3.10; six years of measurement data are used. Therefore, there are annual

maximum soil temperatures for different years. The "$T_{\max}$ "of the "SCAN measurement data" represents the largest annual maximum soil temperature for all the years. For example, in Figure 3.10, the value of $T_{\max}$ is about 18 °C (64 °F), measured at the first year. The "$T_{avg,\max}$ "of the "SCAN measurement data" represents the average of annual maximum soil temperature for different years. The value of $T_{avg,\max}$ usually demonstrates the annual maximum temperature for a typical year (not too hot or cold), therefore, it is always 1-2°C (2-4°F) lower than the $T_{\max}$ , which indicates the maximum temperature for the hottest year. At the depth of 50 cm (20"), the predicted $T_{\max}$ based on 1D numerical model and Kusuda and Achenbach model is 1-2°C (2-4°F) different from the value of $T_{\max}$ and $T_{avg,\max}$ calculated from the measurement data.

Table 3.2: Annual maximum soil temperature at the depth of 50 cm (20")

| SCAN Site Name | SCAN Measurement data,°C(°F) | | | 1D model result,°C(°F) | K&A model result,°C(°F) |
|---|---|---|---|---|---|
| | $T_{max}$ | $T_{avg,max}$ | Number of year of SCAN data | $T_{max}$ | $T_{max}$ |
| Roger Farm,NE | 24.0(75.2) | 23.3(73.9) | 5 | 24.7(76.5) | 23.4(74.1) |
| WTARS,AL | 27.9(82.2) | 26.7(80.0) | 5 | 25.9(78.6) | 25.3(77.5) |
| Mandan,ND | 18.8(65.8) | 17.9(64.3) | 11 | 19.4(66.9) | 17.6(63.7) |
| Cresent Lake,MN | 20.8(69.4) | 19.3(66.8) | 6 | 21.0(69.8) | 18.1(64.6) |
| EROS Data Center,SD | 22.5(72.5) | 20.7(69.2) | 6 | 21.3(70.3) | 20.6(69.1) |
| Mason,IL | 27.1(80.8) | 25.7(78.2) | 5 | 23.5(74.3) | 22.4(72.3) |
| Rock Springs,PA | 22.4(72.3) | 20.8(69.4) | 6 | 23.1(73.6) | 21.5(70.7) |
| Molly Caren,OH | 25.3(77.5) | 23.1(73.5) | 5 | 25.7(78.3) | 23.5(74.3) |
| Pee Dee,SC | 29.4(84.9) | 27.9(82.2) | 9 | 28.4(83.1) | 27.0(80.6) |
| Watkinsville,GA | 27.5(81.5) | 26.0(78.8) | 10 | 26.2(79.2) | 25.8(78.4) |
| Tidewater AREC,VA | 28.0(82.3) | 26.6(79.9) | 7 | 28.7(83.7) | 26.7(80.1) |

Table 3.3: Annual maximum soil temperature at the depth of 100 cm (40")

| SCAN Site Name | SCAN Measurement data,°C(°F) | | | 1D model result,°C(°F) | K&A model result,°C(°F) |
|---|---|---|---|---|---|
| | $T_{max}$ | $T_{avg,max}$ | Number of year of SCAN data | $T_{max}$ | $T_{max}$ |
| Roger Farm,NE | 20.8(69.4) | 20.0(68.1) | 5 | 21.1(70.0) | 21.0(69.8) |
| WTARS,AL | 23.5(74.3) | 22.7(72.9) | 5 | 23.5(74.3) | 23.4(74.1) |
| Mandan,ND | 15.8(60.4) | 14.7(58.4) | 11 | 16.3(61.3) | 15.2(59.4) |
| Cresent Lake,MN | 17.9(64.2) | 16.4(61.5) | 6 | 17.1(62.8) | 15.6(60.1) |
| EROS Data Center,SD | 18.3(64.9) | 17.3(63.1) | 6 | 18.3(64.9) | 18.0(64.4) |
| Mason,IL | 24.7(76.5) | 23.7(74.6) | 5 | 20.1(68.2) | 19.9(67.8) |
| Rock Springs,PA | 20.0(68.0) | 18.9(66.0) | 6 | 19.9(67.8) | 19.4(66.9) |
| Molly Caren,OH | 21.8(71.2) | 20.3(68.5) | 5 | 22.4(72.3) | 21.2(70.2) |
| Pee Dee,SC | 27.4(81.3) | 26.3(79.4) | 9 | 25.7(78.3) | 25.2(77.4) |
| Watkinsville,GA | 25.3(77.5) | 24.0(75.1) | 10 | 24.0(75.2) | 24.0(75.2) |
| Tidewater AREC,VA | 26.0(78.8) | 25.1(77.1) | 7 | 25.6(78.1) | 24.9(76.8) |

Tables 3.4 and 3.5 summarizes the prediction of annual minimum soil temperature $T_{\min}$ with the 1D numerical model and Kusuda and Achenbach model and the annual minimum soil temperature $T_{\min}$ or $T_{avg,\min}$ calculated based on measurement data, at the depth of 50 cm (20") and 100 cm (40"). The 1D model and Kusuda and Achenbach model gives overall good results compared with the experimental measurement, however, at the SCAN site in North Dakota, South Dakota, they are far below the recorded data. As discussed and shown in Figure 3.11, the simulation result may improve if the snow cover effect is included. There is a big difference of 4 °C (7°F) between the simulation result and measurement result observed at the site Moly Caren, Ohio. There is no clear explanation of that.

At the depth of 100 cm (40"), a lower degree of temperature difference between the simulation result and measured result (less than 2 °C (3.6°F)) have been observed for most measurement sites. At the site of Tidewater arec, VA, the simulation results of both the 1D numerical model and Kusuda and Achenbach model are more than 5 °C (9°F) different from the measurement data.

Table 3.4: Annual minimum soil temperature at the depth of 50 cm (20")

| SCAN Site Name | SCAN Measurement data,°C(°F) | | | 1D model result,°C(°F) | K&A model result,°C(°F) |
|---|---|---|---|---|---|
| | $T_{min}$ | $T_{avg,min}$ | Number of year of SCAN data | $T_{min}$ | $T_{min}$ |
| Roger Farm,NE | 1.8(35.2) | 2(35.7) | 5 | 0.6(33.1) | 0.7(33.3) |
| WTARS,AL | 4.8(40.6) | 6.1(43.0) | 5 | 3.5(38.3) | 6.7(44.1) |
| Mandan,ND | -3.8(25.2) | -2(28.4) | 11 | -7.5(18.5) | -4.8(23.4) |
| Cresent Lake,MN | -5(23.0) | -2.3(27.8) | 6 | -6.7(19.9) | -5.2(22.6) |
| EROS Data Center,SD | -1.9(28.6) | -0.7(30.8) | 6 | -5.4(22.3) | -3.7(25.3) |
| Mason,IL | 2.1(35.9) | 2.9(37.2) | 5 | -0.2(31.6) | -0.6(30.9) |
| Rock Springs,PA | 1.1(34.0) | 1.6(34.9) | 6 | 0.5(32.9) | 1.4(34.5) |
| Molly Caren,OH | 4.7(40.5) | 5.3(41.5) | 5 | 1.1(34.0) | 2.7(36.9) |
| Pee Dee,SC | 6.3(43.3) | 8(46.5) | 9 | 8.2(46.8) | 10.6(51.1) |
| Watkinsville,GA | 4.9(40.8) | 7(44.7) | 10 | 5.3(41.5) | 8.3(46.9) |
| Tidewater AREC,VA | 4.2(39.6) | 5.8(42.5) | 7 | 6.3(43.3) | 10.2(50.4) |

Table 3.5: Annual minimum soil temperature at the depth of 100 cm (40")

| SCAN Site Name | SCAN Measurement data,°C(°F) | | | 1D model result,°C(°F) | K&A model result,°C(°F) |
|---|---|---|---|---|---|
| | $T_{min}$ | $T_{avg,min}$ | Number of year of SCAN data | $T_{min}$ | $T_{min}$ |
| Roger Farm,NE | 2.8(37.0) | 3.7(38.7) | 5 | 2.8(37.0) | 3.1(37.6) |
| WTARS,AL | 8.7(47.7) | 10.1(50.1) | 5 | 7.2(45.0) | 8.7(47.7) |
| Mandan,ND | 0.3(32.5) | 1.4(34.5) | 11 | -0.1(31.8) | -2.4(27.7) |
| Cresent Lake,MN | -2.1(28.2) | -0.2(31.6) | 6 | -0.3(31.5) | -2.8(27.0) |
| EROS Data Center,SD | 0.1(32.2) | 0.8(33.5) | 6 | 0.5(32.9) | -1.1(30.0) |
| Mason,IL | 3.4(38.1) | 4.2(39.6) | 5 | 1.7(35.1) | 1.8(35.2) |
| Rock Springs,PA | 2.1(35.8) | 2.6(36.7) | 6 | 2.7(36.9) | 3.5(38.3) |
| Molly Caren,OH | 5.5(41.9) | 6.2(43.2) | 5 | 4.1(39.4) | 4.9(40.8) |
| Pee Dee,SC | 8.4(47.1) | 10.4(50.6) | 9 | 11.8(53.2) | 12.4(54.3) |
| Watkinsville,GA | 8.0(46.4) | 9.4(48.8) | 10 | 8.7(47.7) | 10.1(50.2) |
| Tidewater AREC,VA | 5.4(41.7) | 6.8(44.2) | 7 | 10.5(50.9) | 11.9(53.4) |

In all, the validation results of 1D numerical model are reasonably good, considering the complexity of actual heat transfer process in the soil. There are few reasons that may cause the differences between the simulation results from the 1D numerical model and measured data:

- The 1D numerical model utilized a typical year weather data file (TMY3) for computing the soil temperature. Therefore, the 1D numerical with TMY3 weather file used can not predict soil temperatures for the non-typical year, when the weather gets too hot or cold. Therefore, the 1D numerical model does not match well with some year (too hot or cold) of the measured results.

- The 1D numerical model utilize the weather files collected from around one hundred miles away from the soil measurement site, thus, the weather data used in the model is different from the one measured at the soil measurement site, this will result in the difference between the calculated and measured soil temperature.

- The 1D model does not include snow cover. In practical, under the same weather conditions, whether there is snow cover or not on the earth's surface has a great effect on the ground temperature. As can be seen in Figure 3.11, considering the snow cover in the 1D numerical model could significantly reduce the difference between the model result and experimental result.

- The 1D model calculate the evapotranspiration on the earth surface by assuming a grass cover on the measurement site with a constant height, in practical, the grass may go dormant in winter and less evapotranspiration will be observed. Therefore, the numerical model calculate more heat loss through the evapotranspiration in winter by assuming a grass surface with constant height, the calculated soil temperature will be lower as a result.

The accuracy of the analytical solution (Kusuda and Achenbach model) is limited by the accuracy of the 1-D numerical model. Furthermore, by comparing the 1D numerical model result and Kusuda and Achenbach model result in Tables 3.2-3.5, it has been found out that the simplified Kusuda and Achenbach model does not provides a satisfactory representation of the 1D

numerical model result for some locations. The Kusuda and Achenbach model cannot account for the freezing of soil. Therefore, a revised version the Kusuda and Achenbach model, which includes higher harmonics, is considered for the further improvement of the one-dimensional ground heat transfer model.

# CHAPTER 4

## FHX NUMERICAL MODEL

The foundation heat exchanger numerical model is an explicit two-dimensional finite volume model with a rectangular, non-uniform grid, and it is implemented in the HVACSIM+ environment. The two-dimensional model represents the three dimensional geometry soil domain with a plane perpendicular to the tube (Figure 4.1), with the assumptions that there is no heat transfer through the soil along the length of the tube and the effect of the corners is not important. As shown in Figure 4.1, the simulated soil domain is bounded by a basement (which may be temperature-conditioned or unconditioned), the earth surface and the surrounding ground. The inside basement wall and basement floor boundaries are convective so that the FHX tubes may extract some heat from the basement, and this is called the "short-circuiting heat transfer". "Short-circuiting heat transfer" will drive up the heating load and will be discussed later in this chapter.

For example purposes, some of the input parameters for soil domain are fixed but can be modified when needed. Currently, the soil domain is 5 meters (16.4 ft) deep and extends 4 meters (13.1 ft) from the basement wall to the right boundary, and it extends 6 meters (19.7 ft) from the basement wall to the center of the building. The basement wall is 2.5 meters (8.2 ft) deep and extends 0.3 meters (1.0 ft) above the ground. The above-grade insulation is 25 mm (1 inch) thick with a resistance of 2.11 $m^2$•K/W (12 Btu/hr•$ft^2$•°F), and the below-grade insulation, which covers the entire basement wall of basement floor, is 25 mm (1 inch) thick with a resistance of

2.11 $m^2$•K/W(12 Btu/hr•$ft^2$•°F). Two of the FHX tubes are located in a horizontal line and the other four are located in an inclined line.

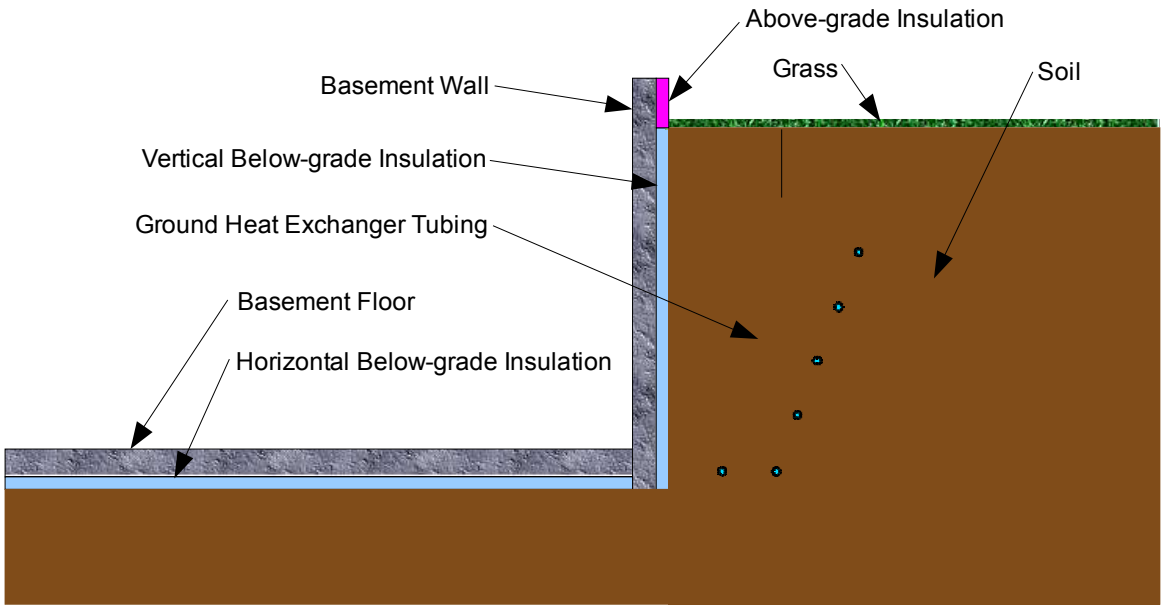


Figure 4.1: Cross-section of foundation heat exchanger

## 4.1 Non-uniform Grid

The soil domain geometry and tube locations are inputs for the FHX model and the non-uniform grid is formed automatically. The non-uniform grid (cells with variable spacing) with ~13000 cells shown in Figure 4.2 is used to model the domain. The FHX tube is represented as rectangular tube which is the same size as the smallest cell but covers portions of four cells. The grid spacing is smaller near the earth surface and tube surfaces and expands towards adiabatic surfaces (left and right sides of the soil domain) and the bottom of the soil domain. The method of generating the non-uniform grid is discussed in this section.

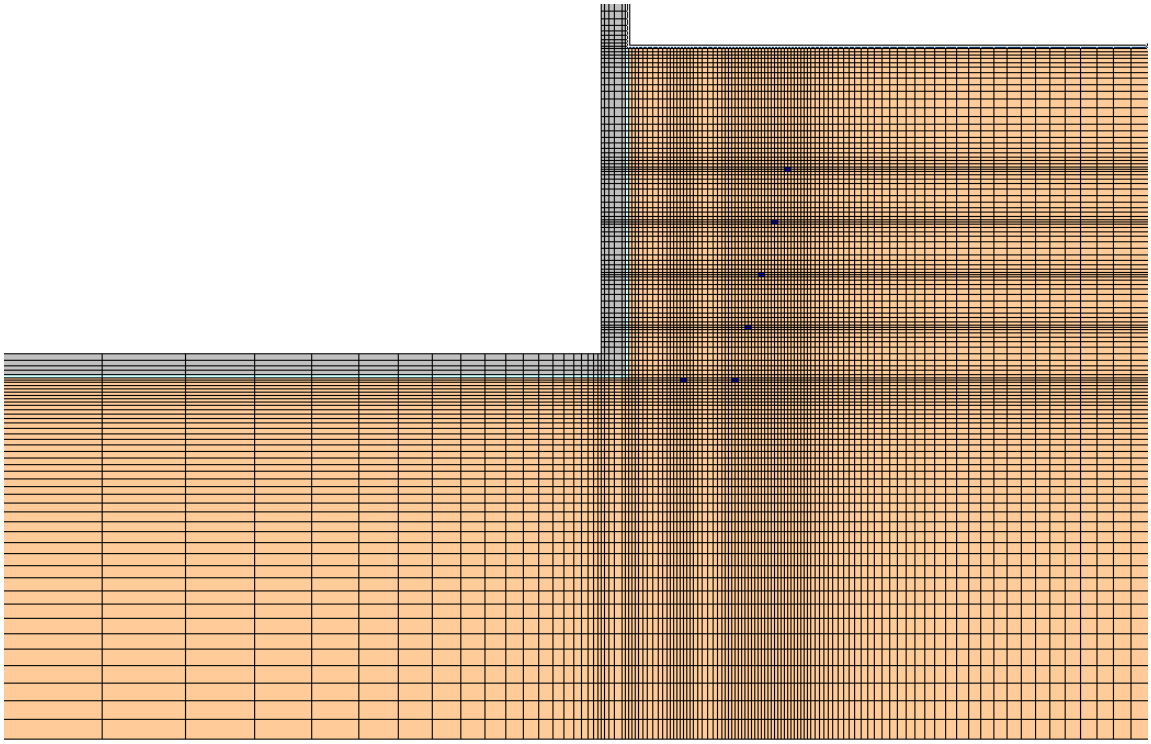

Figure 4.2: Non-uniform grid

In Figure 4.2, there are six tubes, all which are assumed to have the same inside and outside diameters. Each FHX tube is represented as a square tube and has the same size as the smallest cell. The grid spacing is reduced near boundaries between the soil and the surface of the earth; the tubes and the basement. The grid spacing is increased away from their surface and near the adiabatic surface.

In the *x* direction (horizontally), the grid spacing expands from the FHX tube which is closest to the foundation wall towards the farthest left boundary. Between two FHX tubes, the grid spacing expands from tubes towards their mid point. And the grid spacing expands between the right-most tubes and the right boundary. In the *y* direction (vertically), between the shallowest tube and the surface of the earth, the grid spacing expands from the surface of the earth and the tube towards the mid point. And the grid spacing expands from the deepest tube towards the bottom boundary.

In order to generate the non-uniform grid, the FHX tube locations, soil domain size, the desired number of cells between each two FHX tubes, the desired number of cells between the FHX tube and soil domain boundary are inputs for the model. The expansion ratio between each two FHX tubes or between FHX tube and soil domain boundary can be automatically calculated, therefore the non-uniform grid can be automatically generated. Figure 4.3 shows how the non-uniform grids are located between two FHX tubes. Between the two FHX tubes, the grid spacing expands symmetrically from the center line of two FHX tubes towards their mid point. Cell ($m$,$n$) is the smallest cell which is calculated bases on the FHX tube perimeter. The expansion ratio can be calculated with Equation 4-1:

$$\sum_{n=1}^{N/2} l \times (1+R)^{(n-1)} = L \qquad (4\text{-}1)$$

Where:

$N$ is the number of cells between two FHX tubes;

$R$ is the unknown grid spacing expansion ratio needs to be determined with Equation 4-1.

$l$ is the smallest cell length in horizontal or vertical direction, in m or ft;

$L$ is the horizontal or vertical distance between one FHX tube center and the mid point between the two FHX tubes, in m or ft;

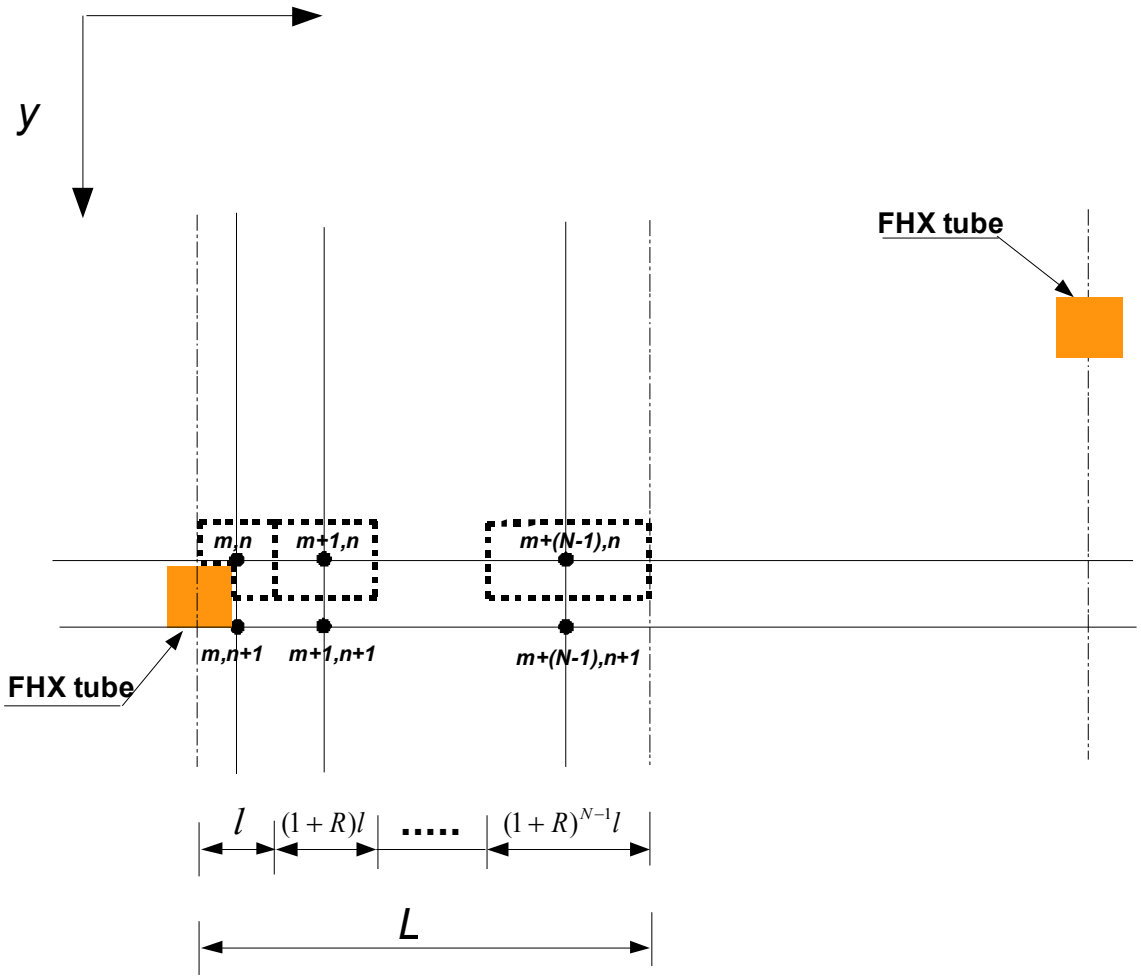


Figure 4.3: Non-uniform grid detailed plot

As discussed before, the smallest grid cell is determined by the FHX tube perimeter; each of the six FHX tubes is represented as a square tube and four cells plotted with dash line surrounds the square tube as shown in Figure 4.4. Four cell centers are located on the square tube outside wall and the inside tube wall is neglected. It is assumed that the square tube and FHX tube have the same perimeter, and the four cells all have the same perimeter as the square tube:

$$4l_x = 4l_y = \pi \times d_o \qquad (4\text{-}2)$$

$l_x$ and $l_y$ is the cell length in $x$ direction (horizontally) and $y$ direction (vertically), $d_o$ is the FHX tube outside diameter; the Equation 4-2 is derived basement the assumption that the square

tube and FHX tube has the same perimeter so that the tube wall area which is perpendicular to the soil domain is the same for the square tube and FHX tube, and this makes the heat transfer rate through the tube wall the same for them.

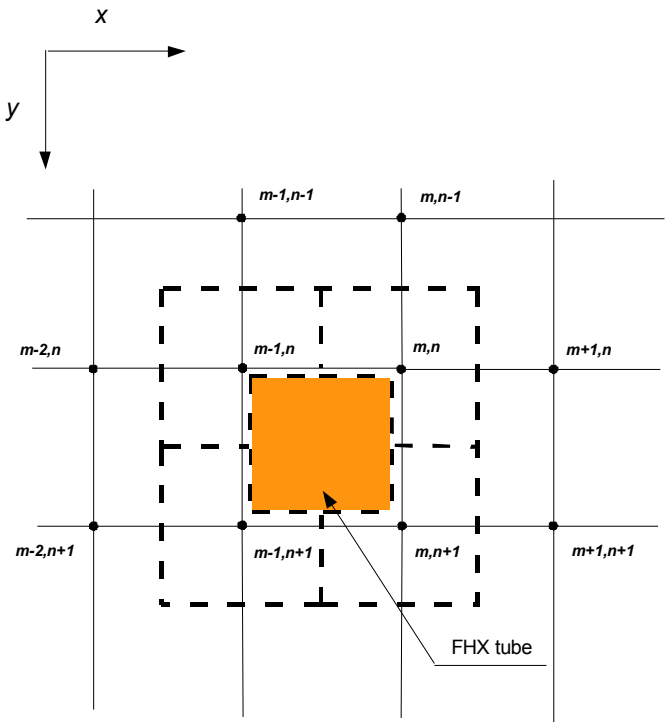


Figure 4.4 FHX tubes grid plot

## 4.2 Finite Volume Equations

The numerical model is based on the finite volume method; for most cells, it follows standard formulations for interior cells with conduction heat transfer, cells with adiabatic boundaries, convective boundaries and temperature-specified boundaries. In Section 4.2 the difference equations for cells at the earth's surface that include convection, radiation, and evapotranspiration and cells that represent tubes are described. All the difference equations are obtained by applying a conservation of energy to a control volume (cell).

Figure 4.5 shows a cell labeled ($m$,$n$) at the earth's surface, which means it is the $m^{th}$ cell in the $x$ direction and the $n^{th}$ cell in the $y$ direction. The cell on the farthest left boundary of the soil domain is the first cell in the $x$ direction, and the cell on the top of the foundation wall is the first cell in the $y$ direction. In order to find the soil temperature at earth's surface directly, a half cell is used as shown in Figure 4.4. An energy balance can be written as:

$$q_1 \Delta x_{(m,n)} L_p + q_2 \frac{\Delta y_{(m,n)}}{2} L_p + q_3 \Delta x_{(m,n)} L_p + q_4 \frac{\Delta y_{(m,n)}}{2} L_p = \rho_s c_{Ps} V \Delta T_{(m,n)} \qquad (4\text{-}3)$$

Where:

$\Delta x_{(m,n)}$ is the cell ($m$,$n$) length in $x$ direction, in m or ft;

$\Delta y_{(m,n)}$ is the cell (m,n) length in $y$ direction, in m or ft;

$\rho_s$ is soil density, in kg/m$^3$ or lb/ft$^3$;

$c_{Ps}$ is the soil heat capacity, in J/kg•K or Btu/lb•°F;

$V$ is the cell volume, in m$^3$ or ft$^3$;

$\Delta T_{(m,n)}$ is the temperature increase in cell ($m$,$n$), in °C or °F ;

$L_p$ is the length of the FHX tube, in m or ft;

$q_2$, $q_3$ and $q_4$ is the heat conduction flux from surrounding cell, in W/m$^2$ or Btu/ft$^2$•hr;

$q_1$ is the net heat gain at the earth's surface, in W/m$^2$ or Btu/ft$^2$•hr;

$\rho_s c_{Ps} V \Delta T_{(m,n)}$ is the heat stored in the cell, in W or Btu/hr;

The left side of Equation 4-3 represents the net heat gain to the cell and the right side represents the increase in energy for the cell for a specific time step. The heat transfers $q_2, q_3$ and $q_4$ are computed based on conduction only. The conduction heat transfer $q_2$ can be calculated as shown in Equation 4-4:

$$q_2 = \frac{k_s \Delta T}{\left(\left(\Delta x_{(m,n)} + \Delta x_{(m+1,n)}\right)/2\right)} \qquad (4\text{-}4)$$

Where:

$k_s$ is soil conductivity, in W/m•K or Btu/ft•°F •hr;

$\Delta x_{(m,n)}$ is the length of cell (*m*,*n*) in the *x* direction., in m or ft;

$q_3$ and $q_4$ can be calculated in a similar way. The heat transfer rate $q_1$ represents the net heat gain due to absorbed short wave irradiation, long wave radiation to and from the environment, convection to and from the outdoor air, and heat loss by evapotranspiration:

$$q_1 = q_{rad\_s} + q_{rad\_L} + q_{conv} + q_{evap} \qquad (4\text{-}5)$$

Where:

$q_{rad\_s}$ is the absorbed short wave radiation in W/m$^2$ or Btu/ft$^2$•hr;

$q_{rad\_L}$ is the net long wave radiation absorbed by the surface, in W/m$^2$ or Btu/ft$^2$•hr;

$q_{conv}$ is convection heat transfer to the surface, in W/m$^2$ or Btu/ft$^2$•hr;

$q_{evap}$ is heat transfer to the surface through evapotranspiration (this will usually be negative, unless condensation is occurring), in W/m$^2$ or Btu/ft$^2$•hr;

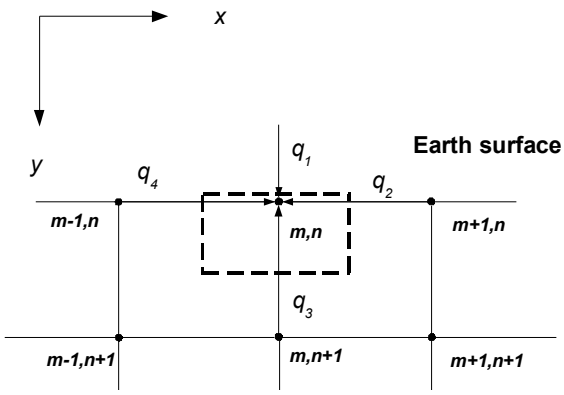


Figure 4.5: Earth surface cell

The absorbed short wave radiation on a horizontal surface is determined from a TMY3 weather file. An absorptivity of 0.77 is chosen for grass cover, based on the recommendation of Walter et al (2005) . The net long wave radiation is based on the procedure recommended by Walter, et al (2005), which utilizes an effective sky emissivity, based on humidity and cloudiness. The convection to and from the outdoor air is determined by a convection correlation recommended by Allen (not sure about the source of the paper) based on the air density, air heat capacity, wind speed and unit less air resistance. Evapotranspiration (ET) is the loss of water from the earth's surface through two processes; evaporation from soil to plant surface and plant internal transpiration. The evapotranspiration model (Walter, et al. 2005) gives the evaporation rate in mm/hr as a function of the type of vegetation. For FHX numerical model, a 12 cm clipped or cool-season grass surface is implemented. Once the ET rate is calculated, the heat loss by evaporation is determined by multiplying the ET rate by density and the latent heat of evaporation. Inclusion of evapotranspiration has a significant impact in the prediction of the ground temperature. The calculation of the evapotranspiration, short wave radiation, long wave radiation, and the convection heat transfer have been described, in detail, in Section 3.1.

As discussed in Section 4.1, the FHX tube is treated as a square tube, four cells center are located on the square tube as shown in Figure 4.4, the orange square is the square tube which represents

the FHX tube, and the tube wall temperature is taken as the average of the temperatures of the four surrounding cells. As an example of how this is done, consider the (*m*,*n*) cell shown in Figure 4.6. According to the conservation of energy in the cell, the conduction heat transfer from the surrounding cell and convection heat transfer from the fluid to the cell (*m*,*n*) sum to the heat stored in the cell at a specific time step, and this heat balance is calculated with the following equations:

$$\frac{T^P_{(m,n+1)} - T^P_{(m,n)}}{R_1} + \frac{T^P_{(m+1,n)} - T^P_{(m,n)}}{R_2} + \frac{T^P_{(m,n-1)} - T^P_{(m,n)}}{R_3} + \frac{T^P_{(m-1,n)} - T^P_{(m,n)}}{R_4} + \frac{T^P_f - T^P_{(m,n)}}{R_5} = \frac{3}{4}(\rho_s C_{Ps})\Delta x_{(m,n)}\Delta y_{(m,n)}\frac{T^Z_{(m,n)} - T^P_{(m,n)}}{\Delta t} \quad (4\text{-}6)$$

$$R_1 = \frac{(\Delta y_{(m,n)} + \Delta x_{(m,n)})/2}{K_s \Delta x_{(m,n)}/2} \quad (4\text{-}7)$$

$$R_5 = \frac{1}{U(\Delta x_{(m,n)} + \Delta y_{(m,n)})/2} \quad (4\text{-}8)$$

Where:

$T^P_f$ is the fluid temperature at previous time step, it is represented as a time-dependent boundary, in °C or °F;

$T^P_{(m,n)}$ is the cell (*m*,*n*) temperature at previous time step, in °C or °F;

$T^Z_{(m,n)}$ is the cell (*m*,*n*) temperature at current time step, in °C or °F;

*U* is the overall conductance through the fluid to the tube outside, in W•K/ $m^2$ or Btu•°F/$ft^2$•hr;

$\Delta x_{(m,n)}$ is the cell ($m$,$n$) length in $x$ direction, in m or ft;

$\Delta y_{(m,n)}$ is the cell ($m$,$n$) length in $y$ direction, in m or ft;

$\rho_s$ is soil density, in kg/m$^3$ or lb/ft$^3$;

$c_{Ps}$ is the soil heat capacity, in J/kg•K or Btu/lb•°F;

$K_s$ is soil conductivity, in W/m•K or Btu/ft•°F •hr;

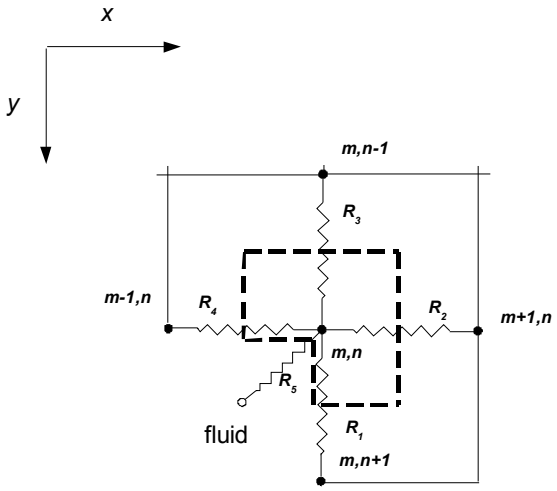


Figure 4.6: Nodes around the FHX tube

$R_1, R_2, R_3$ and $R_4$ are the heat conductance resistances between cell ($m$,$n$) and the surrounding cells; they are all calculated in a similar way. However, the resistance $R_5$ between the fluid and the ($m$,$n$) cell node is calculated so that it is equal to the resistance between the fluid and ¼ of the outside tube wall. $U$ in Equation 4-8 is calculated by adding the convective resistance between fluid and inside tube wall, calculated with the Dittus-Boelter correlation, and the conductive resistance of the tube wall, then taking the inverse of the sum, as shown in Equations 4-9 to 4-11:

$$U = \frac{1}{R_f + R_t} \tag{4-9}$$

$$R_f = \frac{1}{\pi d_i h_p} \tag{4-10}$$

$$R_p = \log(d_o / d_i)/(2\pi K_p) \tag{4-11}$$

Where:

$R_f$ is the thermal resistance between fluid and inside tube wall, in m/W•K or ft•hr/Btu•°F;

$R_p$ is the thermal resistance between inside and outside tube wall, in m/W•K or ft•hr/Btu•°F;

$d_i$ is the inside tube diameter, in m or ft,

$h_p$ is the tube wall convection coefficient, in W/m$^2$•K or Btu/ft$^2$•°F•hr;

$d_o$ is the outside tube diameter, in m or ft;

$K_p$ is the tube conductivity, in W/m•K or Btu/ft•°F•hr ;

The resistance between the fluid and inside tube wall is calculated by Equation 4-10, and the resistance between the inside and outside tube wall is calculated by Equation 4-11, both of which are based on cylindrical tubing, not square tubing.

## 4.3 Boundary Condition and Model Algorithm

As shown in Figure 4.1, the soil domain is bounded by the earth surface, convective basement wall and basement floor, left side adiabatic boundary, right side adiabatic boundary and bottom

side temperature-specified boundary. Initial conditions and the lower boundary conditions are set with the Kusuda and Achenbach (1965) model. The inside basement wall and basement floor boundaries are convective, exchanging heat with the basement, which is assumed to be held at a constant air temperature for the results presented here. The vertical boundaries in the soil domain are assumed adiabatic – on the left hand side, this is due to symmetry; on the right hand side, the size of the domain was set so as to have negligible influence on the result by the right hand boundary.

Fluid inside FHX tubes is treated as a time-dependent inside boundary. The fluid temperature used in the 2D cross-section of FHX tube is the average fluid temperature along the length of the tube. The 2D FHX model assumes that there is no heat transfer in the third dimension and therefore the soil temperature will not change in the third dimension. However, the fluid temperature is changing along the length of the tube. Therefore, the FHX is treated as a soil-fluid heat exchanger in the 3D soil domain and an NTU method is implemented as shown in Equations 4-12 to 4-18:

$$C_{\min} = m_f C_{Pf} \tag{4-12}$$

$$C_{\min} / C_{\max} = 0 \text{, and } C_{\max} \to 0 \tag{4-13}$$

$$NTU = UA / C_{\min} \tag{4-14}$$

$$\varepsilon = 1 - e^{-NTU} \tag{4-15}$$

$$Q_{\max} = C_{\min}(T_i - T_{tw}) \tag{4-16}$$

$$Q_{flu} = \varepsilon Q_{\max} \tag{4-17}$$

$$Q_{flu} = UA(T_f - T_{tw}) \tag{4-18}$$

Where:

$m_f$ is the fluid mass flow rate, in kg/s or lb/s;

$C_{pf}$ is fluid heat capacity, in J/kg•K or Btu/lb•°F,

$T_f$ is the fluid temperature, in °C or °F;

$T_{tw}$ is the tube wall temperature, in °C or °F;

$T_i$ is the inlet fluid temperature, in °C or °F;

$Q_{flu}$ is the heat transfer through the fluid to the tube wall, in W or Btu/hr;

In Equation 4-13, the $C_{\max}$ goes to infinity is based on the assumption that the heat transfers between the soil and fluid will not change the soil temperature in the third dimension. For Equations 4-12 to 4-15, the fluid-soil heat exchanger efficiency can be calculated based on the fluid mass flow rate and heat capacity and *U*, the overall conductance through the fluid to the 1/4 tube outside wall. From Equation 4-16 and 4-17, the average fluid temperature along the length of the tube can be calculated from previous time step inlet fluid temperature $T_i$ and tube wall temperature $T_{tw}$.

## 4.4 Short-Circuiting Heat Transfer

The inside basement wall and basement floor boundaries are convective, which make it possible that the FHX tube is extracting heat from the basement; this will drive up the heating load. This is called short-circuiting heat transfer. For the temperature-conditioned basement, in order to quantify the short-circuiting heat transfer, it is convenient to hold the basement air temperature constant and compare the heat transfer rate (heat extracted from the basement). An unconditioned

basement, for which the short-circuiting heat transfer may be low but for which the basement temperature may vary, can be readily modeled. The method of calculating the short-circuiting heat transfer for both the temperature-conditioned or unconditioned basement will be described here. The short-circuiting heat transfer results will be discussed later in Chapter 7.

For temperature-conditioned basements, the basement air temperature is assumed constant for the entire year, and the heat transfer between the basement air and basement wall $Q_{Bw}$ can be calculated with Equation 4-19. The heat transfer between the basement air and the basement floor $Q_{Bf}$ can be calculated with Equation 4-20. The heat extracted from the basement is the summation of $Q_{Bf}$ and $Q_{Bw}$ :

$$Q_{Bw} = \frac{1}{R_{Bw}}\left(T_a - T_w\right) \qquad (4\text{-}19)$$

$$Q_{Bf} = \frac{1}{R_{Bf}}\left(T_a - T_f\right) \qquad (4\text{-}20)$$

Where:

$Q_{Bw}$ is the heat transfer from the basement air to the basement wall, in W/m$^2$ or Btu/ft$^2$•hr;

$Q_{Bf}$ is the heat transfer from the basement air to the basement floor, in W/m$^2$ or Btu/ft$^2$•hr;

$T_a$ is the constant basement air temperature, in °C or °F;

$T_w$ is the average basement wall temperature, in °C or °F;

$T_f$ is the average basement floor temperature, in °C or °F;

$R_{Bw}$ is the thermal resistance between the basement air and basement wall, in $m^2$•K/W or $ft^2$•°F•hr/Btu;

$R_{Bf}$ is the thermal resistance between the basement air and basement floor, in $m^2$•K/W or $ft^2$•°F•hr/Btu;

Using typical values (McQuiston, et al. 2005, p. 139)"check to see if it is the right place" for film resistances, the thermal resistance between the basement air and the basement wall is taken as 0.12 $m^2$•K/W (0.68 $ft^2$•°F•hr/Btu), and the thermal resistance between the basement air and the basement floor is taken as 0.16 $m^2$•K/W (0.9 $ft^2$•°F•hr/Btu),. Both the basement air temperature, the basement wall and basement floor temperature are known, therefore the heat extracted from the basement can be calculated.

An unconditioned basement can be modeled by holding the house temperature as constant and adding the thermal resistance between basement air and house air, to Equation 4-19 and Equation 4-20. Then the heat transfer between the basement air and the basement wall will be:

$$Q_{total} = \frac{1}{R_{Bw} + R_h}\left(T_a - T_w\right) + \frac{1}{R_{Bf} + R_h}\left(T_a - T_f\right) \qquad (4\text{-}21)$$

Where:

$Q_{total}$ is the total heat extracted from the basement wall and basement floor, in W/$m^2$ or Btu/$ft^2$•hr;

$R_h$ is the thermal resistance between the house air and basement air, in $m^2$•K/W or $ft^2$•°F•hr/Btu

# CHAPTER 5

## FHX ANALYTICAL MODEL

The analytical model relies on superposition of line heat sources, in space and time. Compared to more detailed numerical models, the analytical model makes several approximations:

1. The basement wall is assumed to be adiabatic.
2. The adiabatic basement wall, in effect, extends downward to infinity. This allows the analytical model to be developed using mirror sources, but neglects any heat storage to/from the ground below the basement wall.
3. The analytical model uses the Kusuda and Achenbach (1965) model to predict the undisturbed ground temperature; this is superimposed upon the other inputs (line sources and mirror line sources).
4. Freezing of the soil is not explicitly considered.

Two analytical models are developed; an hourly time-step analytical model implemented in the HVACSIM+ environment and a simplified monthly time-step analytical model implemented in an interpreted language. Both models are based on the approximations listed above. Furthermore, the monthly time-step analytical model simplifies the hourly loads, which are treated as monthly

constant loads and monthly peak loads. The simplified representation of loads gives significantly reduced computation time compared with the numerical model and the hourly time-step analytical model. The simplified model takes less than five minutes in order to size the FHX, even when the algorithm has been implemented in an interpreted language. Therefore, the simplified monthly time-step analytical model can be used as a design tool.

In the analytical model, each FHX tube is represented as a line heat source. The ground surface is treated as being isothermal with an imposed undisturbed ground temperature profile. The basement wall is approximated as an adiabatic vertical surface, of infinite extent. The basement wall and ground surface are represented using a sink/source method, which will be described in Section 5.2. The response of multiple tubes to a single step heat pulse can be determined by superimposing the temperature response of all tubes and their mirrored sinks/sources. Using the superposition, the outer wall temperatures for each tube are calculated. The mean fluid temperature, the average of the entering and exiting fluid temperatures, inside each FHX tube can be calculated from the tube wall temperature, knowing the fluid-to-tube-wall thermal resistance and the heat transfer rate. The exiting and entering fluid temperature can be calculated from the mean fluid temperature, if the heat transfer rate between the fluid and soil, fluid mass flow rate and heat capacity is known.

Furthermore, the actual loads can be represented as a series of step heat pulses which give responses that superimposed in time. This load devolution and superimposing method is described in Section 5.4.

In practice, the step heat pulses used in Section 5.4 are estimated from the building heating and cooling loads. A heat pump model as described in Section 5.5 is used to determine the heat transfer rate to and from the GHE.

The undisturbed soil temperature as a function of depth and time of year is an input to the analytical model and it has great effect on the FHX exiting fluid temperature. The analytical model (1965) relies on the Kusuda and Achenbach model to predict undisturbed ground temperature. It relies upon four empirical parameters-average soil temperature, surface temperature amplitude, soil diffusivity and phase angle at the surface. A model for prediction of the Kusuda and Achenbach parameters based on TMY3 weather data and a one-dimensional conduction heat transfer model has been developed and introduced in Chapter 3. The Kusuda and Achenbach model is described in Section 5.3.

## 5.1 Single FHX Tube

Single FHX tube, buried in a homogeneous, infinite medium can be treated as a line heat source. The line source theory assumes that the line heat source (FHX tube) rejects/extracts a certain amount of heat $q$ to the earth in the radial direction only; the heat is absorbed/rejected by the earth in a cylinder of radius $r_\infty$ surrounding the tube. The earth temperature inside the cylinder will be affected by the line heat source. Outside the cylinder, which has a distance *r* greater than $r_\infty$ from the center of the line source, the earth temperature will be the undisturbed ground temperature $T_\infty$. Line source theory and simplified equations for the Kelvin line source equation have been explained in Chapter 2. Hart and Couvillion (1986) integrated the line source equation and derived a new equation which calculates the time-dependent cylinder boundary $r_\infty$ and define the temperature distribution surrounding the tube, which has a radius $r_o$:

$$t \cdot \alpha_s = 0.0649 \cdot r_\infty{}^2 + 0.2409 \cdot r_o{}^2 - \frac{r_o{}^2}{2} \cdot \ln \frac{r_\infty}{r_o} \qquad (r_o \le r_\infty < 15 r_o) \qquad \text{(5-1)}$$

$$r_\infty = 4\sqrt{\alpha_s t} \qquad (r_\infty \ge 15 r_o) \qquad \text{(5-2)}$$

$$T'(r,q,t) = (\frac{q}{4 \cdot \pi \cdot k_s}) \times [\ln \frac{r_\infty}{r} - 0.9818 + \frac{4 \cdot r^2}{2 \cdot r_\infty{}^2} - \frac{1}{4 \cdot 2!} \cdot (\frac{4 \cdot r^2}{r_\infty{}^2})^2 + \mathsf{L} + \frac{(-1)^{N+1}}{2 \cdot N \cdot N!} \cdot (\frac{4 \cdot r^2}{r_\infty{}^2})^N]$$

$$(r_o \le r_\infty) \qquad (5\text{-}3)$$

Where:

$t$ is the simulation time, in s;

$r_\infty$ is the radius of an imaginary cylinder surrounding the tube, which is assumed to absorb all the heat rejected by the tube, and which varies with time, in m or ft;

$r_o$ is the FHX tube outside wall radius, in m or ft;

$r$ is the distance from the center of the tube to the earth, at which the temperature response need to be obtained, in m or ft;

$T'(r,q,t)$ is the temperature change of the earth, at a distance r from the center of the tube, in response to a single heat pulse $q$ for a period of time $t$, in °C or °F;

$q$ is heat rejected or absorbed by the tube per unit length, in W/m or Btu/ft•hr;

$\alpha_s$ is soil thermal diffusivity, in $m^2/s$ or $ft^2/s$;

$k_s$ is soil thermal conductivity, in W/m•K or Btu/ft•°F•hr;

The value of $r_\infty$ can be determined by Equations 5-1 and 5-2. In practice, Equation 5-2 is evaluated first. When the value of $r_\infty$ obtained by Equation 5-2 is 15 times greater than $r_o$, the value of $r_\infty$ is maintained. If the value of $r_\infty$ obtained by Equation 5-2 was between the value of $r_o$ and $15r_o$, $r_\infty$ will be determined by Equation 5-1. Equation 5-3 defines the temperature change

of the earth surrounding the FHX tube when $r \geq r_o$. Evaluating Equation 5-3 at $r = r_o$, and superimposing the undisturbed ground temperature, one may obtain the temperature of any arbitrary point $\alpha$ on the tube outside wall:

$$T_{o,\alpha} = T'(r_o, q, t) + T_{UG}(y_\alpha, t_c) \qquad (5\text{-}4)$$

Where:

$T_{o,\alpha}$ is the temperature of the point $\alpha$ on the tube outside wall, in °C or °F;

$T'(r_o, q, t)$ is the temperature change of the point $\alpha$, in response to a single heat pulse $q$ for a period of time $t$, in °C or °F;

$q$ is heat rejected or absorbed by the tube per unit length, in W/m or Btu/ft•hr;

$r_o$ is the FHX tube outside wall radius, in m or ft;

$t$ is the simulation time, in s;

$T_{UG}(y_\alpha, t_c)$ is the undisturbed ground temperature at the point $\alpha$, which is a function of depth and time of the year, in °C or °F;

$y_\alpha$ is the depth of the point $\alpha$, in m or ft;

$t_c$ is the calendar time in days start with at midnight, January 1, in day;

According to Equation 5-4, the temperature of any point $\alpha$ on the tube outside wall is determined by superimposing the temperature change $T'$ and the undisturbed soil temperature $T_{UG}$ at the point. The temperature change of the point is determined by the tube outside wall radius $r_o$, heat transfer rate $q$ and simulation time t. $T_{UG}$ is a function of depth $y_\alpha$ and time of the year $t_c$.

Different points on the tube outside wall surface are at different depths; therefore, the value of $T_{UG}$ varies for different points, and the wall temperature of different point varies depending on depth. The outside tube wall temperature $T_o$, which is supposed to be the average temperature the tube outside wall surface, is represented as the average temperature of four points 1, 2, 3 and 4 as shown in Figure 5-1 on the tube wall surface in the analytical model:

$$T_o = \frac{1}{4}\sum_{\alpha=1}^{4} T_{o,\alpha} \qquad (5\text{-}5)$$

Where:

$T_o$ is the tube outside wall temperature, in °C or °F;

$T_{o,\alpha}$ is the temperature of the point $\alpha$ on the tube outside wall, in °C or °F;

The four points used in Equation 5-5 are located symmetrically and uniformly on the tube wall. According to the study, the temperature differences between each two of the four points are no more than 0.05 °C (0.09 °F) even in August.

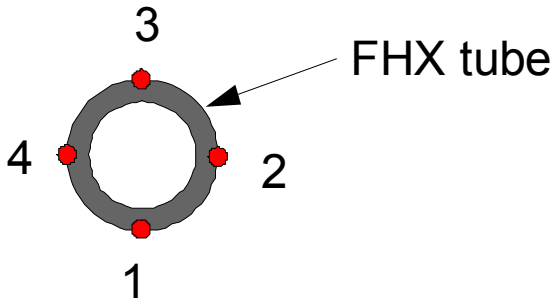


Figure 5.1: The schematic of a single FHX tube

The mean fluid temperature inside the tube, which is an average of tube entering and exiting fluid temperatures, can be calculated from the tube outside wall temperature by Equation 5-6, if the

fluid-to-tube-wall thermal resistance and the heat transfer rate is known. Equation 5-6 is a one-dimensional and steady-state heat transfer equation. It assumes that the heat rejected/absorbed by the tube is only transferred in the radial direction; there is no temperature gradient along the length of the tube. Equation 5-7 gives the resistance between the fluid and inside surface of the tube $R_f$; the fluid convective coefficient $h_f$ is calculated with the Dittus-Boelter correlation. Equation 5-8 gives the conductive resistance of the tube wall $R_t$:

$$T_f - T_o = q(R_f + R_t) \tag{5-6}$$

$$R_f = \frac{1}{2\pi r_i h_f} \tag{5-7}$$

$$R_t = \frac{1}{2\pi k_t} \ln(\frac{r_o}{r_i}) \tag{5-8}$$

Where:

$T_o$ is the tube outside wall temperature, calculated by Equation 5-5 , in °C or °F;

$T_f$ is the fluid temperature inside the FHX tube, in °C or °F;

$R_f$ is the thermal resistance between the fluid and tube inside wall, in m•K/W or ft•°F•hr/Btu;

$R_t$ is the thermal resistance between the tube inside wall and outside wall, in m•K/W or ft•°F•hr/Btu;

$q$ is heat rejected or absorbed by the FHX tube per unit length, in W/m or Btu/ft•hr;

$k_t$ is FHX tube conductivity, in W/m•K or Btu/ft•°F•hr;

$h_f$ is FHX tube convection coefficient, in W/m$^2$•K or Btu/ft$^2$•°F•hr;

$r_o$ is the FHX tube outside wall radius, in m or ft;

$r_i$ is the FHX tube inside wall radius, in m or ft;

The tube exiting fluid temperature can be calculated from the mean fluid temperature. Equation 5-9 is derived based on the energy balance assumption. It assumes that heat rejected/extracted from the earth $Q$ by the tube is totally absorbed by the fluid inside the tube. The mean fluid temperature $T_f$ is the average of tube entering and exiting fluid temperature, so that $2(T_{out} - T_f)$ is equal to the temperature difference of entering and exiting fluid temperatures. The total heat absorbed in the fluid $Q$ is equal to $2(T_{out} - T_f)\dot{m}\,c_{pf}$ :

$$T_{out} = T_f + \frac{Q}{2\dot{m}\,c_{pf}} \qquad (5\text{-}9)$$

Where:

$T_{out}$ is the exiting fluid temperature, in °C or °F;

$T_f$ is the fluid temperature inside the FHX tube, in °C or °F;

$Q$ is the total heat rejected/extracted by the tube, in W or Btu/hr;

$\dot{m}$ is the mass flow rate of the fluid, in kg/s or lb/s;

$c_{pf}$ is the fluid heat capacity, in J/kg•K or Btu/lb•°F;

The fluid temperature described in Section 5.1 and 5.2 represents the mean fluid temperature, or average temperature of the tube entering and exiting fluid temperature. In infinite space, the fluid temperature of a single FHX tube, in response to a step heat pulse can be calculated from Equations 5-1 to 5-8. In practice, there are multiple FHX tubes buried in the soil domain, furthermore, the soil domain is bounded by the basement wall and ground surface. The fluid temperature of each FHX tube is affected by the boundary conditions. The ground surface and the basement wall will be accounted by using the sink/source method.

## 5.2 Sink/Source Method

The ground surface is being treated as isothermal and imposed with undisturbed ground temperature profile. This is accounted by adding a mirrored line sink symmetrically above the line source as shown in Figure 5.2. The basement wall is assumed as an adiabatic vertical surface, extending to infinity, by placing mirrored heat sources symmetric on the other side of the basement wall. Another mirrored heat sink is located above the ground surface, on the other side of the basement, in order to make the above surface basement wall adiabatic and the basement isothermal. Individual tube locations are specified in Cartesian coordinates relative to the building foundation; mirrored sources and sinks are automatically located.

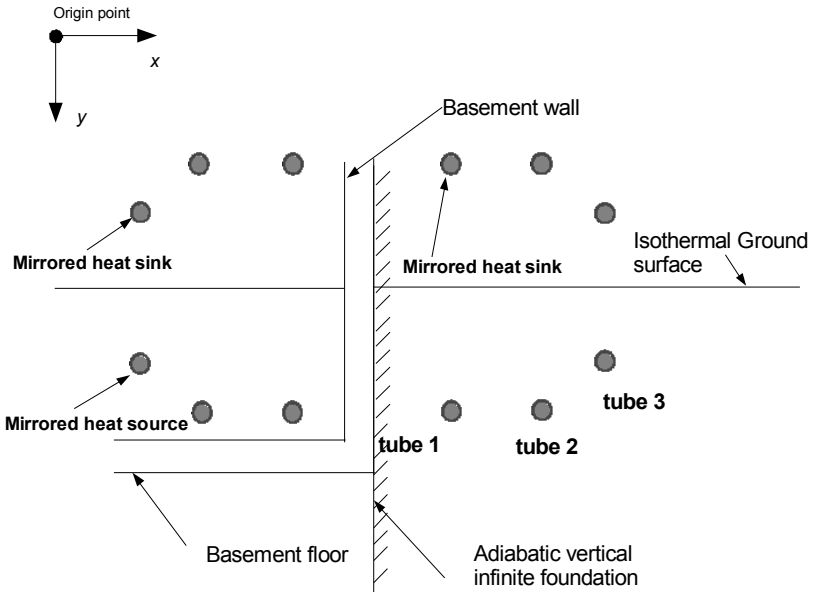


Figure 5.2: Application of mirror-image sources and sinks

As shown in Figure 5.2, three FHX tubes are located under the ground, their mirrored sinks and sources are automatically located. All the tubes are assumed to have the same heat transfer rate $q$ all the time. The temperature response of the earth, in which multiple tubes are buried, can be obtained by superimposing the temperature change, in response to each tube, sink and source. Thus, in Figure 5.2, the temperature change of arbitrary point $\alpha$, which is on the tube $j$ outside wall surface, is the summation of temperature responses at the point due to tube 1, 2, 3 and their mirrored sinks and sources, which is the term $\sum_{i=1}^{m} T'\left(r_{ij,\alpha}, q, t\right)$ in Equation 5-10. The temperature of point $\alpha$ is the undisturbed soil temperature at the point $T_{UG}$ superimposed with the temperature change. For each tube $j$, the outside wall temperature is the average temperature of four points located on the tube $j$ outside wall surface:

$$T_{oj}(q,t) = \frac{1}{4}\sum_{\alpha=1}^{4}\left( T_{UG}\left(y_{j,\alpha}, t_c\right) + \sum_{i=1}^{m} T'\left(r_{ij,\alpha}, q, t\right)\right) \qquad (5\text{-}10)$$

Where:

$T_{oj}(q,t)$ is the outside wall temperature of the tube $j$, in response to the single heat pulse $q$ for a period of time $t$, in °C or °F;

$j$ is the FHX tube number, which could be tube 1, 2 or 3 in Figure 5.2;

$q$ is heat rejected or absorbed by each tube per unit length, in W/m or Btu/ft•hr;

$t$ is the simulation time, in s;

$T_{UG}(y_{j,\alpha},t_c)$ is the undisturbed ground temperature of any point $\alpha$ at the outside wall of tube $j$, which is a function of depth and time, in °C or °F;

$y_{j,\alpha}$ is the depth of the point α on the tube $j$ outside wall surface, in m or ft;

$\alpha$ is the point number, which could be point 1, 2, 3 or 4 in Figure 5.1;

$t_c$ is the calendar time in days start with at midnight, January 1, in day; $T'(r_{ij,\alpha},q,t)$ is the temperature change of point $\alpha$ at the tube $j$ wall surface, in response to heat source $i$, it could be one of the FHX tubes, or their sinks/sources, in °C or °F;

$m$ is the total number of all the FHX tubes , their sinks and sources, this would be 12 in Figure 5.2;

$i$ is the number of the heat source/sink, or the FHX tubes in Figure 5.2, the FHX tubes are numbered 1,2,3, the sources and sinks are numbered 4-12;

$r_{ij,\alpha}$ is the distance between the point α on the tube $j$ outside wall and center of the $i_{th}$ heat sources, which could be any one of the tubes, heat sources, or heat sinks, in m or ft;

Similar to Equation 5-6, the fluid temperature of tube $j$ can be calculated with the outside tube wall temperature, heat transfer rate and the thermal resistance between the fluid and tube outside wall:

$$T_{fj}(q,t) = T_{oj}(q,t) + q(R_{fj} + R_{tj}) \quad (5\text{-}11)$$

Where:

$T_{fj}(q,t)$ is the fluid temperature inside the tube $j$, in response to the single heat pulse $q$ for a period of time $t$, in °C or °F;

$T_{oj}(q,t)$ is the outside wall temperature of the tube $j$, in response to the single heat pulse $q$ for a period of time $t$, in °C or °F;

$R_{fj}$ is the thermal resistance between the fluid and tube $j$ inside wall, in m•K/W or ft•°F•hr/Btu;

$R_{tj}$ is the thermal resistance between the tube $j$ inside wall and outside wall, in m•K/W or ft•°F•hr/Btu;

Over all, in a finite soil domain, bounded by the isothermal earth surface and vertical adiabatic basement wall which extends to infinity, the same heat pulse $q$ is imposed on the center of each FHX tube for a period of time, the outside wall temperature and mean fluid temperature of any tube can be calculated by Equations 5-10 and 5-11 respectively.

## 5.3 Undisturbed Ground Temperature

The undisturbed ground temperature is required as a function of depth and time for the analytical model and it has great effect on the FHX tubes' performance. The analytical model is based on the Kusuda and Achenbach model to predict undisturbed ground temperature versus time of year and depth. It relies upon four empirical parameters-average soil temperatures, surface temperature amplitude, soil diffusivity and phase angle at the surface:

$$T_{UG}(y,t_c) - T_{\infty A} = -SAe^{-\sqrt{\frac{\pi}{365\alpha_s}}y} \cos[\frac{2\pi}{365}(t_c - pl) - \sqrt{\frac{\pi}{365\alpha_s}}y] \qquad (5\text{-}12)$$

Where;

$T_{UG}(y,t_c)$ is the undisturbed ground temperature in depth $y$ and $t_c$ day, in °C or °F;

$y$ is the depth, in m or ft;

$t_c$ is the calendar time in days start with at midnight, January 1, in day;

$T_{\infty A}$ is the average soil temperature of different time and depth, in °C or °F;

$SA$ is the surface temperature amplitude, in °C or °F;

$pl$ is the phase lag, the day minimum surface temperature occurs, in days;

$\alpha_s$ is soil thermal diffusivity, in $m^2/s$ or $ft^2/s$;

In the continental U.S. average soil temperature may be estimated from a map based on Collin's (1925)original measurements; surface temperature amplitude may be estimated from a map based on Chang (1958); soil diffusivity may be estimated from physical measurement of a specific soil.

Kusuda and Achenbach showed that for a handful of continental U.S. sites, minimum surface temperature occurring between phase lags of 26 and 44 days.

However, the above procedures for estimating undisturbed ground temperature are limited in applicability to the continental U.S. and they are hard to read accurately. A model for prediction of the Kusuda and Achenbach parameters based on TMY3 weather data and a one-dimensional conduction heat transfer model is developed and has been described in detail in Chapter 3. It is similar to the two-dimensional numerical model described above, except, it does not account for the foundation or FHX tubing. The one-dimensional undisturbed ground temperature model has been validated against sub-surface measurements made at weather stations in Oklahoma and at stations throughout the US maintained by the USDA Soil Climate Analysis Network.

The soil diffusivity could also be estimated from empirical equations. According to previous study on the modeling of soil conductivity and soil heat capacity (Hendrickx, et al. 2003; Cote and Konrad 2005; Lu, et al. 2007), the soil properties are mostly determined by the water content, the percent of clay and sand in the soil. Figures 5.3 and 5.4 are the sample plots of soil thermal properties vs. water content in Oklahoma. The sample soil used for modeling has around 29% quartz, the bulk density is 1330 $Kg/m^3$ (83 $lb/ft^3$), and saturated water content is 0.5. In Figure 5.3, all four models predict the thermal conductivity increases when the water content increases, and the speed of increasing decreases. As shown in Figure 5.4, the modeled heat capacity is linearly proportional to the water content.

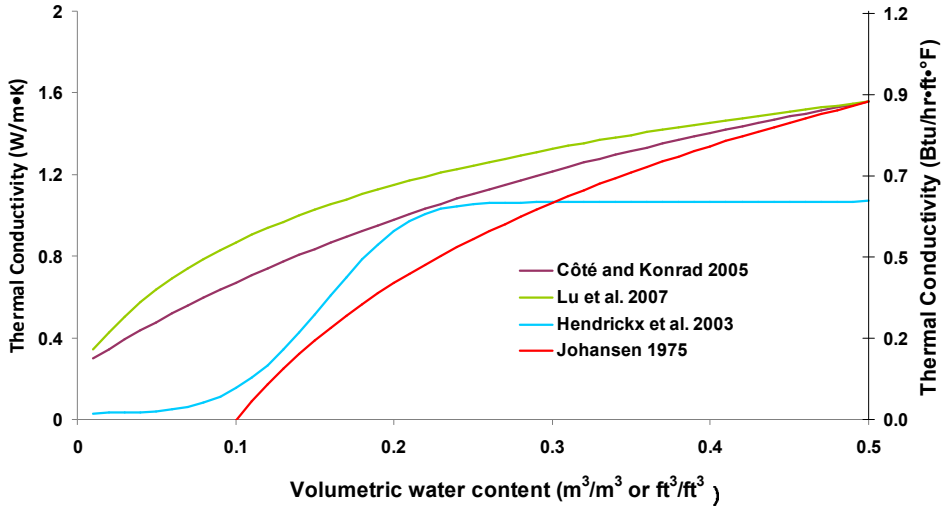


Figure 5.3: Thermal conductivity vs. water content in certain location in Oklahoma

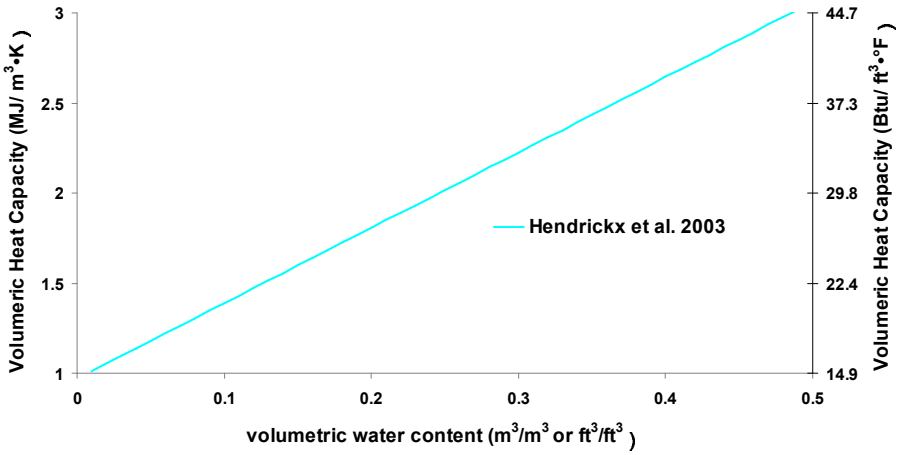


Figure 5.4: Thermal heat capacity vs. water content in certain location in Oklahoma

## 5.4 Load Devolution Superimposition Method

The total number of tubes, tube locations relative to the building foundation, tube conductivity, the soil conductivity, soil heat capacity, four empirical parameters used in Kusuda and Achenbach model are inputs for the analytical model. The fluid temperature of each FHX tube

can then be represented as a function of heat pulse and simulation time *t*. Once the fluid temperature of each tube is represented with a function, the fluid temperature of any tube, in response to any arbitrary heat rejection/extraction function can be determined, by devolving the heat rejection/extraction into a series of step functions, and superimposing the response to each step function. For hourly and monthly time-step analytical model, the processes of devolving loads are slightly different from each other.

The process of devolving loads in the hourly analytical model is graphically demonstrated in Figure 5.5, for $t_e$ hours of heat rejection/extraction from the tube to the earth. It is assumed that each FHX tube is applied with the same heat pulse at any time. The basic heat pulse from zero to $q_1$ is applied on tube $j$ for the entire duration of $t_e$ hours and is effective as $q_1' = q_1$. The subsequent pulses are superimposed as $q_2' = q_2 - q_1$ effective for $t_e - 1$ hours, $q_k' = q_k - q_{k-1}$ effective for $t_e - t_{k-1}$ hours and finally $q_e' = q_e - q_{e-1}$ effective for 1 hour. The heat pulse applied on each tube is calculated from hourly heating and cooling loads applied on the heat pump; the heat pump model is introduced in Section 5.5. Therefore, the temperature response of each FHX tube to the actual hourly loads $q_e$, at the end of $t_e$, is calculated by superimposing the temperature response to the devolved loads $q_k' = q_k - q_{k-1}$ for a period of $t_k' = t_e - t_{k-1}$, which becomes $\sum_{k=1}^{e} T'(q_k', t_k')$, as shown in Figure 5.6.

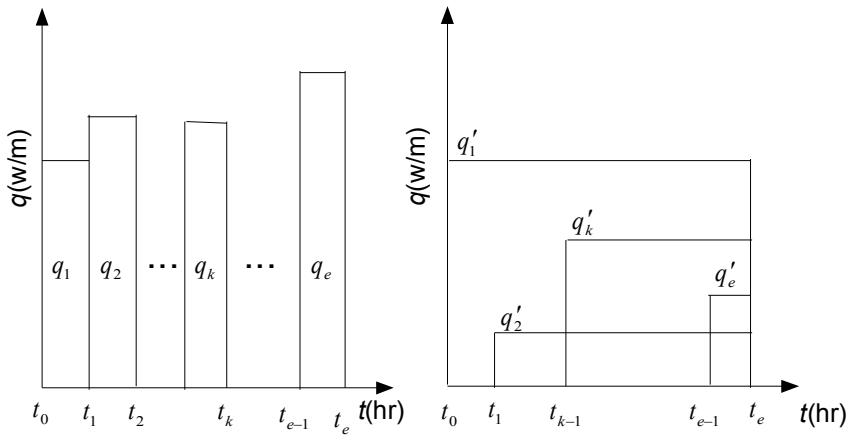


Figure 5.5 Loads devolution method (hourly loads)

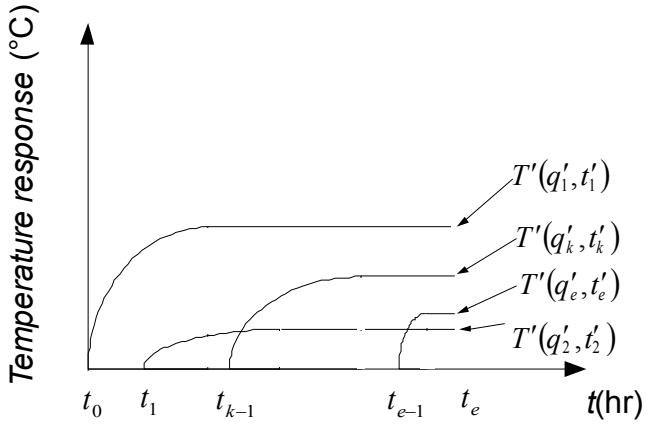


Figure 5.6 Temperature response superimposition method (hourly loads)

The temperature response of point $\alpha$ at the tube $j$ outside wall surface, at the end of $e^{th}$ hour, can be determined by adding the temperature response to *m* heat sources (including all the tubes and their sinks/sources), for the $e$ step functions, and it becomes the term of $\sum_{k=1}^{e}\sum_{i=1}^{m} T'\left(r_{ij,\alpha}, q_k - q_{k-1}, t_e - t_{k-1}\right)$ in Equation 5-13. The temperature of point $\alpha$ is the summation of the temperature response and undisturbed soil temperature. The outside wall temperature of tube $j$ is represented as the average temperature of four points on the outside wall of tube $j$:

$$T_{oj} = \frac{1}{4}\sum_{\alpha=1}^{4}\left(\sum_{k=1}^{e}\sum_{i=1}^{m} T'\left(r_{ij,\alpha}, q_k - q_{k-1}, t_e - t_{k-1}\right) + T_{UG}\left(y_{j,\alpha}, t_c\right)\right) \quad (5\text{-}13)$$

$$T_{fj} = T_{oj} + q_e\left(R_{fj} + R_{ij}\right) \quad (5\text{-}14)$$

Where:

$T_{fj}$ is the mean fluid temperature inside tube $j$, at the end of the $e^{th}$ hour, in °C or °F;

$T_{oj}$ is the tube $j$ outside wall temperature, at the end of the $e^{th}$ hour, in response to any arbitrary heat rejection or extraction of the tube to the earth, in °C or °F;

$T'\left(r_{ij,\alpha}, q_k - q_{k-1}, t_e - t_{k-1}\right)$ is the temperature change of point $\alpha$ at the tube $j$ wall surface, in response to heat source/sink or FHX tube $i$, due to the heat pulse $q_k - q_{k-1}$, at the period of time $t_e - t_{k-1}$ hours, in °C or °F;

$r_{ij,\alpha}$ is the distance between the point $\alpha$ at the outside wall of tube $j$ and center of any heat source/sink or FHX tube $i$, in m or ft;

$q_k$ is heat rejected or absorbed by FHX tube $j$ per unit length during the $k^{th}$ hour, in W/m or Btu/ft•hr;

$t_e$ is the entire duration, in hour/month;

$t_k$ is the kth hour during the simulation , in hour;

$R_{fj}$ is the thermal resistance between the fluid and tube $j$ inside wall, in m•K/W or ft•°F•hr/Btu;

$R_{tj}$ is the thermal resistance between the tube $j$ inside wall and outside wall, in m•K/W or ft•°F•hr/Btu;

$j$ is the number of the tube, for example, tube 1, 2 or 3;

$T_{UG}\left(y_{j,\alpha}, t_c\right)$ is the undisturbed ground temperature of the point $\alpha$ at the outside wall of tube $j$, which is a function of depth $y_{j,\alpha}$ and time $t_c$ days, in °C or °F;

$y_{j,\alpha}$ is the depth of point $\alpha$ at the outside wall of the tube $j$, in m or ft;

$t_c$ is the calendar time in days start with at midnight, January 1, in day;

m is the total number of all the FHX tubes , their sinks and sources;

Equation 5-14 calculates the fluid temperature inside tube *j* at the end of $e^{th}$ hour. The analytical model assumes all FHX tubes have the same exiting fluid temperature and entering fluid temperature, which is the average temperature of all FHX tubes.

The process used for the monthly analytical model is graphically demonstrated in Figure 5.7, for $t_e$ months of heat rejection/extraction from the tube to the earth. The heat transfer rate $q$ apply on each tube, shown in Figure 5.7, is monthly values with monthly peak heat pulse, it is converted from actual hourly heat pulse used in the hourly model. The procedure of determine the monthly value and peak heat pulse is introduced in Section 5.5. Mean fluid temperature of each tube at the end of $e^{th}$ month can be calculated by Equation 5-13 and 5-14, with exact the same procedure described above. The minimum and maximum FHX ExFT at the end of month *e* can be calculated by adding the temperature response of the monthly peak loads $q_{pe} - q_e$ to the FHX exiting fluid temperature at the end of the month *e*. Calculation of the exiting fluid temperature at

the end of each month could be accomplished by applying Equation 5-9, knowing the mean fluid temperature.

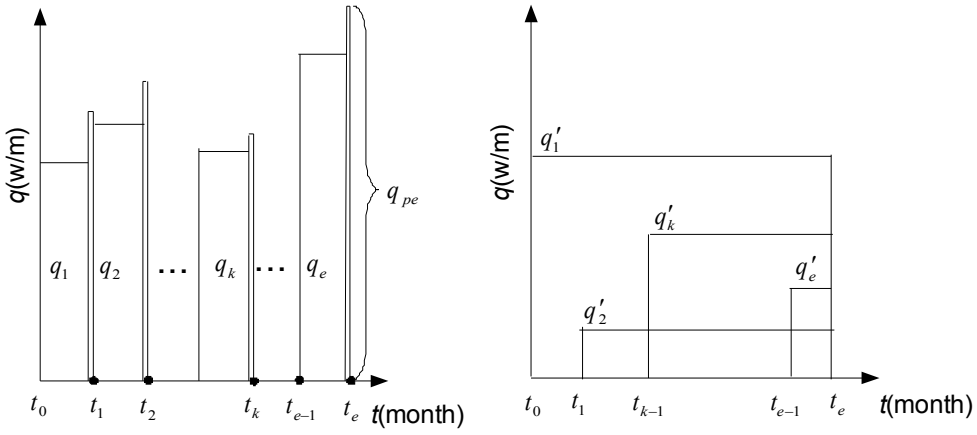


Figure 5.7 Loads devolution method (monthly loads)

## 5.5 Heat Pump Model

It is assumed that the FHX analytical model is connected to a heat pump model in series. Hourly heating and cooling loads applied on the heat pump are estimated from a building simulation program, such as EnergyPlus. Users are required to input the information of the modeled building, including geometry, construction information, internal heat gains and weather data. Then the program will estimate the hourly heating and cooling loads of the building.

The model uses two polynomial equations to relate heating loads to heat extraction and cooling loads to heat rejection:

$$NHq_k = Q_{hk}\left(C_1T_{out}^0 + C_2T_{out}^1 + C_3T_{out}^2\right) - Q_{ck}\left(C_4T_{out}^0 + C_5T_{out}^1 + C_6T_{out}^2\right) \qquad (5\text{-}15)$$

Where:

$Q_{hk}$ is the building heating load for $k^{th}$ hour/month, in W or Btu/hr;

$Q_{ck}$ is the building cooling load for $k^{th}$ hour/month, in W or Btu/hr;

$T_{out}$ is the FHX ExFT (or heat pump EFT) for the $k^{th}$ hour/month, in °C or °F;

$q_k$ is the heat pulse applied on each tube per unit length for the $k^{th}$ hour/month, in W/m or Btu/Ft•hr;

$N$ is the total number of the FHX tubes;

$H$ is the length of the FHX tubes, in m or ft;

$C_n$ is value used for determining the ratio of heating or cooling, $n$ could be 1, 2, etc;

For a specific heat pump, the ratio of heating/cooling at different heat pump EFT can be calculated from the data provided by the manufacture. The value of $C_n$ can then be found by curve fitting the manufacturer's data.

For hourly time-step analytical model, the hourly heat pulse applied on each tube, used in Figure 5.5, can be calculated by Equation 5-16, knowing the building hourly heating and cooling loads and the coefficients $C_1$ - $C_6$. For the monthly time-step analytical model, the actual hourly loads applied to the heat pump are represented as two components-a monthly average load, applied over the whole month, and a monthly peak load, typically applied over a period of 1-8 hours at the end of the month. The procedure of determining the peak load magnitude and duration is described by Cullin (2008), knowing building hourly heating and cooling loads for a full year. The heat pulse applied on each tube, shown in Figure 5.7, which is constant heat pulse over the whole month and a peak heat pulse at the end of the month, can be calculated by Equation 5-16, knowing the building monthly loads and peak load at the end of the month.

# CHAPTER 6

## VERIFICATION AND EXPERIMENTAL VALIDATION

Verification and experimental validation of the FHX numerical is presented in this chapter. The explicit finite volume numerical model described in Chapter 4 is implemented in the HVACSIM+ environment; It utilizes a full heat balance at the earth surface including short wave radiation, long wave radiation, convection heat transfer and evapotranspiration. HVACSIM+ stands for HVAC Simulation Plus other systems, was developed at the National Bureau of Standards (NBS), which provides advanced equation solving techniques to perform dynamic simulations of the building/HVAC systems. The bottom boundary is temperature-specified, which is calculated from the Kusuda and Achenbach model. The left side boundary is connected to the temperature-conditioned or un-conditioned basement. The right side boundary is set to be adiabatic, at the distance far away from the FHX pipes. Non-uniform grids have been used. The number of FHX tubes, tubes distance relative to the basement, tube depths and tube configurations are defined by the users.

Section 6.1 introduces the verification of the FHX numerical model, the time step independency test and non-uniform grid test are performed. The analytical validation of numerical model, which compares the numerical model result to line source for step pulse, is introduced in Section 6.2. Section 6.3 covers the numerical model validation against experimental data for a period of 10

months, starts on January 1st, 2010. The experimental data is collected from a two-story house built in Oak Ridge, Tennessee, by the Oak Ridge National Laboratory Team. The undisturbed soil temperature at multiple depths, the FHX exiting fluid temperature (heat pump entering fluid temperature), the temperature at the FHX tube wall and disturbed soil temperature near the FHX tubes at multiple depths are validated.

## 6.1 FHX Numerical Model Verification

Section 6.1 includes the time step independency and non-uniform test. Time step independency test are designed for showing the numerical model result are independent of the time steps used in the numerical model. The non-uniform grid test is performed by comparing the simulation results with non-uniform grid and the uniform grid implemented in the numerical model, which verifies the accuracy of non-uniform grid scheme implemented in the numerical model.

### 6.1.1 Time Step Independency Test

Because the FHX numerical model is included in the HVACSIM+ package as a modular component, there are two time steps used; HVACSIM+ time step and internal FHX model time step. HVACSIM+ has a variable time step that can be constrained or fixed by the users. The internal FHX model time step is the time step used for solving the finite volume equations in the FHX model. Both time step independency have been tested. Figure 6.1 shows the calculated FHX exiting fluid temperature (ExFT) of numerical model in response to a constant building heating load of 1kw (3412.1 Btu/hr) during a period of 24 hours, for selected HVACSIM+ time step at 300 second, 900 second and 3600 second. The minimum HVACSIM+ time step can be chosen for this model is 300 s. Results show that the variation of HVACSIM+ time step has very small effect on the simulation result. Figure 6.2 shows the simulation result of numerical model is independent of internal numerical model time step. The simulation is run with internal numerical model time step of 25 second, 50 second and 100 second. For the simulation, the HVACSIM+

time step is fixed at 3600 second. The internal numerical model time step is calculated by the FHX numerical model itself, for each HVACSIM+ time step. It is the maximum time step which allows the explicit method used in the model to be numerically stable.

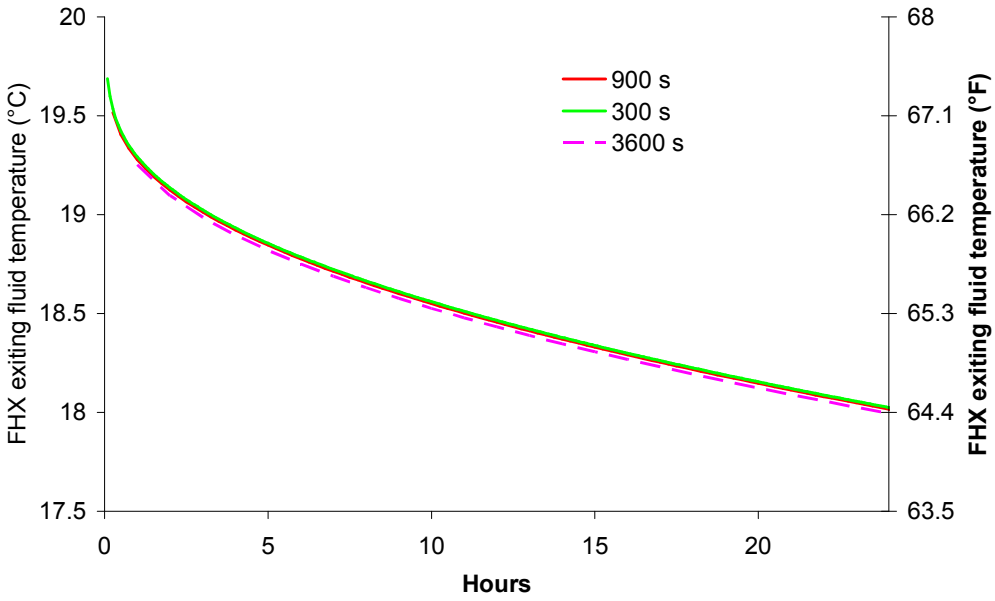


Figure 6.1: HVACSIM+ time step independency study

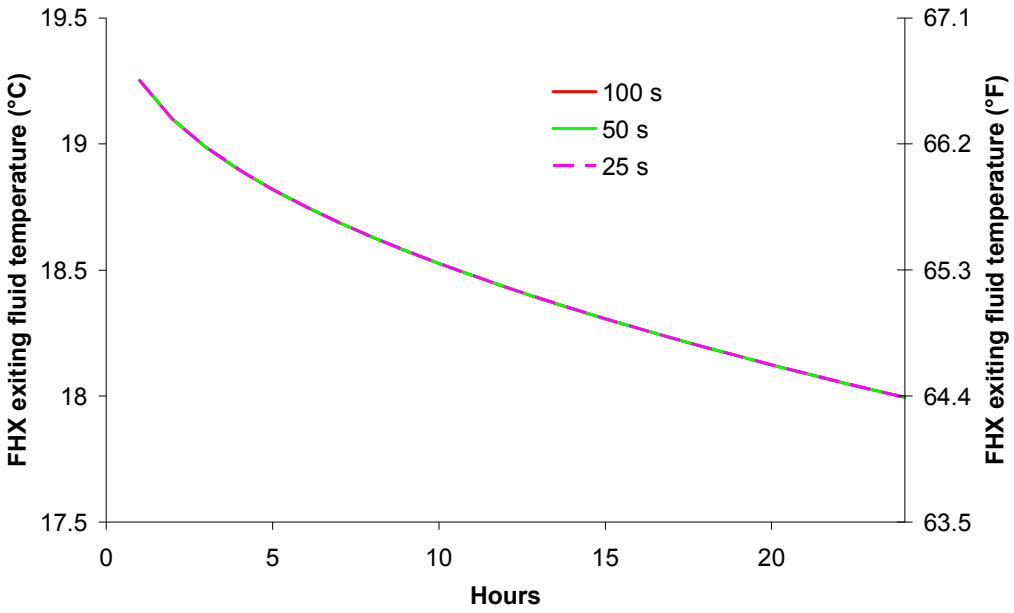


Figure 6.2: Inter numerical model time step independency study

### 6.1.2 Non Uniform Grid Test

In order to save the computational time, a non-uniform grid is implemented in the numerical model; a detailed discussion of the non-uniform grid is given in Section 4.1. The non uniform grid test is designed to ensure the non-uniform grid scheme implemented in the numerical model is defined properly. The simulation result with non-uniform grid implemented are compared to the result utilizes the uniform grid, as shown in Figure 6.3. Six FHX tubes are chosen for the test, the tube locations are chosen based on the experimental set up, which is, three tubes are in a horizontal line at the depth of 1.52 m and the other three tubes are in slope. The accurate location of each tube is shown in Figure 6.7. Once the tube location is fixed in the simulation, the user can define the cells numbers between each of two tubes, and between the tubes and simulation boundaries. The model will automatically calculate the expansion ratio of the non-uniform grid, based on the distance of two tubes and the cell numbers defined by the users. The curve marked "non-uniform grid" represents the calculated FHX ExFT from the numerical model which utilizes 123 x 116 (14268) non-uniform grid. The curve marked "uniform grid" represents the result from numerical model which utilize the close to uniform grid by adjusting the expansion ratio of the non-uniform grid to near 0, a number of 169 x 144 (24336) grid has been used. As shown in Figure 6.3, the result of numerical model with non-uniform grid or uniform grid is only 0.06 °C (0.11 °F) difference, at the end of 72 hours. This test served to gain some confidence in the non-uniform grid utilized for the experimental validation, introduced in Section 6.3. However, the grid expansion ratio should be carefully adjusted so that it will not decrease computational time at a big cost of result accuracy. For the geometry used in this test, it is suggested that the grid expansion ratio is kept within the range of 10%-20%.

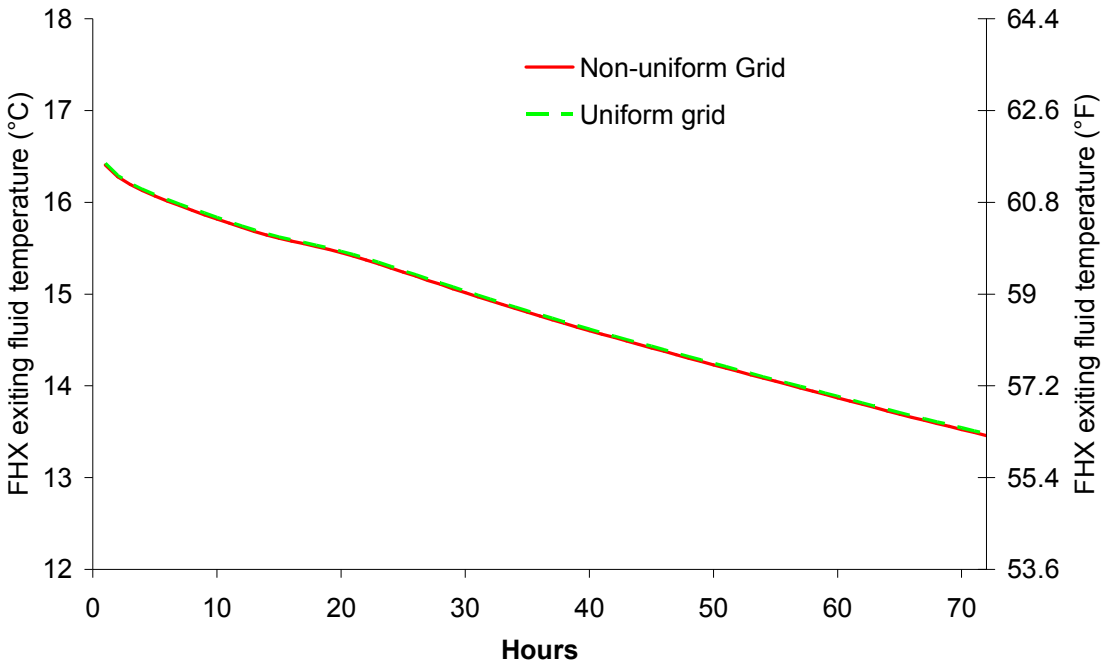


Figure 6.3: Non-uniform grid test

## 6.2 Analytical Validation of Numerical Model

The numerical model is validated against the analytical solution (line source), by comparing the temperature response of a single tube to a step heat pulse using the two models. During the test, both the numerical model and line source are set to an initial uniform soil temperature, 17 °C (62.6 °F). The tube extracts heat constant rate of 9.6 W/m (10.0 Btu/hr•ft) from the ground continually. The thermal resistance between the fluid and tube outside wall is set to be constant value of 9.8 W/m•K (68 Btu/hr•ft$^2$•°F). The result of the validation is shown in Figure 6.4. The two curves represent the calculated FHX ExFT from the line source model and FHX numerical model respectively. The two model results are about 0.03 °C (0.05 °F) difference at the beginning of the simulation, the difference gradually increases to 0.25 °C (0.45 °F) after 10 hour, and stays almost constant until the end of 240 hr. The comparison of the FHX ExFT calculated from the

numerical model to the line source model result gains more confidence of the accuracy of the numerical model. The numerical model represents the FHX tube as a square tube and calculates the tube wall temperature as an average temperature of four nodes located on the square tube, the accuracy of this method is now tested with analytical solution.

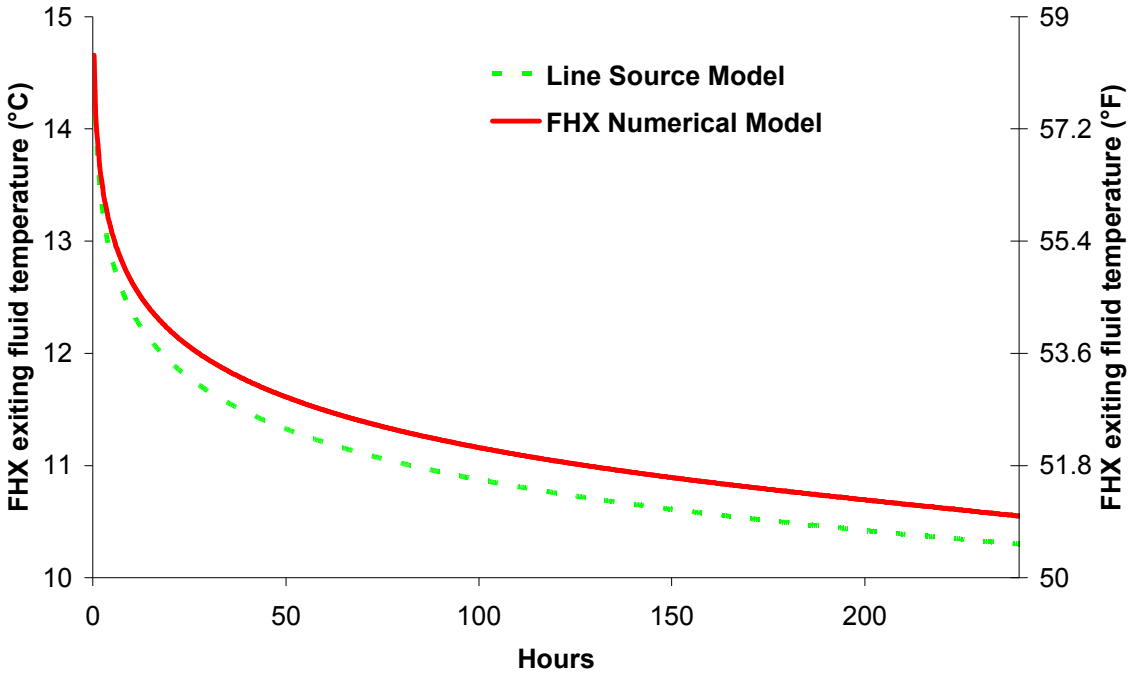


Figure 6.4: FHX analytical model test against FHX numerical model

## 6.3 Experimental Validation

The FHX numerical model is validated with experimental data collected by the ORNL team from a very well insulated house located in Oak Ridge, Tennessee. The house built with structural insulated panel, is shown in Figure 6.5. The geometry of the house and the tube configurations is shown in Figure 6.6. There are three types of tubes have been implemented in the experiment. The site marked “rain garden” represents the sites where conventional horizontal ground heat

exchangers are buried, under the "rain garden". The rain garden is a place where various plants grow for capturing or using rainwater that may run off. The sites marked “Conventional Earth” is the sites where traditional horizontal ground heat exchangers are buried in. The tubes locate near the west and north wall of the house are the foundation heat exchanger tubes. There are six tubes in parallel, three of them for supplying the fluid and others for returning the fluid. The heat pump is located inside the house, where it is marked “A” in the figure. The fluid leaves the heat pump, passes through the manifold and flows into the HGHX tubes buried under the rain garden. After the rain garden, the fluid goes through the conventional HGHX tubes buried on the southwest of the house and enters the FHX tubes buried on the west side of the house, and then reach the conventional HGHX tubes buried at the northeast of the house and returns to the heat pump. The fluid is a mixture of water and 20% propylene glycol.

Figure 6.5: Experimental house built in Oak Ridge, Tennessee

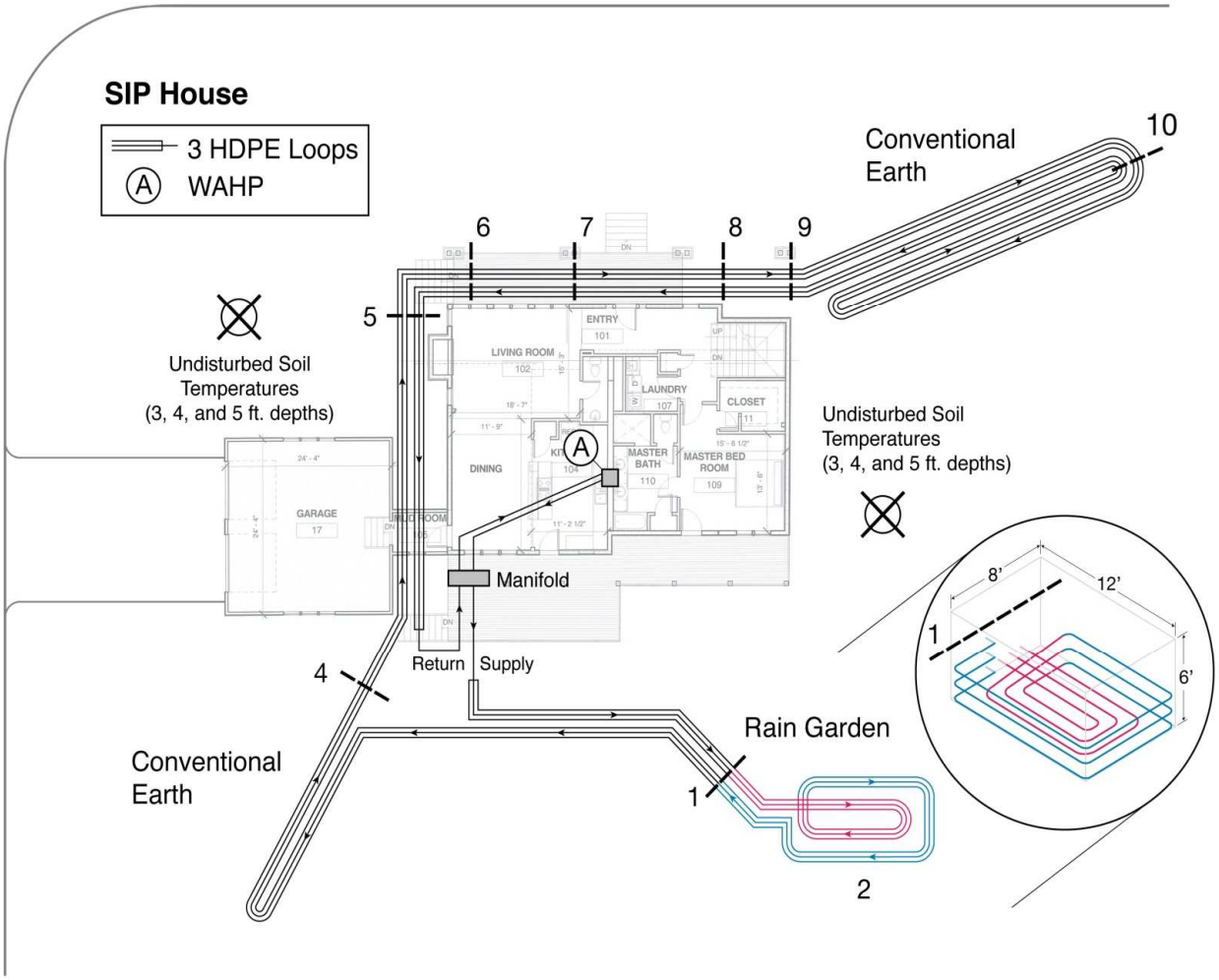


Figure 6.6: SIP house and FHX pipes locations (Im 2009)

An FHX model and an HGHX model are used to model only their respective parts of the system; the rain garden and other components are modeled as a horizontal ground loop heat exchanger. Since entering and exiting heat pump fluid temperature are known from experimental data, no heat pump model is included in the simulation at present time, exiting heat pump fluid temperature is treated as input in FHX model. The input parameters to the FHX and HGHX numerical model are listed below. Figure 6.7 shows the geometry of the simulation domain used for the FHX numerical model. The experimentally measured air temperature, humidity of the air, solar radiation, wind speed, heat pump ExFT (FHX EFT) and heat pump flow rate are treated as

15 minute time step boundary conditions. Both the FHX numerical model and HGHX numerical model initial soil temperature are computed with Kusuda and Achenbach model (1965), the Kusuda and Achenbach parameters are calculated with the 1D ground heat transfer model described in Chapter 3 using TMY3 weather file in Knoxville, Tennessee. The computed annual average soil temperature is 15.5 °C (60 °F), the surface amplitude is 12.8 °C (23 °F), and the phase lag is 17.3 days.

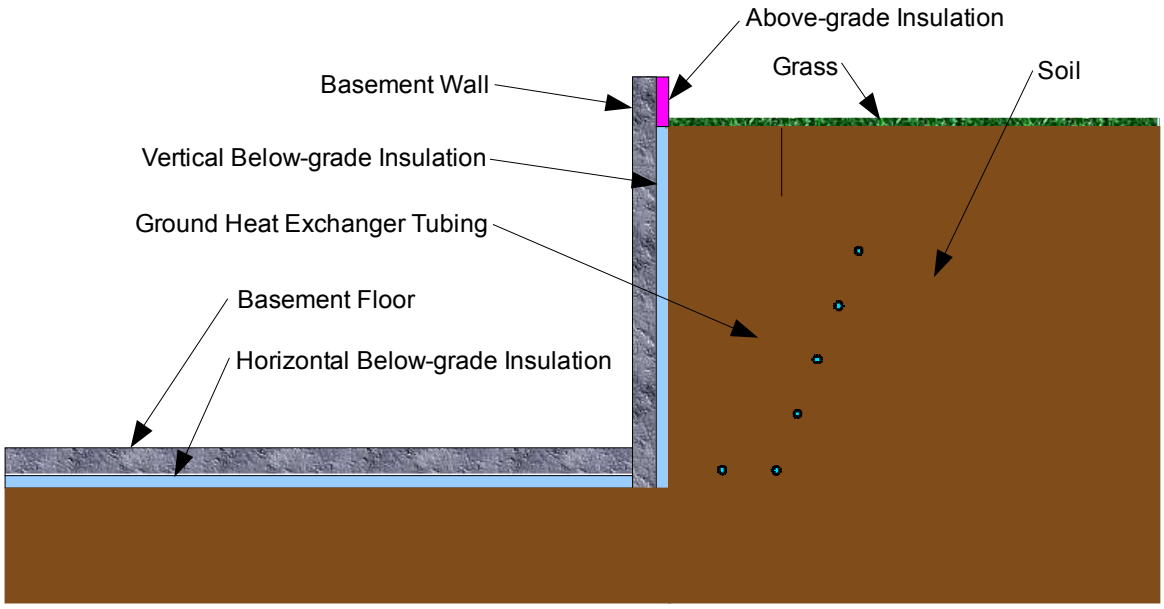


Figure 6.7: Cross-section of foundation heat exchanger.

*Geometry of the simulation domain*

- Depth of the soil domain, from the earth surface to the bottom of the soil domain: 5 m (16.4 ft) (assumed based on the boundary independence study)

- Vertical basement wall depth, the basement wall under the earth: 2.54 m (8.33 ft) (based on experimental house)

- Vertical basement wall height, the basement wall above the earth: 0.41 m (1.33 ft) (based on experimental house)

- Vertical basement wall thickness: 0.3 m (12") (from the experimental house)
- Basement floor width: 11.9 m (39.0 ft) (The 2D FHX numerical model treats the under-the-basement floor soil domain as having a width equal to half of the basement floor width. This width is approximated as the square root of the floor area, which is 141 $m^2$ (1518 $ft^2$) for the experimental house)
- Basement floor thickness: 0.25 m (10") (from the experimental house)
- Vertical below-grade insulation depth: 2.54 m (8.33 ft) ( from the experimental house, the basement wall and floor are fully insulated)
- Above-grade insulation height: 0.41 m (1.33 ft)
- Horizontal below-grade insulation length: 11.9 m (39.0 ft)

*Thermal properties*

- Soil thermal conductivity: 1.17 W/m•K (2.03 Btu/hr•ft•°F) (the average soil conductivity measured at six different depths and six different locations around the house )
- Soil volumetric heat capacity (calculated based on effective heat capacity method) 2.48 $MJ/m^3$•K ( $T_{soil}$>0 °C (32 °F))

  b) 242 M $J/m^3$•K (-0.5 °C (31.1 °F)≤ $T_{soil}$ ≤0°C (32 °F))

  c) 1.78 $MJ/m^3$•K ( $T_{soil}$ <-0.5 °C (31.1 °F))
- Vertical foundation and basement floor thermal conductivity: 1.7 W/m•K (2.9 Btu/hr•ft•°F ) (The experimental house uses foundation wall and basement floor made of concrete, the thermal values of the concrete have not been measured, therefore, a typical

thermal conductivity specific heat and density of concrete have been chosen for the simulation, within the range of values tabulated by ASHRAE (1997))

- Vertical foundation and basement floor density: 2240 kg/$m^3$ (140 lb/$ft^3$)
- Vertical foundation and basement floor specific heat: 920 J/kg•K (0.22 Btu/lb•°F)
- Vertical foundation and basement floor insulation thickness: 0.06 m (2.375") (from the experimental house, the house uses fiberglass as the insulation)
- Thermal conductivity of insulation (fiber glass) : 0.038 W/m•K (0.067 Btu/hr•ft•°F) ( The thermal conductivity and volumetric heat capacity have not been measured, therefore, a typical value for the fiber glass are chosen for the experimental validation (Incropera and Dewitt 1996))
- Volumetric heat capacity of insulation: 0.27 MJ/$m^3$•K (4.0 Btu/$ft^3$•°F)

*FHX and HGHX Tubing information*

The geometry of the FHX tubes and HGHX tubes are shown in Figured 6.8 and 6.9, the depths and distances of the tubes relative to the foundation wall are in meters, for both of them, there are six tubes in parallel, three of the tubes for supplying the water-antifreeze mixture, and the others for returning the fluid. The depths of each FHX and HGHX tube are and the distances between different tubes in parallel are not consistent, therefore, the depth are estimated as an average value based on the experimental house.

- Length of each FHX tube: 36.8 m (120.7 ft) (experimental measurement)
- Length of each HGHX tube: 54.6 m (179.1 ft) (experimental measurement)

- Inside diameter of the tube: 21.84 mm (0.86 inch) (the experimental house utilizes 3/4" HDPE tube, the inside and outside diameter is based on standard dimension for the type of tube used in the experimental house)
- Outside diameter of the tube: 26.67 mm (1.05 inch)
- Tube wall conductivity: 0.39 W/m•K (0.67 Btu/hr•ft•°F ) (typical value for HDPE pipe)

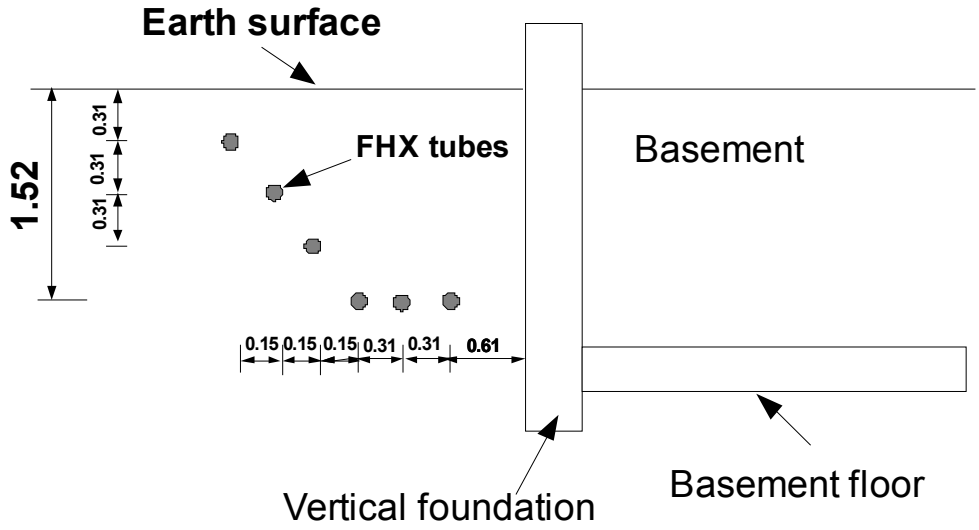


Figure 6.8: The geometry of FHX tubes: dimensions given in m

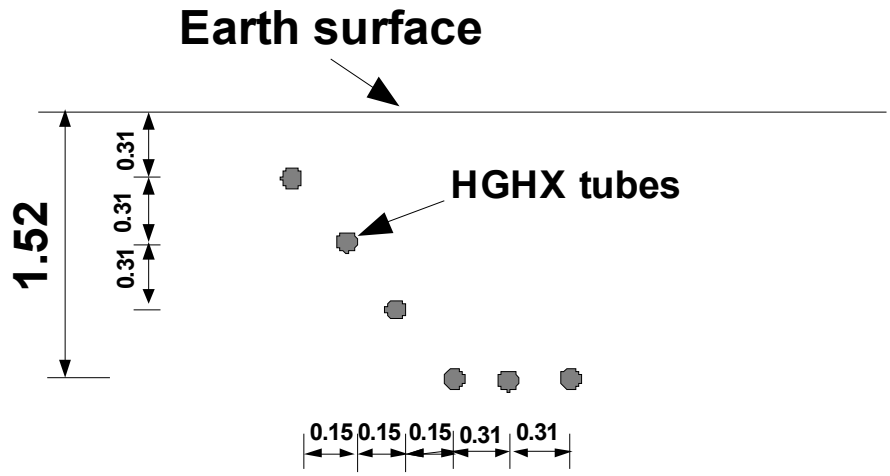


Figure 6.9: The geometry of HGHX tubes

*Other parameters*

- Basement are set to constant temperature 21°C (70 °F) (experimental measurement)
- Fluid type: water mixed with 20% Propylene glycol
- Longitude of the house: 84.12° W
- Latitude of the house: 35.95° N
- Attitude: 286 m (938.3 ft)

### 6.3.1 Validation of Undisturbed Ground Temperature Model

First, the undisturbed ground temperature was tested by looking at the temperature response of the ground far away from the foundation when there is no heating or cooling load input to the FHX, and the foundation surface is assumed adiabatic. The model initialized the soil temperature with the Kusuda and Achenbach model, using parameters tuned from the TMY3 weather data which is collected at the Knoxville McGhee Tyson Airport. Results were compared against the measured ground temperature stations at depths of 0.31m (1 ft), 0.61 m (2 ft), 0.91 m (3 ft), 1.52 m (5 ft) and 1.83 m (6 ft) below the ground surface for a period of 10 months, starts on January 1st 2010. There is one measurement site located in the rain garden, measure the undisturbed soil temperature at the depths of 0.31m (1 ft), 0.61 m (2 ft), and 0.91 m (3 ft). Another measurement site is 4.6 m (15 ft) away from the west foundation wall of the house; it measures the soil temperature at 0.91 m (3 ft), 1.52 m (5 ft) and 1.83 m (6 ft). Results are shown in Figures 6.10 to 6.14, respectively. For the shallow depths, 0.31m (1 ft), 0.61 m (2 ft) and 0.91 m (3 ft), the simulation results follow the trend of measurement sites quite well, the

temperature differences of modeled result and experiment measurement are a bit high during the January and February, but this can be attributed to the assumption that the measurement site is assumed to be covered with 12 cm (4.7 inch) tall grass for an entire year. In the winter, the grass will die out or go dormant, and the effect of evapotranspiration will be smaller than assumed in the model, therefore, the soil temperature should be higher than what calculated in the model. The result might be improved by making a seasonal correction to the value of evapotranspiration calculated in the model. The experimental data show a higher degree of fluctuation than predicted by the model at the depth of 0.31 m (1 ft). For the 3 ft depth measurement, the simulated results are really close to the measured soil temperature at site 2; the overall difference is within 1.0 °C (2 °F). In Figure 6.12, it shows that the there might be something wrong with the measurement data at site 2, the thermometer possibility stop working, need to be further checked.

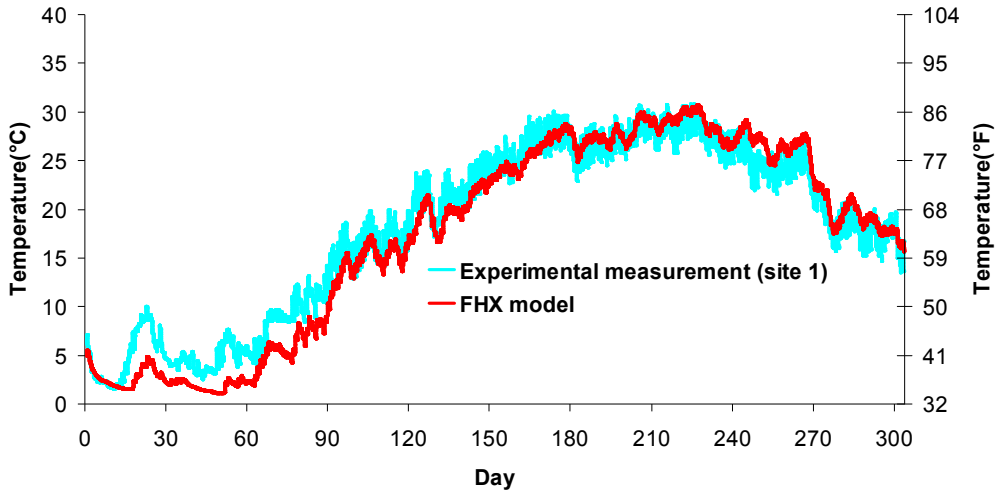


Figure 6.10: Undisturbed ground temperature at 0.31m (1 ft) depth

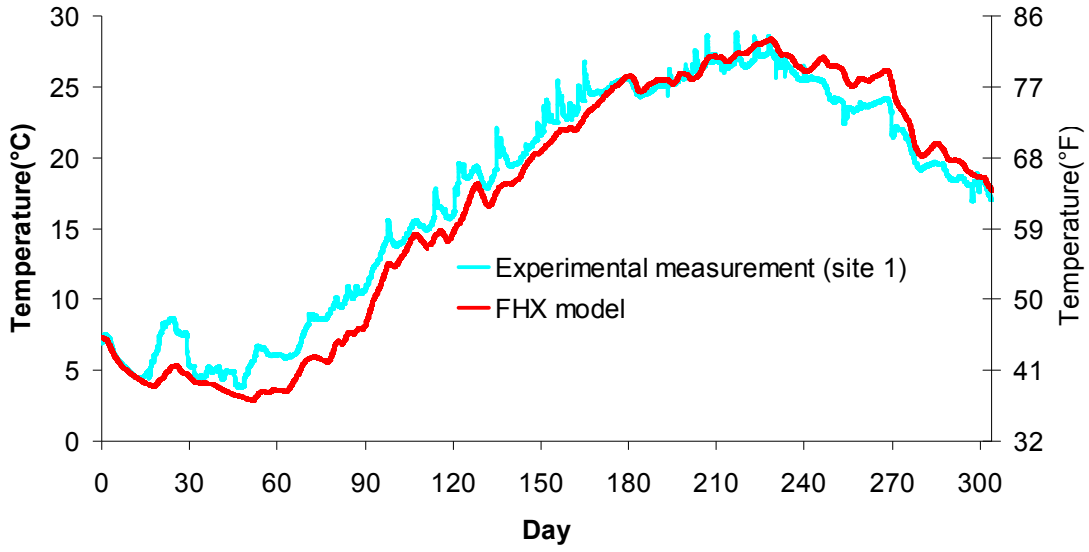


Figure 6.11: Undisturbed ground temperature at 0.61m (2 ft) depth

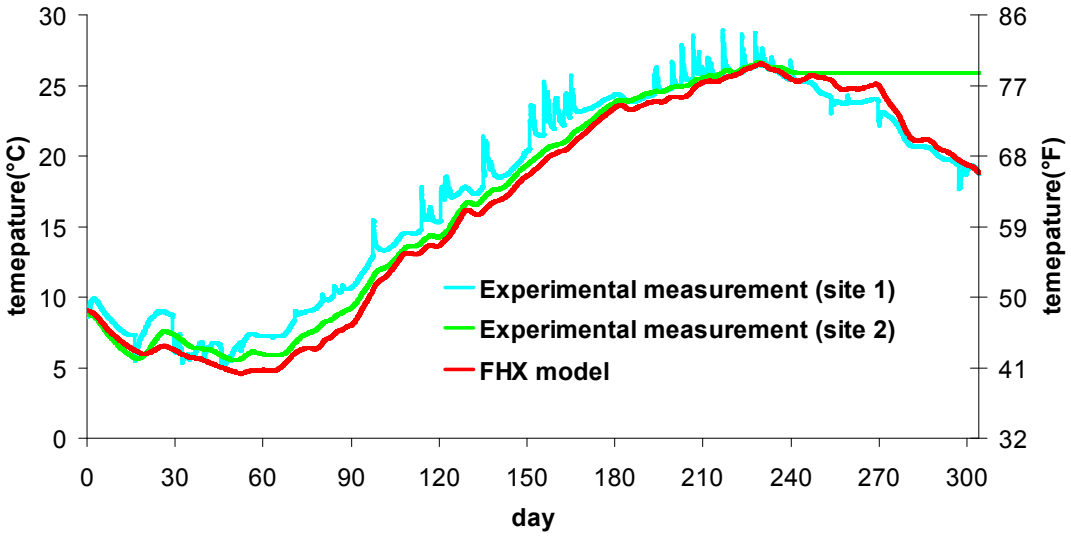


Figure 6.12: Undisturbed ground temperature at 0.91m (3 ft) depth

At a deeper depth, the depths of 1.52 m (5 ft) and 1.83 m (6 ft), the model result follow the trend of the measurement data quite well. The calculated undisturbed ground

temperature is higher in winter and lower in summer compared with the experimental result, with a temperature difference of 1-2°C (1.8-3.6°F).

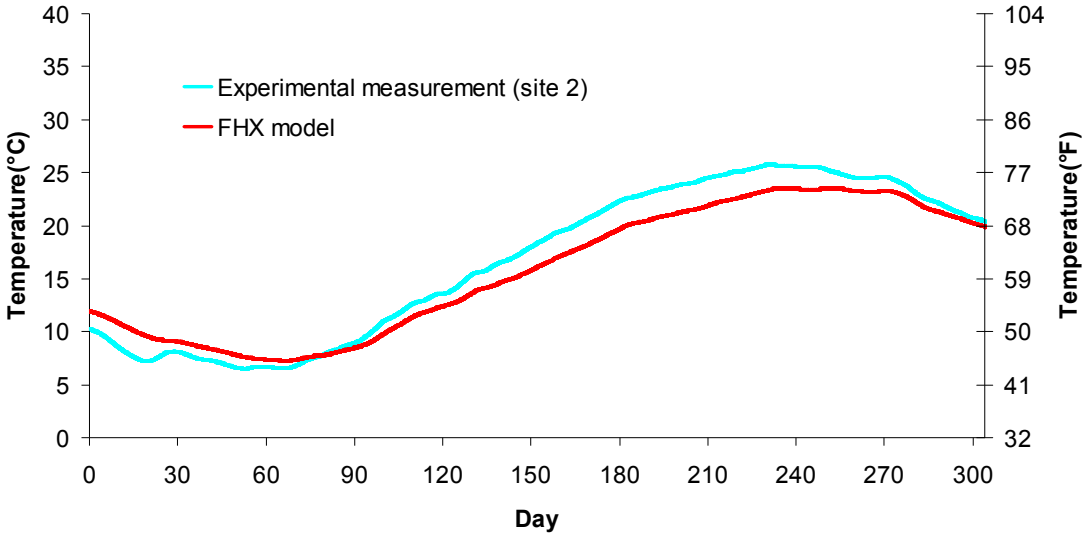


Figure 6.13: Undisturbed ground temperature at 1.52 m (5 ft) depth

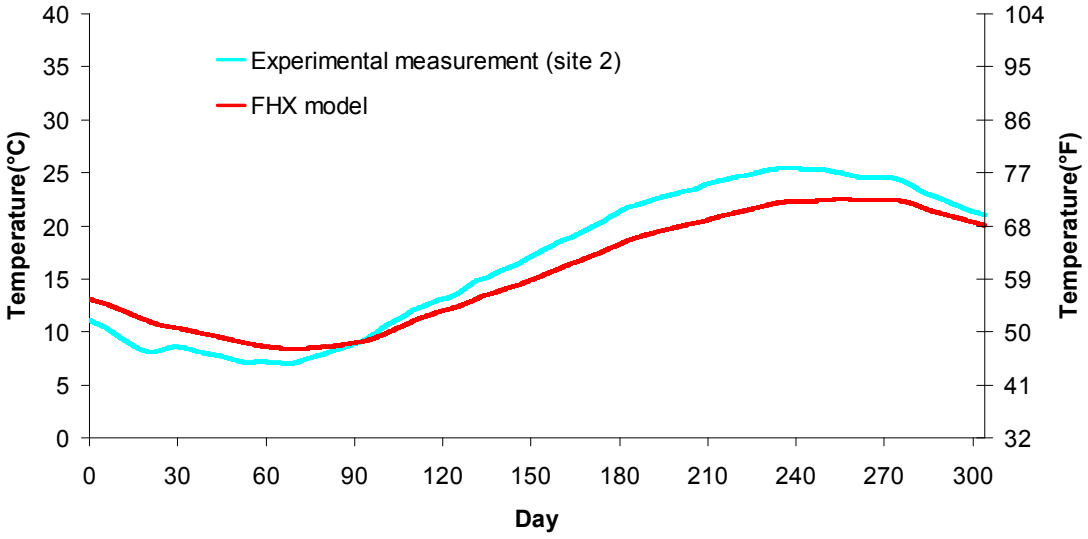


Figure 6.14: Undisturbed ground temperature at 1.83 m (6 ft) depth

### 6.3.2 Post-processing of Experimental Data

Two problems were found with the experimental data: the measured heat pump EFT and ExFT are "wrong" at low flow rate, the measured heat pump flow rate is wrong at low flow rate. An hourly simulation of the FHX+HGHX system was performed. It was found out that the resulting heat pump entering fluid temperature poorly matches with the experimental results at low flow rate. After further checking, it was found that the 15-minute data received (measured heat pump EFT or ExFT) are raw averages of minutely data, this causes the poor match during low flow rate periods. The heat pump EFT and ExFT are measured inside the conditioned house; when the heat pump is off, the slaved circulating pump will also be off. During these times, the measured heat pump EFT and ExFT drift towards room temperature, which is about 20°C (68°F). Including these drifting temperatures in the averages leads to problems with both the simulation input (measured heat pump exiting fluid temperature) and comparison of the simulation results to "measured" values (heat pump exiting fluid temperature). Therefore, the average heat pump EFT and ExFT using a flow rate weighted average needed to be provided for the experimental validation, not a simple averages of minutely data. In order to correct the "wrong" heat pump exiting fluid temperature and entering fluid temperature, minutely data of heat pump flow rate, heat pump EFT and ExFT needed to be provided.

Another problem was found in the experimental measured flow rate. The heat pump flow is calculated from recorded pressure drop across the heat pump, by using an equation fit. The equation fit is correlated only for the normal operation range of the heat pump, thus, according to the "problematic" correlation; the zero flow rates correspond to about 2.07 Kpa (0.3 psi). I developed a procedure for backing out the pressure drop, based on the equation fits used to correlate the fluid flow rate and pressure drop across the heat pump, and used a new equation relating flow rate to pressure drop to correct the flow rates.

For the first seven month of validation, only 15 minutely data are provided, 1 minutly data of heat pump flow rate, heat pump EFT and ExFT are recorded since August 1st. Therefore, I back out the pressure drop from the 15 minutes flow rate data provided for the first seven months. There are five equation fits for flow rate and pressure drop used in the experiment, for the five different mean heat pump fluid temperatures (the average of heat pump EFT and ExFT): -1 °C (30 °F) , 10 °C (50°F), 21°C (70°F), 32 °C (90°F) and 43 °C (110°F). The procedure to back out the pressure drop involves interpolation and is described by example - if I have a flow rate as 0.32 l/s (5.14 GPM) and the mean heat pump EFT and ExFT is 6.0 °C (42.9 °F), what is the corresponding pressure drop across the heat pump?

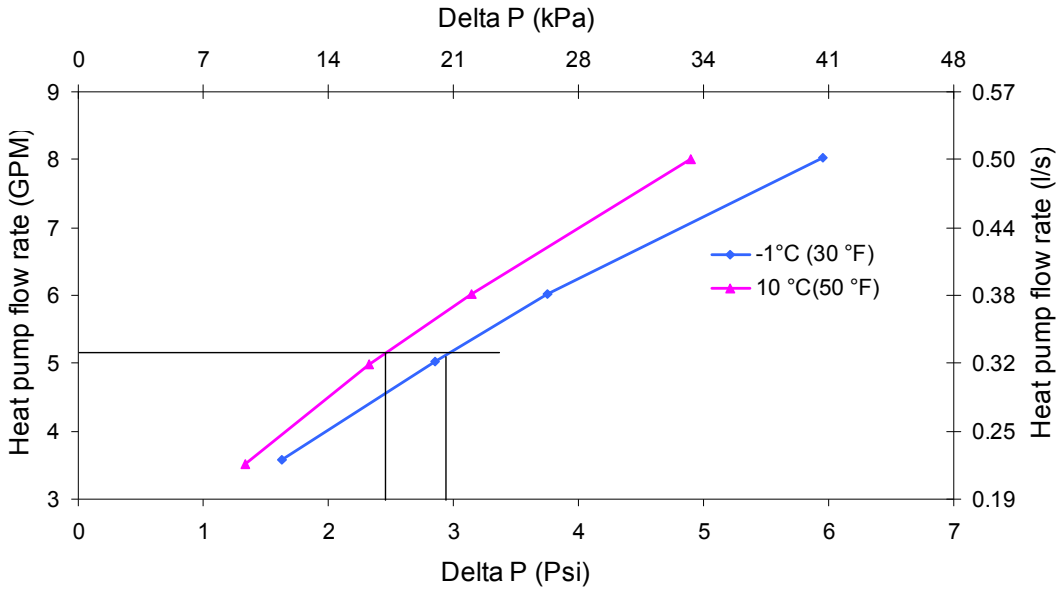


Figure 6.15: Heat pump flow rate and pressure drop correlation

First, calculate the $\Delta P$ from the correlations for fluid temperatures of -1 °C (30°F) and 10 °C (50°F) separately. As shown from Figure 6.15, when the flow rate is 0.32 l/s (5.14 GPM), the corresponding $\Delta P$ at the fluid temperatures of -1 °C (30°F) and 10 °C (50°F) are 20 kPa (2.9 Psi) and 17.2 kPa (2.5 Psi) respectively. Second, interpolate by the temperature in order to find the $\Delta P$ at the temperature of 6.0 °C (42.9 °F) as shown in Equation 6-1:

$$\Delta P|_{42.9} = \Delta P|_{30} + \frac{\left(\Delta P|_{50} - \Delta P|_{30}\right)}{50-30} \times (42.9-30) = 15.8kPa(2.3Psi) \qquad (6\text{-}1)$$

$\Delta P|_{42.9}$ is the pressure drop across the heat pump when the mean fluid temperature is 6.0 °C (42.9 °F). After backing out the pressure drop, a new equation fit relating the pressure drop across the heat pump to the flow rate can now be applied.

As mentioned before, there are five equation fits for the pressure drop and flow rate for different mean fluid temperatures and all of them need to be corrected, and in Figure 6.16, I only show one of them, the curve for a mean heat pump fluid temperature of -1°C (30 °F). "Experiment" is the experimentally measured data points the ORNL team provided, "Equation fit_experiment" is the correlation curve based on the equation fit that ORNL team used before, and "Equation fit_corrected" is the corrected correlation curve.

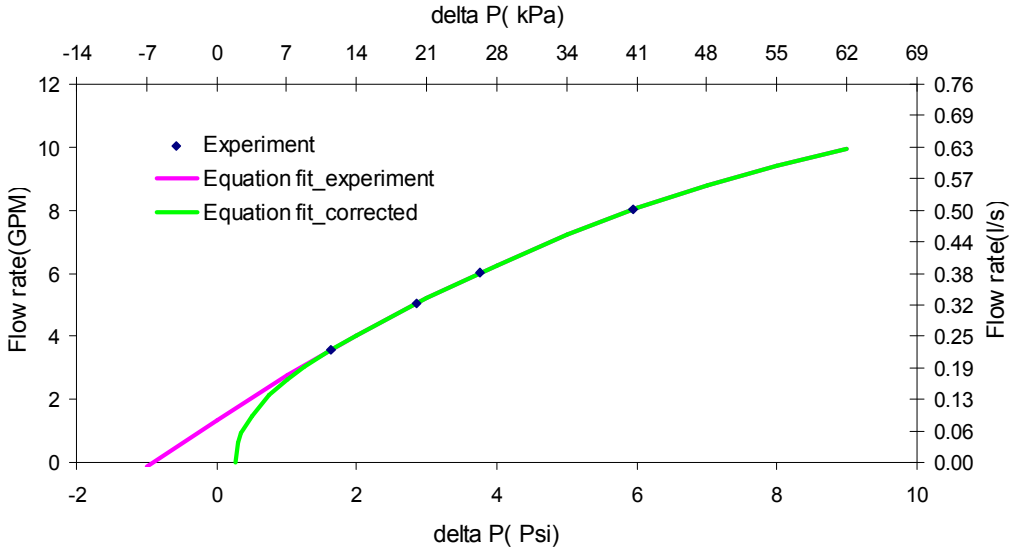


Figure 6.16: Correlation between flow rate and pressure drop

The corrected equation fit can be summarized as follows, this correlation works on IP unit.

At -1°C (30 °F) and $\Delta P \geq 1.6301 Psi$

$$\dot{V} = -0.054323(\Delta P)^2 + 1.44435(\Delta P) + 1.35863 \qquad \text{(6-2a)}$$

At -1°C (30 °F) and $1.6301 Psi > \Delta P \geq 0.26 Psi$

$$\dot{V} = 3.05(\Delta P - 0.26)^{0.5} \qquad \text{(6-2b)}$$

At -1°C (30 °F) and $0.26 Psi > \Delta P$

$$\dot{V} = 0 \qquad \text{(6-2c)}$$

Where:

$\dot{V}$ is the heat pump flow rate, in GPM;

$\Delta P$ is the pressure drop across the heat pump, in Psi;

The actual coefficients for the Equation 6-2a and 6-2b vary with mean fluid temperature. The somewhat unusual form of the correlations is indented to give reasonable results under conditions when the heat pump is off for all or part of the 15-minutes averaging period.

The validation data on 1-minute measurement intervals is available at the beginning of the eighth month. A modified procedure is needed to correct the data. First, from the measured heat pump flow rate, pressure drop, and mean fluid temperature, the corrected flow rate is determined from the pressure drop/flow rate correlation used previously for the 15-minute data. Any missing data is treated as the heat pump is not in operation for that minute. The heat pump EFT and ExFT are then computed on a 15-minute weighted average basis with the adjusted flow rates. To test this new procedure for the 1-minute data, a simulation was run using this data, after using the 15-minute data for all previous seven months. Additionally, a second

simulation was run using the provided 15-minute data corrected with the previous procedure for all ten months. The undisturbed soil temperature validation is independent of heat pump flow rate and fluid temperature; therefore, it does not need to be rerun.

As Figure 6.17 shows, the resulting daily average FHX ExFTs using each data scheme are nearly identical, with both model results deviating from the measured data less than 0.5°C(0.9 °F) since the beginning of April. The models results are showing a deviation of about 1.5°C (1.8 °F) from the measurement result on March and April (60-90 days) when the system has a low run time fraction. The same deviation is observed in the undisturbed soil temperature validation, the result could be improved by investigating the undisturbed soil temperature calculation. On the tenth month, models results of using difference data scheme start to deviate, the simulation result using flow rate corrected from 1-minutes flow rate shows a better match with the experiment data. When the system is off, the measured fluid temperature drifts towards the room temperature where the temperature sensors are located. Therefore, the "wrong" measured fluid temperatures when system is off are not plotted in the Figure. Figure 6.18 shows the FHX ExFTs for a sample day, 10 August. Overall, the model follows the trend of the measured data quite well for both the 1- and 15-minute data processing schemes; however, there are certain points around 7am and 9am for this sample day where the 1-minute processing deviates from the 15-minute processing by as much as 1°C. The reason for this differential is not clear at present, and needs further investigation.

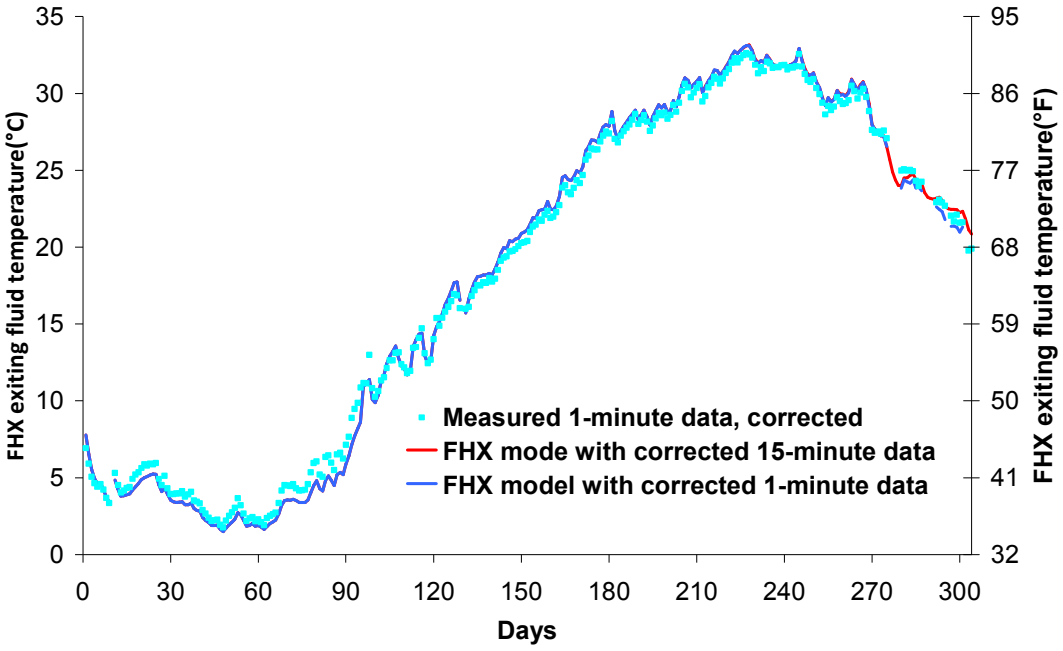


Figure 6.17: Comparison of daily average simulated and measured FHX ExFT

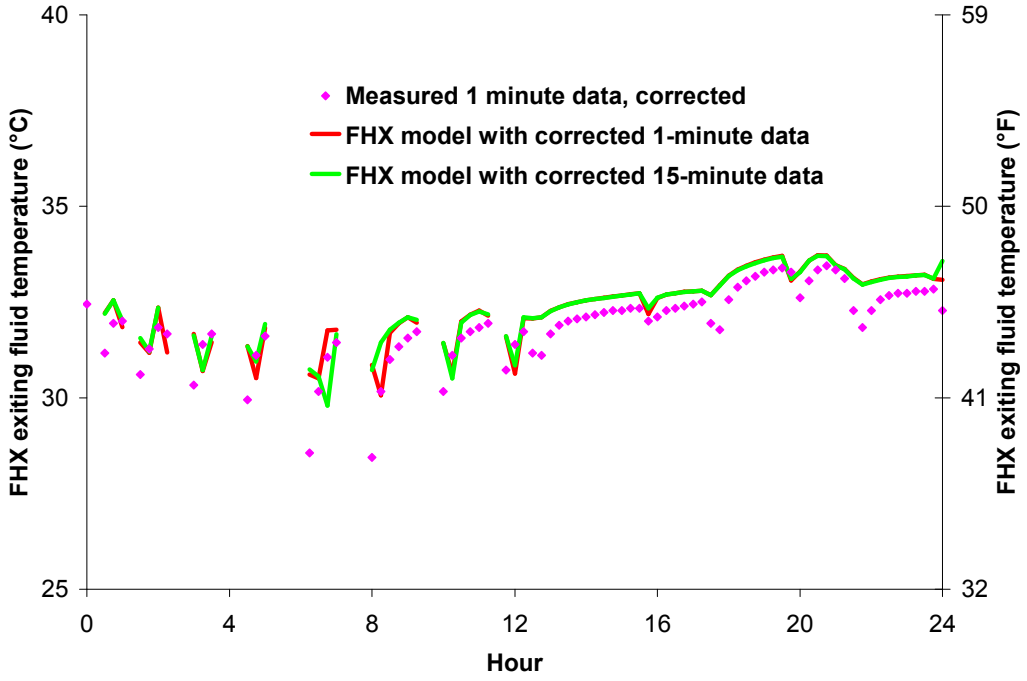


Figure 6.18: Comparison of FHX ExFTs with 1- and 15- minute data for 10 August

Figure 6.19 shows experimental validation of the pipe wall temperature-the measured data is an average of six measurements from each of five stations. In general, the simulation result using the 1- and 15- minute data processing schemes matches the measured data quite well, there are higher deviations during the period of April (100-120 days) and October (270-300 days), when the run time fraction is low.

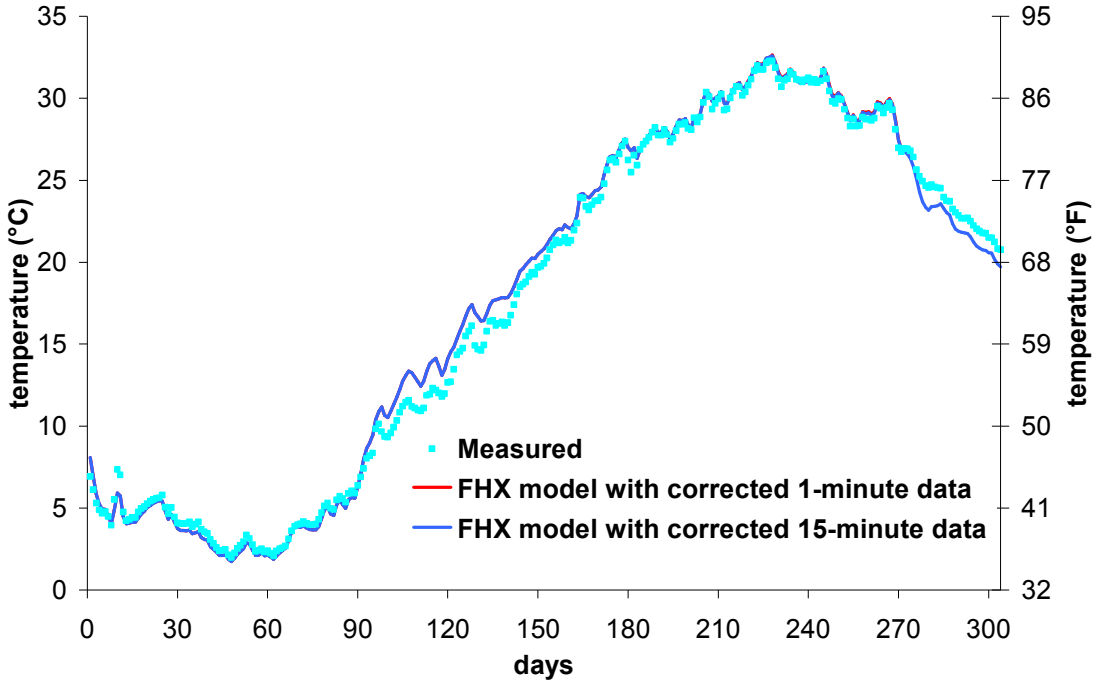


Figure 6.19: Daily average measured and modeled pipe wall temperature

Figures 6.20 and 6.21 show the FHX model predicted and measured disturbed soil temperatures at the depth of 0.38 m (15 inch) and 1.07 m(42 inch), respectively, at a distance of 0.61 m (24 inches) from the north foundation wall. The FHX model predicts a higher disturbed soil temperature than the measured data, as shown in Figures 6.17 and 6.18. Since the experimental measurement site 1 and 2 are on the north side of the house, covered by a deck, and further shaded by eaves, therefore, there will likely be a substantial shading effect. To understand how

much the presence of shading can explain the difference between the modeled and measured results, the FHX model was run with zero solar radiation, the simulation result is marked as "FHX model_no solar radiation" in the figures. As the figures demonstrate, after an initial model warm-up period, the FHX model with full incident solar radiation and the FHX model with absolutely no solar radiation bracket the soil temperature measurements. This would suggest that including partial shading might provide the most accurate temperature results.

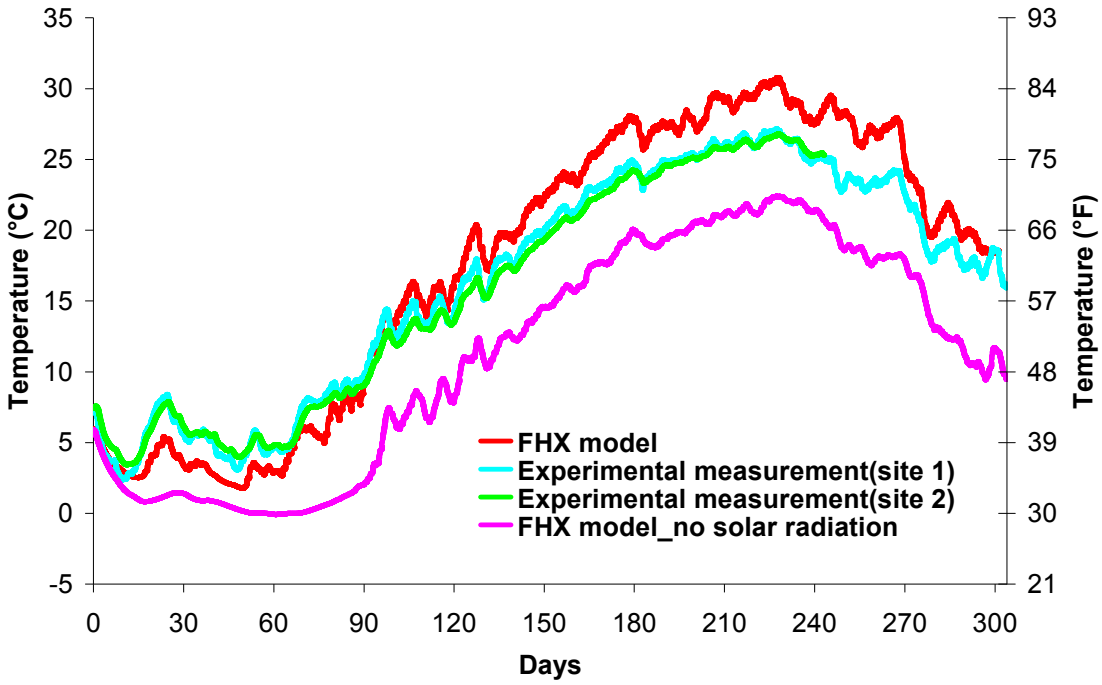


Figure 6.20: Soil temperature at 0.38 m (15 ") depth, measured and modeled

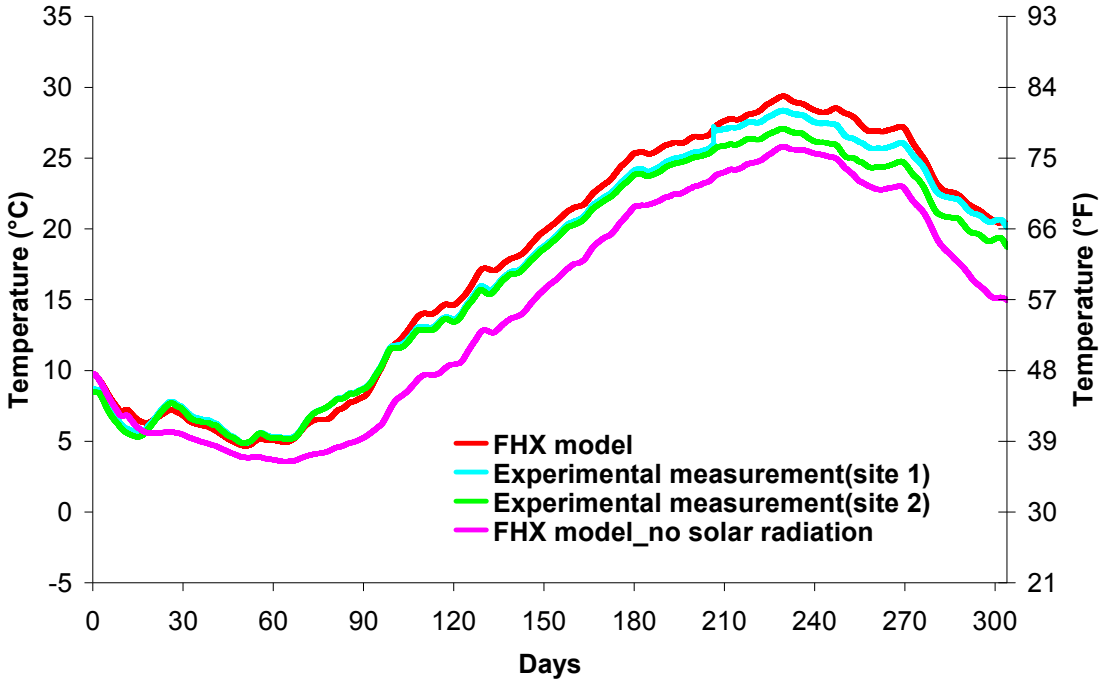


Figure 6.21: Soil temperature at 1.0 m (42 ") depth, measured and modeled

The presence of shading could explain the difference in soil temperature measurements, but what about other quantities such as the FHX fluid temperature, or the pipe wall temperature? The same analysis was performed, comparing a simulation with zero shading to one with no solar radiation at all, to determine the FHX exiting fluid temperature and mean pipe wall temperature. As before, the model including full solar radiation with no shading, and the model with no solar radiation at all, bracket the measured data for both the FHX ExFT and mean pipe wall temperature. This provides a strong indication that some degree of shading in the model could improve the overall results. The degree of shading to apply, and the best method for including it in the model, is a subject for further study.

So far, the numerical model has been well validated with the experimental data for a period of ten month. The validated numerical model can then be used for two purposes: design tool or make

energy analysis. Be used as a design tool, the users need to input the length and locations of the FHX tubes, the numerical model will calculate and output the hourly heat pump EFT and ExFT. The tube length and configuration needed to be iteratively adjusted by the users so that annual minimum or maximum the heat pump EFT reaches the "constraining heat pump EFT limit". The 2D numerical model could also be used to analyze the energy consumption of simulated house, which utilize the GSHP system with FHX tubes.

# CHAPTER 7

## INTERMODEL VALIDATION

In this thesis, two models have been developed for the simulation of foundation heat exchangers; a detailed hourly time step numerical model and a simplified monthly time step analytical model based on the line source solutions. A parametric study has been performed in order to compare the results of the two models and investigate the difference between them. Six geographically-diverse locations are chosen for the parametric study. In order to compare the models over a range of conditions, six climates were chosen and may be categorized based on Briggs et al. (2003) as shown in Table 7.1. A single, well insulated house is modeled in EnergyPlus for each climate to generate hourly heating and cooling loads.

Table 7.1: Climate zones

| Location | Climate Zone | Briggs Classification |
|---|---|---|
| Albuquerque, New Mexico | Mixed-Dry | 4B |
| Knoxville, Tennessee | Mixed-Humid | 4A |
| Phoenix, Arizona | Hot-Dry | 2B |
| Salem, Oregon | Mixed-Marine | 4C |
| San Francisco, California | Warm-Marine | 3C |
| Tulsa, Oklahoma | Warm-Humid | 3A |

The house has a rectangular plan, 15.24 x 9.75m (50 x 32ft) , with the longer sides facing north and south. 3% of the wall area is covered by glazing on the east and west façades. 29% of the north and south facades are glazed. On the south side, half of the glazing is shaded by an

overhang. The overall R-value of the walls is 4.75 $m^2$•K /W (27 $ft^2$•°F•hr/Btu), the overall roof R-value is 7.39 $m^2$•K /W (42 $ft^2$•°F•hr/Btu). The windows have a U-value of 2.49 W/$m^2$•K (0.44 Btu/ $ft^2$•°F•hr) and a solar heat gain coefficient of 0.36.

For the occupied space in the house, the occupant density was set presuming a family of four in the household, and combined lighting and casual gains of 8.2 W/$m^2$ (2.6 Btu/ hr• $ft^2$) and constant infiltration rates of 0.5 ACH. Schedules for the people, equipment, and lighting were created assuming a typical residential schedule. In heating, the daytime (6am-9pm) set point temperature is 22.2°C (72 °F), with a setback temperature of 20°C (68 °F) at night. In cooling, the daytime set point is 25°C (77 °F), with a nighttime temperature of 26.7°C (80 °F). For this study, soil is assumed to be clay loam, with conductivity of 1.08 W/m•K (2.0 Btu/ hr•ft•°F) and volumetric heat capacity is 2.479 MJ/$m^3$•K (41 Btu/$ft^3$•°F). Six tubes are located at depths of 2.5(8.2), 2.5(8.2), 2.1(6.9), 1.7(5.6) and 0.9(3) m(ft), with the distance to the vertical foundation wall of 0.4(1.3), 0.8(2.6), 0.9(3), 1.0(3.3), 1.1(3.6) and 1.2(3.9) m(ft)respectively.

Whether ground heat exchanger models are used for design or energy analysis, the key output is the exiting fluid temperature (ExFT), which is also the entering fluid temperature (EFT) for the heat pump. For design purposes, the minimum and maximum heat pump EFTs are the key design constraints that control the size of the ground heat exchanger. The analytical model, which is intended for use in design simulations, gives monthly minimum and maximum FHX ExFT, which are compared to ExFT generated by the numerical model in Figures 7.1-7.6 for the six locations.

For all locations, the simulations are run with both models for a two year period and the second year simulation results are shown. By the second year, the results have essentially converged to a steady periodic result. Running the simulations for a third year will not change the minimum or maximum FHX ExFT more than 0.01°C (0.018 °F) compared with the second year.

Figures 7.1-7.6 all show two sets of results for the numerical model and the maximum and minimum FHX ExFT for each month calculated with the analytical model. Ideally, the numerical results should vary between the minimum and maximum FHX ExFT for each month. The curves marked "Numerical result" represent the output from the numerical model as described above. The curves marked "Numerical result/adiabatic foundation" are from a modified version of the numerical model, described below, which will be used to help identify the sources of the differences between the numerical and analytical models.

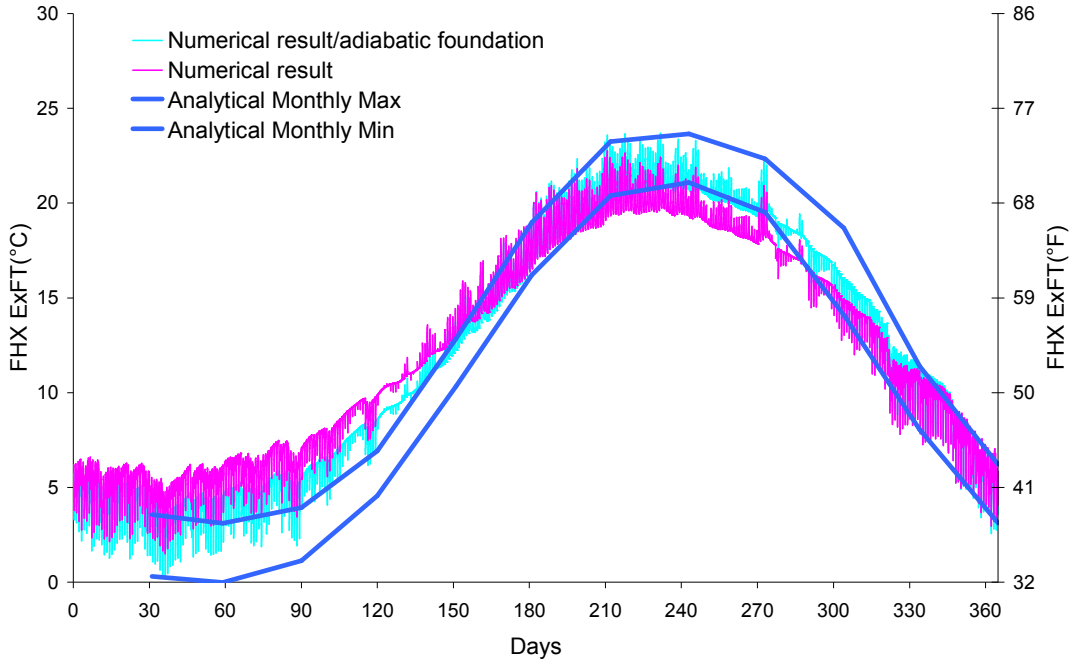


Figure 7.1: FHX exiting fluid temperature predictions for Albuquerque, NM

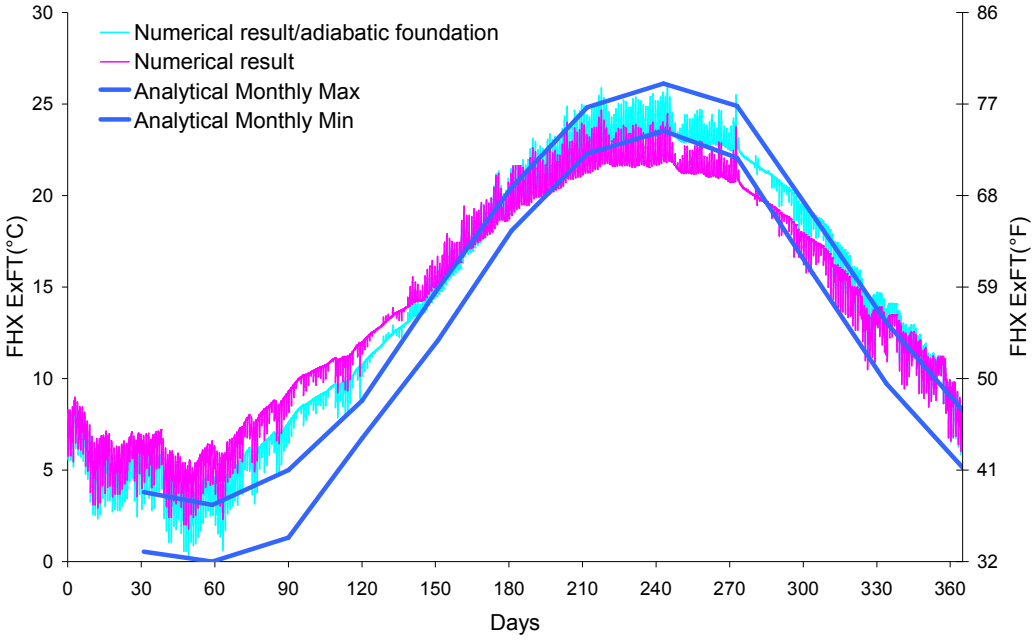


Figure 7.2: FHX exiting fluid temperature predictions for Knoxville, TN

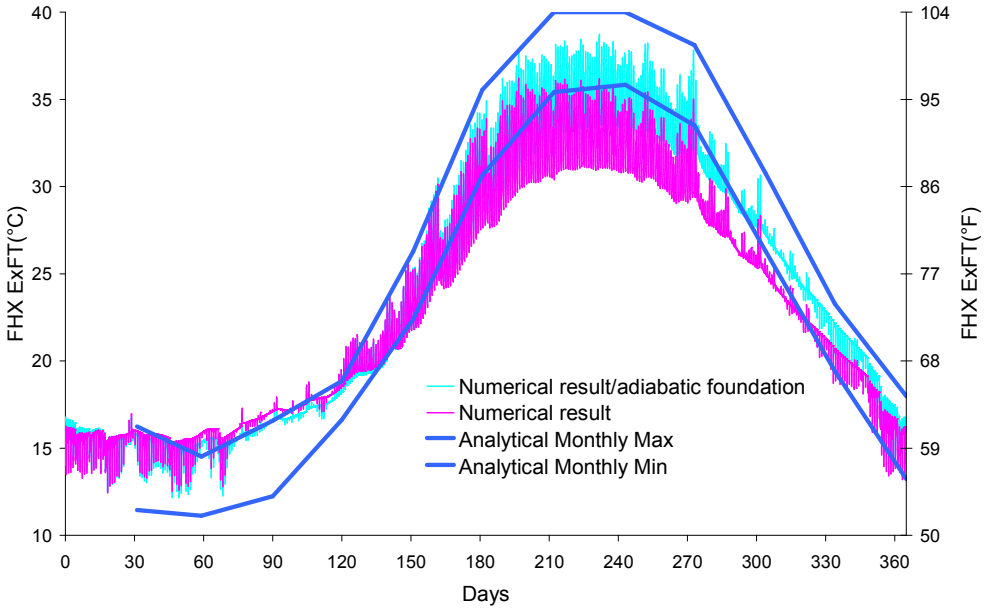


Figure 7.3: FHX exiting fluid temperature predictions for Phoenix, AZ

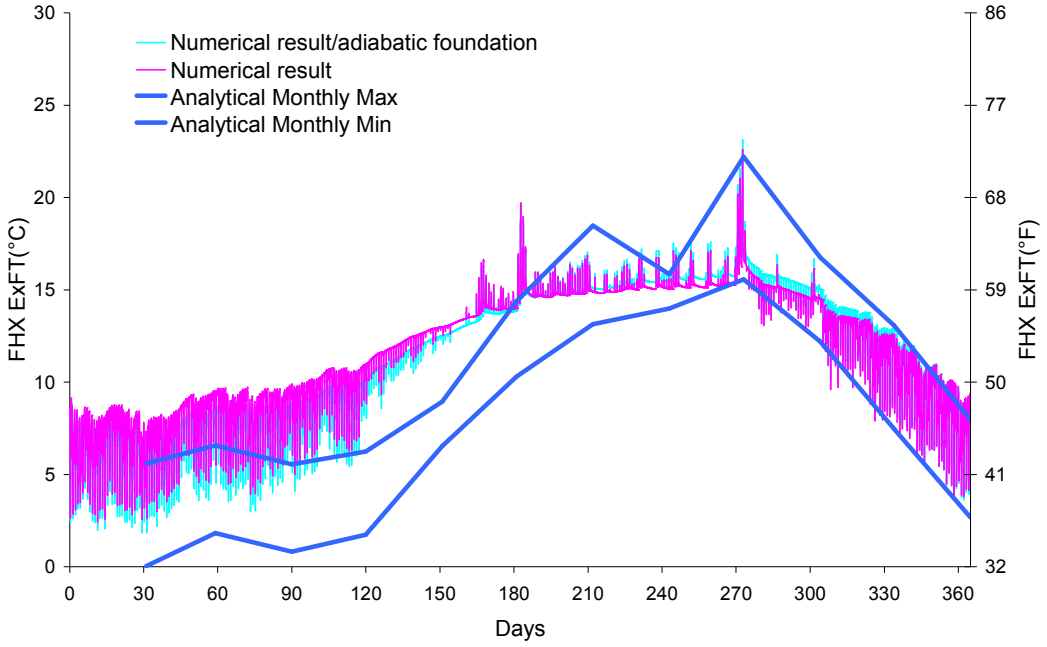


Figure 7.4: FHX exiting fluid temperature predictions for SanFrancisco, CA

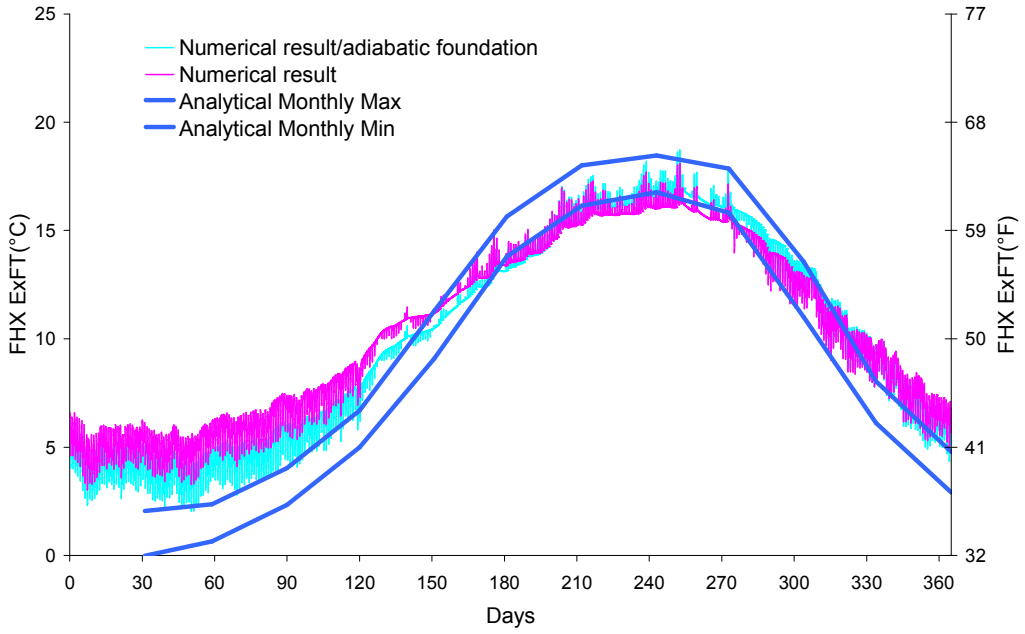


Figure 7.5: FHX exiting fluid temperature predictions for Salem, OR

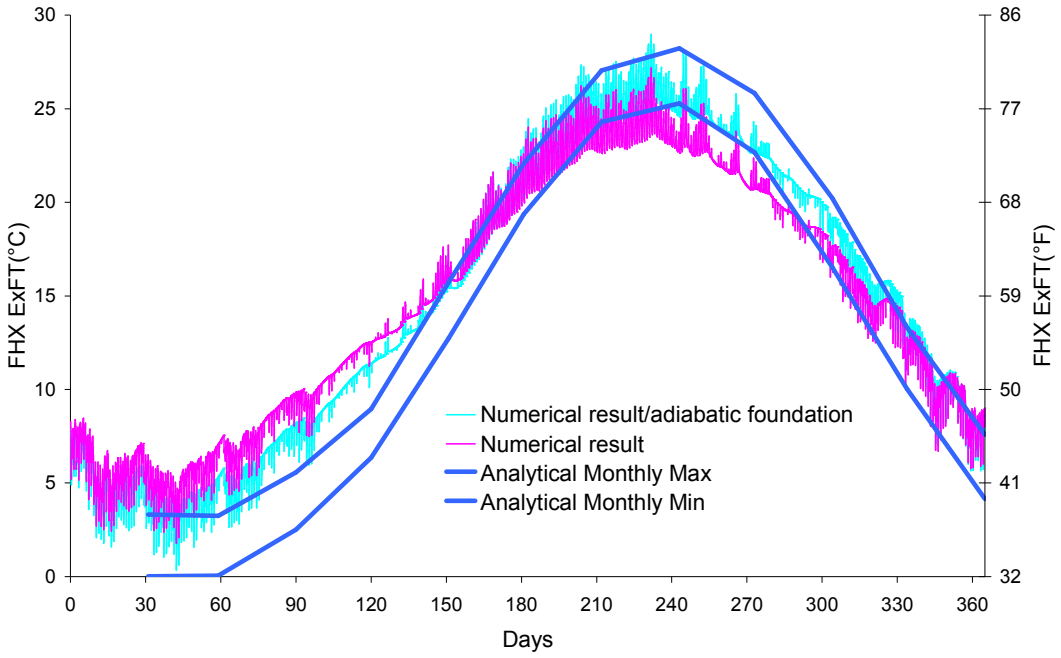


Figure 7.6: FHX exiting fluid temperature predictions for Tulsa, OK

For each case, the difference between the two models may be characterized in at least two ways. First, for a given length of FHX tubing, calculated with the analytical model, there will be a difference in the peak FHX ExFT calculated by the numerical model and the analytical model. This error in the analytical model prediction, treating the numerical model results as “correct” is summarized in Table 7.2. The "constraining HP EFT limit" is chosen to allow the system to operate within the limits specified by the manufacturer, within the limits of the working fluid, with acceptable capacity, and with acceptable energy efficiency. The temperature range for the heat pump operation chosen here is 0-40 °C (32-104°F) as shown in Table 7.2. For each case, the peak FHX ExFT calculated by the analytical model exactly meets the constraining HP EFT limit.

Table 7.2: Peak FHX ExFT error

| Locations | Constraining HP EFT limit °C(°F) | Corresponding numerical model peak FHX ExFT °C(°F) | Peak FHX ExFT error °C(°F) |
|---|---|---|---|
| Salem | 0(32) | 3(37.4) | -3(-5.5) |
| Phoenix* | 40(104) | 36.2(97.2) | 3.8(6.8) |
| Albuquerque | 0(32) | 1.5(34.7) | -1.5(2.7) |
| Knoxville | 0(32) | 1.8(35.2) | -1.8(-3.2) |
| San Francisco | 0(32) | 2.4(36.3) | -2.4(-4.3) |
| Tulsa | 0(32) | 1.8(35.2) | -1.8(-3.2) |

* All cases except for Phoenix are constrained by the minimum HP EFT. Phoenix is constrained by the maximum HP EFT.

A second approach for characterizing the error is to compute the size (length) of FHX required to meet the heat pump entering fluid temperature constraints with both the analytical model and the numerical model. In both cases, the models are applied iteratively and the length of the FHX is adjusted until either the minimum or maximum HP EFT limits are reached.

Table 7.3: FHX sizing error

| Locations | Constraining HP EFT limit °C(°F) | FHX length sized with analytical model m(ft) | FHX length sized with numerical model m(ft) | Error in analytical model sizing |
|---|---|---|---|---|
| Salem | 0(32) | 46.3(151.9) | 33(108.3) | 29% |
| Phoenix | 40(104) | 31.7(104) | 25.7(84.3) | 19% |
| Albuquerque | 0(32) | 34.1(111.9) | 28.4(93.2) | 17% |
| Knoxville | 0(32) | 36.8(120.7) | 30.4(99.7) | 17% |
| San Francisco | 0(32) | 18(59.1) | 14.5(47.6) | 19% |
| Tulsa | 0(32) | 39.4(128.9) | 32(105) | 19% |

Looking at Tables 7.2 and 7.3, the errors are higher than desirable. While some oversizing by a simplified design tool is usually acceptable, errors as high as 29% are higher than desired. This leads to the question: why are the errors so high, particularly for the Salem, Oregon case?

To answer this question, first consider the differences between the numerical and analytical models. Table 7.4 characterizes three aspects of the models.

Table 7.4: Comparison of numerical and analytical model features

| Model | Time step | Foundation wall geometry | Ground temperature (UGT) |
|---|---|---|---|
| Numerical model | hourly | Unconditioned basement with finite vertical and horizontal dimensions | Computed with numerical model and includes effects of surface heat balance, soil freezing, and FHX heat transfer |
| Analytical model | monthly | Adiabatic foundation wall, infinite in the vertical direction | Determined with superposition – undisturbed ground temperature portion is computed with Kusuda and Achenbach model |

The effects of the three differences shown in Table 7.4 can be investigated by modifying the numerical model or the analytical model to be closer to each other. The first effect that investigated is the foundation wall geometry. Because the analytical model cannot be modified to account for the actual geometry, I modified the numerical model to have an adiabatic foundation wall that was infinite in the vertical direction. These results are shown for every location in Figures 7.1-7.6 and are labeled "Numerical result/adiabatic foundation." In all locations, except perhaps San Francisco, the numerical model with the adiabatic foundation comes much closer to the analytical model results. This indicates that the infinite adiabatic foundation wall assumption made by the analytical model is responsible for a significant amount of the error in the analytical model. Table 7.5 summarizes the peak FHX ExFT errors; compared to the results in Table 7.2, the peak FHX ExFT errors are nearly eliminated for Albuquerque, Knoxville and Tulsa. For San Francisco, Phoenix, and Salem, the errors are higher. Salem has the highest error and will be investigated further.

Table 7.5: Peak FHX ExFT error with adiabatic foundation

| Locations | Constraining HP EFT limit °C(°F) | Corresponding numerical model (with adiabatic foundation) peak FHX ExFT °C(°F) | Peak FHX ExFT error °C(°F) |
|---|---|---|---|
| Salem | 0(32) | 2.0(35.6) | -2.0(-3.6) |
| Phoenix | 40(104) | 38.7(101.6) | 1.3(2.3) |
| Albuquerque | 0(32) | 0.2(32.4) | -0.2(-0.3) |
| Knoxville | 0(32) | 0.3(32.5) | -0.3(-0.5) |
| San Francisco | 0(32) | 1.8(35.2) | -1.8(-3.2) |
| Tulsa | 0(32) | 0.3(32.5) | -0.3(-0.6) |

As summarized in Table 7.4, the numerical model uses a heat balance on the surface to compute the ground temperature; the analytical model uses the Kusuda and Achenbach (1965) model to determine the undisturbed ground temperature. It is not feasible to implement a heat balance in the analytical model, but one possible approach is to compute the undisturbed ground temperature with a one-dimensional numerical model, then use it instead of the Kusuda and Achenbach-determined UGT within the analytical model. I have taken this approach, using a 1-d numerical model that has an identical surface heat balance to the FHX numerical model. The resulting UGT are used within the analytical model.

The results are shown in Figure 7.7; using the UGT computed with the 1-d numerical model eliminates most of the error. The peak error in FHX ExFT is reduced from -2°C (-3.6°F) (with the numerical model/adiabatic foundation) to -0.3°C (-0.5°F). So, then most of the differences between the numerical model and the analytical model can be attributed to, first, the analytical model approximation of the basement as a vertical, infinite, adiabatic wall, and, second, use of the Kusuda and Achenbach model for undisturbed ground temperature.

The Kusuda and Achenbach model does not account for freezing in the soil. Freezing in the soil limits the penetration of cold temperatures downwards and accounting for this may require a

revised procedure. It would be possible to extract the UGT from the 1D numerical models. As the 1D numerical model runs very fast (about a minute on a current desktop PC), it conceivably could be run in advance of the analytical model. An analytical solution that does not require such simplified geometry would also be helpful.

Remaining differences are presumably due to differences in time steps: hourly loads for the numerical model and monthly loads and monthly peak loads for the analytical model. Further research may be needed to quantify the importance of these differences.

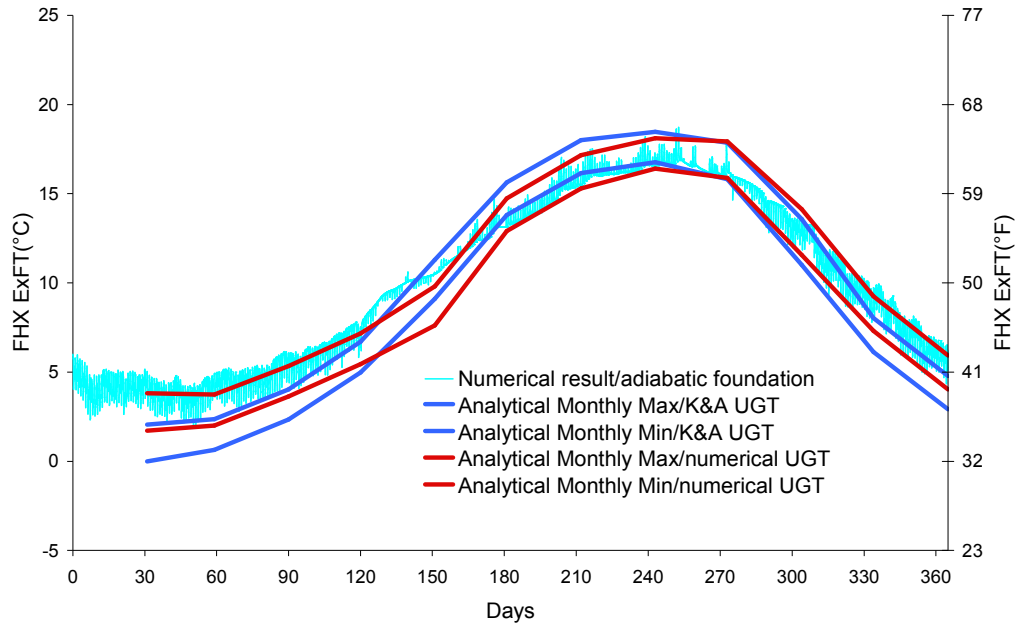


Figure 7.7: Reasons for FHX ExFT difference between two model result in Salem, OR

Also, for all of the cases shown above, the basement is not temperature conditioned. It is expected that some "short-circuiting" will occur when the basement is conditioned and that remains a subject for future research. As a first attempt to look at the sensitivity of the basement to use of an FHX, consider Figure 7.8. Figure 7.8 shows the basement air temperature for a case without FHX (where the house heating and cooling are provided with another system) and the

case with an FHX, in the second year of operation. The maximum difference is about 0.7°C (1.3°F); which seems acceptably small. However, how the short-circuiting will affect cases with conditioned basements is still under investigation.

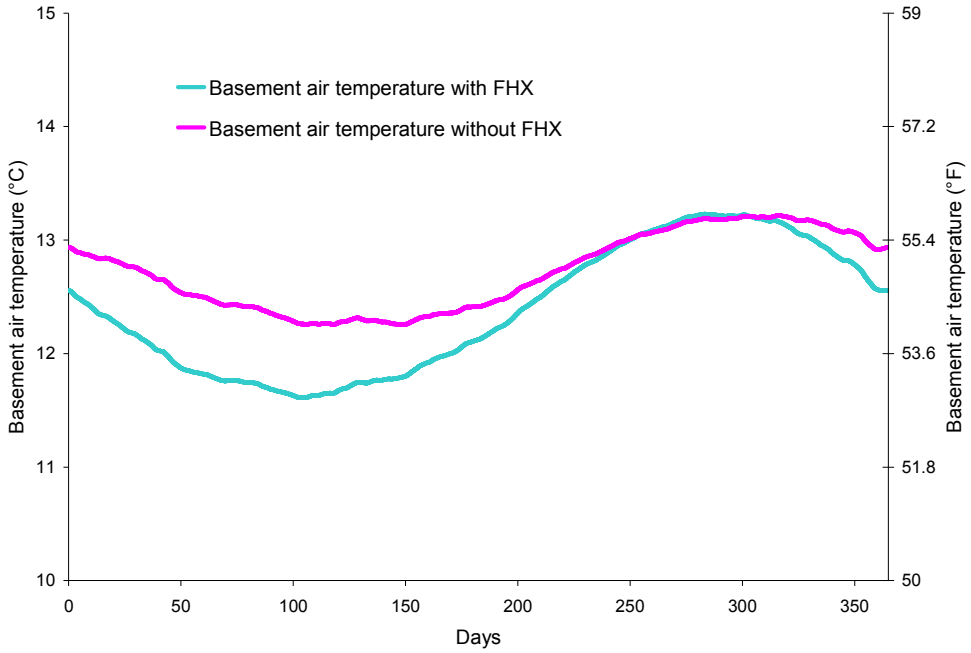


Figure 7.8: Basement air temperature in Salem, OR

In this chapter, simulation results of the FHX numerical model and FHX analytical model are compared and discussed. Six cases at six different locations in the US; Salem, Phoenix, Albuquerque, Knoxville, San Francisco and Tulsa, were chosen for the investigation. For all cases except Salem, Oregon the analytical model oversizes the FHX between 17% and 19%. For Salem, the analytical model oversizes the FHX by 29%. Most of the error is caused by two factors:

- The analytical model approximates the actual basement geometry as an infinite, vertical, adiabatic wall

- The analytical model uses the Kusuda and Achenbach (1965) procedure for determining the undisturbed ground temperature.

The errors in the analytical model are really higher than desirable for a simplified design tool, yet the time required to use a numerical model iteratively for design is unacceptable with current desktop computers. The analytical model runs about 200 times faster than the numerical model, but at the cost of accuracy. Therefore, for the future work, the FHX analytical model needs to be improved. The most promising possibility is to improve the undisturbed ground temperature model – it would be possible to extract the UGT from the 1D numerical models. As the 1D numerical model runs very fast (about a minute on a current desktop PC), it conceivably could be run in advance of the analytical model. An analytical solution that does not require such simplified geometry would also be helpful.

# CHAPTER 8

## CONCLUSION AND RECOMMENDATION

Foundation heat exchangers (FHX) are an alternative to more costly ground heat exchangers utilized in ground-source heat pump (GSHP) systems serving detached or semi-detached houses. Simulation models of FHX are needed for design and energy calculations. This thesis looks at two approaches that have been used for development of simulation models for FHX: a detailed numerical model and a simplified monthly time-step analytical model used as a design tool. The numerical model is a two-dimensional finite volume model with hourly time steps, implemented in the HVACSIM+ environment. The simplified analytical model is based on superimposed line sources and sinks and uses a hybrid monthly time step. Also superimposed is the undisturbed ground temperature calculated with the Kusuda and Achenbach (1965) procedure. The analytical model runs about 200 times faster than the numerical model, but at the cost of accuracy.

The FHX numerical model is validated with experimental measurement collected in a two-story residual building, located in Oak Ridge, Tennessee. The experiment system installed both the foundation heat exchangers and conventional ground heat exchanger tubes buried horizontally. A FHX model and HGHX model are used to model only their respective parts of the system. Since entering and exiting heat pump fluid temperature are known from experimental data, no heat pump model is included in the simulation at present time, exiting heat pump fluid temperature is treated as input in FHX model. The input parameters to FHX model and HGHX numerical

models are mostly obtained from the experimental data. The simulation results of the FHX model; exiting fluid temperature, FHX tube wall temperature, undisturbed soil temperature and disturbed soil temperature, have been compared to the experimental result. The difference of simulated and measured daily average FHX exiting fluid temperature is less than 1°C (1.8°F), for a period of ten months. The validation results provide a strong assurance of the model accuracy.

For the FHX numerical model, the question of short-circuiting needs further investigation. When the FHX tubes are buried besides the convection basement wall, it may extract heat from the basement; this will drive up the heating load. This is called short-circuiting heat transfer. The short-circuiting heat transfer might decrease the coefficient of the system that utilizes the foundation heat exchangers.

Simulation results of the FHX numerical model and FHX analytical model are compared and discussed. Six cases at six different locations in the US; Salem, Phoenix, Albuquerque, Knoxville, San Francisco and Tulsa, were chosen for the investigation. For all cases except Salem, Oregon the analytical model oversizes the FHX between 17% and 19%. For Salem, the analytical model oversizes the FHX by 29%. Most of the error is caused by two factors:

- The analytical model approximates the actual basement geometry as an infinite, vertical, adiabatic wall
- The analytical model uses the Kusuda and Achenbach (1965) procedure for determining the undisturbed ground temperature.

The errors in the analytical model are really higher than desirable for a simplified design tool, yet the time required to use a numerical model iteratively for design is unacceptable with current desktop computers. Therefore, for the future work, the FHX analytical model needs to be improved. The most promising possibility is to improve the undisturbed ground temperature model – it would be possible to extract the UGT from the 1D numerical models. As the 1D

numerical model runs very fast (about a minute on a current desktop PC), it conceivably could be run in advance of the analytical model. An analytical solution that does not require such simplified geometry would also be helpful.

The FHX analytical model calculates the undisturbed ground temperature with the Kusuda and Achenbach model (1965). The FHX numerical model generally depends on the Kusuda and Achenbach model to set the initial temperature profile in the ground and, in some cases, to set the lower boundary conditions. However, the result of the equation depends on having the Kusuda and Achenbach parameters: annual average soil temperature, surface temperature amplitude and phase delay. Therefore, a simpler one-dimensional model that utilizes a 1D numerical model, with full surface heat balance coupled with TMY3 (Typical Meteorological Year 3) weather files (or other equivalent weather files), to estimate all three parameters has been developed. The accuracy of the Kusuda and Achenbach model calculated with the tuned parameters is limited by the accuracy of the 1D numerical model. The simulation results of 1D numerical model and Kusuda and Achenbach model are compared to measured data provided by Soil Climate Analysis Network (SCAN) of the USDA NRCS (See http://www.wcc.nrcs.usda.gov/scan/). Eleven sites in eleven states of the US are chosen for the validation. There are few conclusions made for computing the undisturbed ground temperature with the 1D numerical model and Kusuda and Achenbach model;

- The heat loss from the evapotranspiration is not negligible in the calculation of the surface heat balance, when the soil is cover by grass or plant.
- The soil freezing and snow cover effect have a significant effect on undisturbed ground temperature in colder climate, therefore, needs to be considered in the 1D numerical model.

- Kusuda and Achenbach model, which is not able to estimate soil freezing/melting, gives a poor representation of the hourly 1D numerical model results. Therefore, a revised version of the model with higher harmonics are desired to improve the analytical model.

Using the 1D numerical model coupled with TMY3 weather files to compute the Kusuda and Achenbach parameters, and then estimate the undisturbed ground temperature with the Kusuda and Achenbach model is quite useful and promising. The availability of the TMY3 weather file and the simplified form of analytical model can provide researchers a convenient and accurate way of estimating the undisturbed soil temperature.

For the 1D model which estimates the Kusuda and Achenbach parameters in order to calculate the undisturbed ground temperature, it is suggested to include the snow cover effect in the 1D numerical model to improve the accuracy. Moreover, a revised version of Kusuda and Achenbach could be used to improve the result of the analytical model.

# REFERENCES


Arimilli, R. V., and M. Parang. 1983. Numerical analysis Of heat transfer in buried heat-exchanger tubes. *AlChE Symposium Series*(225): 121-129.

Bose, J. E., J. D. Parker, and F. C. McQuiston. 1985. Design/data Manual for closed-loop ground coupled heat pump systems, American Society of Heating, Refrigerating and Air-Conditioning Engineers.

Bose, J. E., and M. Smith. 1992. Performance of new ground heat exchanger configurations for heat pumps. ASME-JSES-KSES International Solar Energy Conference Part 1 (of 2), Maui, HI, USA385-393.

Braven, D., and E. Nielson. 1998. Performance prediction of a sub-slab heat exchanger for geothermal heat pumps. *Journal of Solar Energy Engineering, Transactions of the ASME* 120: 282-288.

Braven, K. R. D., and C. D. David. 1992. A ground-coupled heat pump system with a buried underfloor heat exchanger. Winter Annual Meeting of the American Society of Mechanical Engineers, Anaheim, CA, USA.28: 97-101.

Carslaw, H. S., and J. C. Jaeger. 1959. Conduction of heat in solids, Clarendon Press, Oxford.

Demir, H., A. Koyun, and G. Temir. 2009. Heat transfer of horizontal parallel pipe ground heat exchanger and experimental verification. *Applied Thermal Engineering* 29: 224-233.

Droulia, F., S. Lykoudis, I. Tsiros, N. Alvertos, E. Akylas, and I. Garofalakis. 2009. Ground temperature estimations using simplified analytical and semi-empirical approaches. *Solar Energy* 83(2): 211-219.

Duan, X., and G. F. Naterer. 2008. Ground heat transfer from a varying line source with seasonal temperature fluctuations. *Journal of Heat Transfer-Transactions of the Asme* 130(11): 111302-111301-111310.

Eicker, U., and C. Vorschulze. 2009. Potential of geothermal heat exchangers for office building climatisation. *Renewable Energy* 34: 1126-1133.

Elias, E. A., R.Cichota, H. H. Torriani, and D. J. V. L. Quirijn. 2004. Analytical soil-temperature model: Correction for temporal variation of daily amplitude. *Soil Science Society of America Journal* 68(3): 784-788.

Esen, H., M. Inalli, and M. Esen. 2006. Technoeconomic appraisal of a ground source heat pump system for a heating season in eastern Turkey. *Energy Conversion and Management* 47(9-10): 1281-1297.

Allen, R. G., L. S. Pereira, D. Raes, and M. Simth. 1998. Crop evapotranspiration-Guidelines for computing crop water requirements. *FAO Irrigation and Drainage Paper No 56*.

Antonopoulos, V. Z. 2006. Water movement and heat transfer simulations in a soil under ryegrass. *Journal of Biosystems Engineering* 95(1): 127-138.

ASHRAE. 1997. ASHRAE Handbook-Fundamentals, Atlanta: American Society of Heating, Refrigerating and Air-Conditioning Engineers, Inc.

Bose, J. E., J. D. Parker, and F. C. McQuiston. 1985. Design/data Manual for closed-loop ground coupled heat pump systems, American Society of Heating, Refrigerating and Air-Conditioning Engineers.

Bose, J. E., and M. Smith. 1992. Performance of new ground heat exchanger configurations for heat pumps. ASME-JSES-KSES International Solar Energy Conference Part 1 (of 2), Maui, HI, USA385-393.

Braven, D., and E. Nielson. 1998. Performance prediction of a sub-slab heat exchanger for geothermal heat pumps. *Journal of Solar Energy Engineering, Transactions of the ASME* 120: 282-288.

Carslaw, H. S., and J. C. Jaeger. 1959. Conduction of heat in solids, Oxford at the Clarendon Press.81-83.

Chang, J. H. 1958. Ground Temperature. Bluehill Meteorological Observatory, Harvard University.

Collins, W. D. 1925. Temperature of water available for industrial use in the United States. United States Geological Survey Water Supply Paper 520-F, Washington: USGS

Cote, J., and J. M. Konrad. 2005. A generalized thermal conductivity model for soils and construction materials. *Canadian Geotechnical Journal* 42: 443-458.

Cullin, J. 2008. Improvements in design procedures for ground source and hybrid ground source heat pump systems. M.S. Thesis. Oklahoma State University. Stillwater.

Demir, H., A. Koyun, and G. Temir. 2009. Heat transfer of horizontal parallel pipe ground heat exchanger and experimental verification. *Applied Thermal Engineering* 29: 224-233.

Droulia, F., S. Lykoudis, I. Tsiros, N. Alvertos, E. Akylas, and I. Garofalakis. 2009. Ground temperature estimations using simplified analytical and semi-empirical approaches. *Solar Energy* 83(2): 211-219.

Eckert, E. R. G., and R. M. Drake. 1959. Heat and Mass Transfer, Mc-Graw-Hill Book Company, New York, Toronto, London.99-107.

Eicker, U., and C. Vorschulze. 2009. Potential of geothermal heat exchangers for office building climatisation. *Renewable Energy* 34: 1126-1133.

Elias, E. A., R.Cichota, H. H. Torriani, and D. J. V. L. Quirijn. 2004. Analytical soil-temperature model: Correction for temporal variation of daily amplitude. *Soil Science Society of America Journal* 68(3): 784-788.

Esen, H., M. Inalli, and M. Esen. 2006. Technoeconomic appraisal of a ground source heat pump system for a heating season in eastern Turkey. *Energy Conversion and Management* 47(9-10): 1281-1297.

Esen, H., M. Inalli, and M. Esen. 2007a. Numerical and experimental analysis of a horizontal ground-coupled heat pump system. *Building and Environment* 42(3): 1126-1134.

Esen, H., M.Inalli, and M. Esen. 2007b. A techno-economic comparison of ground-coupled and air-coupled heat pump system for space cooling. *Building and Environment* 42: 1955-1965.
Gao, J., X. Zhang, J. Liu, K. Li, and J. Yang. 2008a. Numerical and experimental assessment of thermal performance of vertical energy piles: An application. *Applied Energy* 85(10): 901-910.
Gao, J., X. Zhang, J. Liu, K. Li, and J. Yang. 2008b. Thermal performance and ground temperature of vertical pile-foundation heat exchangers: A case study. *Applied Thermal Engineering* 28: 2295-2304.
Hanks, R. J., D. D. Austin, and and O.Wt. 1971. Soil TEMPERATURE ESTIMATION BY A NUMERICAL METHOD. *Soil Science Society of America Proceedings* 35(5): 665-.
Hart, D. P., and R. Couvillion. 1986. Earth-coupled heat transfer, National Water Well Association,Dublin,OH.192.
Hendrickx, J. M. H., R. L. V. Dam, and B. Borchers. 2003. Worldwide distribution of soil dielectric and thermal properties
Herb, W. R., B.Janke, O. Mohseni, and H.G.Stefan. 2008. Ground surface temperature simulation for different land covers. *Journal of Hydrology* 356(3-4): 327-343.
Howell, T. A., and S. R. Evett. 2004. The Penman-Monteith Method. Section 3 in Evapotranspiration: Determination of Consumptive Use in Water Rights Proceedings, Denver, CO
Inalli, M., and H. Esen. 2004. Experimental thermal performance evaluation of a horizontal ground-source heat pump system. *Applied Thermal Engineering* 24(14-15): 2219-2232.
Incropera, F. P., and D. P. Dewitt. 1996. Introduction to Heat Transfer, John Wiley & Sons; 3 Sub edition
Ingersoll, L. R., and H. J. Plass. 1948. Theory of the ground pipe heat source for the heat pump. *Heating, Piping and AIr conditioning* 20: 119-122.
Katsura, T., K.Nagano, and S.Takeda. 2008. Method of calculation of the ground temperature for multiple ground heat exchangers. *Applied Thermal Engineering* 28: 1995-2004.
Katsura, T., K. Nagano, S. Narita, S. Takeda, Y. Nakamura, and A. Okamoto. 2009. Calculation algorithm of the temperatures for pipe arrangement of multiple ground heat exchangers. *Applied Thermal Engineering* 29(5-6): 906-919.
Kusuda, T., and P. R. Achenbach. 1965. Earth Temperature and Thermal Diffusivity at Selected Stations in the United States. *ASHRAE Transactions* 71(1): 61-76.
Laloui, L., M.Nuth, and L.Vulliet. 2006. Experimental and numerical investigations of the behaviour of a heat exchanger pile. *International Journal for Numerical and Analytical Methods in Geomechanics* 30: 763-781.
Lamberg, P., R. Lehtiniemi, and A. M. Henell. 2004. Numerical and experimental investigation of melting and freezing processes in phase change material storage. *Internation Journal of Thermal Sciences* 43(3).
Liu, X. 2005. Development and experimental validation of simulation of hydronic snow melting systems for bridges. Ph.D. Thesis.
Lu, S., T. Ren, Y. Gong, and R.Horton. 2007. An improved model for predicting soil thermal conductivity from water content at room temperature. *Soil Science*

*Society of America Journal* 71: 8-14.
Mei, V. C. 1985. Theoretical heat pump ground coil analysis with variable ground farfield boundary conditions. *AlChE Symposium Series*(245): 7-12.
Mei, V. C. 1986. Horizontal ground-coil heat exchanger theoretical and experimental analysis. Technical report. Oak Ridge National Laboratory.
Mei, V. C. 1988. Heat pump ground coil analysis with thermal interference. *Journal of Solar Energy Engineering, Transactions of the ASME* 110(2): 67-73.
Mei, V. C., and C. J. Emerson. 1985. New approach for analysis of ground-coil design for applied heat pump systems. *ASHRAE Journal* 91(2): 1216-1224.
Metz, P. D. 1983. A Simple Computer Program to Model Three-Dimensional Underground Heat Flow With Realistic Boundary Conditions. *Journal of Solar Energy Engineering* 105(1): 42-49.
Minea, V. 2006. Ground-source heat pumps: Energy efficiency for two Canadian schools. *ASHRAE Journal* 48(5): 28-38.
Morino, K., and T. Oka. 1994. Study on heat exchanged in soil by circulating water in a steel pile. *Energy and Buildings* 21: 65-78.
Moustafa, S., D. Jarrar, H. Elmansy, H. Alshami, and G. Brusewitz. 1981. Arid soil temperature model. *Solar Energy* 27(1): 83-88.
Niu, G. Y., and Z. L. Yang. 2006. Effects of frozen soil on snowmelt runoff and soil water storage at a continental scale. *J. Hydrometeorol.* 7(5): 937-952.
Penman, H. L. 1948. Natural evaporation from open water, bare soil, and grass. Procedeedings of the Royal Society of London Series A.193: 120-146.
Persson, C., and J. Claesson. 2005. Steady state thermal problem of insulated pipes solved with the multipole method. Chalmers University of Technology.
Philippe, M., M.Bernier, and D. Marchio. 2009. Validity ranges of three analytical solutions to heat transfer in the vicinity of single boreholes. *Geothermics* 38(4): 407-413.
Piechowski, M. 1996. A ground coupled heat pump system with energy storage. Ph.D. Melbourne University.
Piechowski, M. 1998. Heat and mass transfer model of a ground heat exchanger: Validation and sensitivity analysis. *International Journal of Energy Research* 22(11): 965-979.
Piechowski, M. 1999. Heat and mass transfer model of a ground heat exchanger: Theoretical development. *International Journal of Energy Research* 23(7): 571-588.
Pulat, E., S. Coskun, K. Unlu, and N. Yamankaradeniz. 2009. Experimental study of horizontal ground source heat pump performance for mild climate in Turkey. *Energy* 34: 1284-1295.
Saastamoinen, J. J. 2007. Unsteady state temperature fields in a slab induced by line sources. *Internation Journal of Heat and Mass Transfer* 50(3-4): 756-765.
Sikora, E., S. C. Gupta, and J. Kossowski. 1990. Soil temperature predictions from a numerical heat-flow model using variable and constant thermal diffusivities. *Soil and Tillage Research* 18(1): 27-36.
Tarnawski, V. R., and W. H. Leong. 1993. Computer analysis, design and simulation of horizontal ground heat exchangers. *International Journal of Energy Research* 17: 467-477.

Van Wijk, W. R., and D. A. de Vries. 1966. Periodic temperature variations in a homogeneous soil, North-Holland Publishing Company, Amsterdam 102-143.

Walter, I. A., R. G. Allen, R. Elliott, D. Itenfisu, P.Brown, M. E. Jensen, B. Mecham, T. A. Howell, R. Snyder, S.Eching, T.Spofford, M.Hattendorf, D.Martin, R.H.Cuenca, and J. L. Wright. 2005. The ASCE standardized reference evapotranspiration equation. Standardization of Reference Evapotranspiration Task Committee Final Report. American Society Civil Engineers, Environmental and Water Resources Institute. Reston, Virginia.

Walter, I. A., R. G. Allen, R. Elliott, M. E. Jensen, D. Itenfisu, B. Mecham, T. A. Howell, R. Snyder, P.Brown, S.Eching, T.Spofford, M.Hattendorf, R.H.Cuenca, J. L. Wright, and D.Martin. 2000. ASCE's standardized reference evapotranspiration equation. Proceeding 4th National Irrigation Symposium, ASAE, Phoenix,AZ209-215.

VITA

Lu Xing

Candidate for the Degree of

Master of Science

Thesis: ANALYTICAL AND NUMERICAL MODELING OF FOUNDATION HEAT EXCHANGERS

Major Field: Mechanical Engineering

Biographical:

Education:

Completed the requirements for the Master of Science with a major in Mechanical Engineering at Oklahoma State University, Stillwater, Oklahoma in December, 2010

Completed the requirements for the Bachelor of Science with a major in Building Environment of Equipment Engineering at Huazhong University of Science and Techonology, Wuhan, China in May, 2008.

Professional Memberships:

ASHRAE student member during master degree study

Name: Lu Xing Date of Degree: December, 2010

Institution: Oklahoma State University Location: Stillwater, Oklahoma

Title of Study: ANALYTICAL AND NUMERICAL MODELING OF FOUNDATION HEAT EXCHANGERS

Pages in Study: 145 Candidate for the Degree of Master of Science

Major Field: Mechanical Engineering

Scope and Method of Study:

Foundation heat exchangers (FHX) are an alternative to more costly ground heat exchangers utilized in ground-source heat pump (GSHP) systems serving detached or semi-detached houses. Simulation models of FHX are needed for design and energy calculations. This thesis looks at two approaches that have been used for development of simulation models for FHX: a detailed numerical model and a simplified monthly time-step analytical model used as a design tool. The numerical model is a two-dimensional finite volume model with hourly time steps, implemented in the HVACSIM+ environment. The simplified analytical model is based on superimposed line sources and sinks and uses a hybrid monthly time step. The numerical model is validated with experimental result for a period of ten months; data are collected from a two-story residual building, located in Oak Ridge, Tennessee. Both the FHX analytical model and FHX numerical model utilize Kusuda and Achenbach model (1965) to calculates the undisturbed ground temperature. However, the result of the Kusuda and Achenbach model depends on having the Kusuda and Achenbach parameters: annual average soil temperature, surface temperature amplitude and phase delay. Therefore, a simpler one-dimensional model that utilizes a 1D numerical model, with full surface heat balance coupled with TMY3 (Typical Meteorological Year 3) weather files (or other equivalent weather files), to estimate all three parameters has been developed. The 1D ground heat transfer model result is validated with experimental data of 11 locations within U.S..

Findings and Conclusions:

The daily average exiting FHX fluid temperature calculated from the numerical model is less than 1°C (1.8 °F) difference from the experimental result, which suggests the FHX numerical model provides simulation result with high accuracy. Simulation results of the FHX numerical model and FHX analytical model are compared and discussed for six cases at six different locations in the US; Salem, Phoenix, Albuquerque, Knoxville, San Francisco and Tulsa. Two models show a sizing error of less than 20% for five locations and 29% sizing error for one location. The analytical model runs about 200 times faster than the numerical model, but needs the further improvement of the model accuracy.

ADVISER'S APPROVAL: Dr. Jeffrey Spitler